

NATIONAL TRANSPORTATION SAFETY BOARD

Office of Research and Engineering
Washington, D.C. 20594

March 14, 2022

Aircraft Performance Study

by John O'Callaghan

Location: Truckee, California

Date: July 26, 2021

Time: 13:18 Pacific Daylight Time (PDT)
(20:18 Coordinated Universal Time (UTC))

Aircraft: Bombardier CL-600-2B16, registration N605TR

NTSB#: WPR21FA286

TABLE OF CONTENTS

A.	ACCIDENT	1
B.	GROUP	1
C.	HISTORY OF FLIGHT	1
	<i>Objective and scope of the Aircraft Performance Study</i>	1
	<i>Summary of results</i>	2
D.	DETAILS OF THE INVESTIGATION	4
I.	The Bombardier CL-600-2B16 Airplane	4
II.	Accident site and surveillance video	5
	<i>Accident site location</i>	5
	<i>Surveillance video</i>	5
III.	Surveillance data	5
IV.	Recorded flight data	6
	<i>FDR and CVR data description</i>	6
	<i>Correlation of FDR, CVR, and ADS-B Times</i>	8
V.	Performance Calculations based on FDR Data	8
	<i>Overview</i>	8
	<i>True airspeed calculation</i>	9
	<i>Pressure-based true altitude and density altitude calculations</i>	10
	<i>True altitude based on radio altimeter and terrain elevation data</i>	11
	<i>Accelerometer data corrections and integration</i>	12
	<i>Accelerometer integration results</i>	13
	<i>Flight path angle (γ) calculation</i>	14
	<i>Wind calculations</i>	14
	<i>Inertial angle of attack (α) and sideslip angle (β) calculations</i>	15
VI.	Additional aircraft performance considerations	15
	<i>Introduction</i>	15
	<i>The CL-605 Stall Protection System (SPS)</i>	16
	<i>The effect of spoiler deployment on normal load factor capability</i>	20
	<i>Flight control inputs following stick shaker and pusher activation</i>	25
	<i>Simulation model comparison of circling maneuver performed by Bombardier</i>	26
E.	CONCLUSIONS	27
F.	REFERENCES	29
G.	GLOSSARY	30
	<i>Acronyms</i>	30
	<i>English symbols</i>	30
	<i>Greek symbols</i>	31
	FIGURES	32
	APPENDIX A: KTRK airport diagram and other information	A1
	APPENDIX B: Bombardier memorandum to NTSB	B1

NATIONAL TRANSPORTATION SAFETY BOARD

Office of Research and Engineering
Washington, D.C. 20594

March 14, 2022

Aircraft Performance Study

by John O'Callaghan

A. ACCIDENT

Location: Truckee, California
Date: July 26, 2021
Time: 13:18 Pacific Daylight Time (PDT)
(20:18 Coordinated Universal Time (UTC))¹
Aircraft: Bombardier CL-600-2B16, registration N605TR
NTSB#: WPR21FA286

B. GROUP

Chairman: John O'Callaghan
National Resource Specialist - Aircraft Performance
National Transportation Safety Board (NTSB)
490 L'Enfant Plaza E, SW
Washington, DC 20594

Members: N/A

C. HISTORY OF FLIGHT

On July 26, 2021, at about 13:18 PDT, a Bombardier Inc., CL-600-2B16 airplane (Challenger 605 or CL-605), N605TR, was destroyed when it was involved in an accident while circling to land at Truckee-Tahoe Airport (KTRK), Truckee, California. The pilot, co-pilot and 4 passengers were fatally injured. The airplane was operated as a Title14 Code of Federal Regulations Part 91 personal flight.

Objective and scope of the Aircraft Performance Study

The objective of this *Aircraft Performance Study* is to determine and analyze the motion of the airplane and the physical forces that produce that motion. In particular, the *Study* attempts to define the airplane's position and orientation during the relevant portion of the

¹ Local time in Truckee on the day of the accident was Pacific Daylight Time (PDT). PDT = UTC - 7 hours. Times in this *Study* use PDT unless otherwise noted.

flight, and determine the airplane's response to control inputs, external disturbances, and other factors that could affect its trajectory.

The data used to determine and analyze the airplane motion includes the following:

- Airplane resting location and ground scars / markings.
- Air Traffic Control (ATC) Automatic Dependent Surveillance - Broadcast (ADS-B) data.
- Flight Data Recorder (FDR) data.
- Cockpit Voice Recorder (CVR) information.
- Surveillance video information.
- Weather information.
- Airplane aerodynamic performance information.
- Output from aircraft performance analysis programs and simulations.

This *Study* describes the results of using the data listed above in defining, as far as possible, the position of N605TR relative to the KTRK runway 11 threshold throughout its approach to that runway. The *Study* introduces the aircraft motion data collected during the investigation, describes the methods used to extract additional aircraft motion information from the FDR, and presents the results of these calculations.

The *Study* also examines the aerodynamic behavior of the airplane during its final maneuvers, and the performance of the Stall Protection System (SPS) at the time. The effect of the deployment of the spoilers on the load factor achievable by the airplane is also considered, as is the effect of erroneous weight data in the airplane's Flight Management System (FMS).

Summary of results

The data listed above indicates that as N605TR was circling to land on runway 11 after approaching KTRK on the RNAV runway 20 instrument approach, the angle of attack (α) exceeded the natural stall angle of attack. The left wing stalled first and the airplane abruptly rolled to the left past 140° and impacted the ground. This asymmetric stall and abrupt roll is consistent with the known natural stall characteristics of the CL-605, which is why the airplane is equipped with a stick pusher system ("pusher") that activates before the natural stall occurs. The α at which the pusher activates defines the "stall" α of the airplane, and is the basis for the definition of operational reference speeds and the α margin provided by the Stall Protection System (SPS), including the stick shaker system ("shaker").

During the circling maneuver, N605TR did not achieve a "downwind" leg parallel to runway 11, and the "base" leg of the approach was not perpendicular to runway 11 (see Figure 5). This contributed to the airplane crossing the extended centerline of runway 11 only 0.85 nm from the threshold, while heading 49° to the right of the runway heading and above a 3° glide path to the runway. The crew's conversation recorded on the CVR indicates that they were aware that they had overshot the centerline and were high, but intended to

continue the landing by maneuvering back towards the centerline. As the airplane crossed the centerline, the flight spoilers were deployed to 40° (i.e., fully deployed) and remained fully deployed until impact.

During the turn back towards the runway centerline, the roll angle reached -37° (left). The left bank increased the lift required from the wings, while at the same time the spoiler deployment reduced the lift provided by the wings at a given α . To meet the lift requirement, the α increased. As the airplane reached a roll angle of -37°, a “sink rate” alert was activated, less than a second later, the shaker activated. Within a second of the shaker activation, the stick pusher also activated, and the elevators moved trailing-edge-down (TED, i.e., in the airplane nose-down direction).

As a result of the pusher activation, the elevators moved to 10° TED. This movement decreased α , and the pusher and shaker de-activated. However, the elevators then moved to about 18° trailing-edge-up (TEU), which propelled α above the natural stall α (re-activating the shaker and pusher), and resulted in an asymmetric aerodynamic stall, uncontrollable roll to the left, and impact with the ground.

The investigation discovered that the airplane empty weight programmed into the FMS was most likely the factory-default weight of 24,000 lb., about 3,000 lb. lighter than the estimated actual airplane empty weight.² Such a discrepancy would have resulted in the FMS computing a landing weight of about 28,300 lb. and a corresponding reference landing speed (V_{REF}) of 118 kt. The estimated correct landing weight (which also results in an excellent simulator match of the circling maneuver) is 31,294 lb., corresponding to a V_{REF} of 124 kt. (6 kt. faster than the V_{REF} likely computed by the FMS). Using a speed additive of 10 kt. to V_{REF} for maneuvering, the target speed during the circling maneuver using the FMS weight would have been 118 kt. + 10 kt. = 128 kt., and the target speed using the estimated correct weight would have been 134 kt. During the last minute of the flight, the calibrated airspeed varied between 120 kt. and 137 kt., and was about 130 kt. (V_{REF} + 6 kt.) at 13:18:05.8, the first time the sound of the stick shaker was recorded on the CVR. Consequently, the erroneous FMS weight did not contribute to the airplane operating with a significantly reduced α margin to the stick shaker during the final maneuver. However, as will be seen, the deployment of the spoilers about 12 seconds before impact did significantly reduce the α margin to stick shaker, stick pusher, and natural stall.

The sections that follow present the data used in this *Study* (as listed above), and describe the methods used to calculate additional performance information from this data. The recorded airplane performance is compared with the results of a simulation of the circling maneuver performed by Bombardier, and the SPS and α -vane parameters recorded on the FDR are compared with the SPS design specifications. The results of these calculations are presented in the Figures and Tables described throughout the *Study*.

² The reasons for this discrepancy are discussed in the *Systems Group Chairman's Factual Report* (Reference 11). As noted below, the default empty weight results in a landing weight consistent with the V_{REF} speed cited by the First Officer on the CVR.

D. DETAILS OF THE INVESTIGATION

I. The Bombardier CL-600-2B16 Airplane

The Bombarider CL-600-2B16, or “Challenger 605,” is a derivative of the Canadair Challenger 600 (CL-600-1A11) originally certificated in 1980.³ The Challenger 605 was certified in 2006, has a maximum takeoff weight of 48,200 lb., and is powered by two General Electric CF34-3B turbofan engines mounted on the aft fuselage, providing 8,700 lb. of takeoff thrust each.⁴ Figure 1 shows a 3-view image of the Challenger 605, taken from Reference 1. N605TR was Bombardier serial number 5715 and was manufactured in 2007. A pre-accident photograph of the airplane is shown in Figure 2.

Table 1 lists some dimensions of the airplane, and Table 2 presents mass properties for N605TR at the time of the accident. The mass properties were estimated by Bombardier for their simulator match of the circling maneuver, based on the fuel quantities and stabilizer position recorded on the FDR, and a December 2007 Aircraft Weight and Balance Report for serial number 5715 (the accident airplane).

Item	Value
<i>Reference dimensions:</i>	
Wing area	450 ft. ²
Wing span	64.33 ft.
Mean Aerodynamic Chord (MAC)	92.64 inches (7.72 ft.)

Table 1. Dimensions of the Challenger 605 airplane.

Item	Weight (lb.)	Fuselage station (inches)
Basic Operating Weight (BOW, from 12/2007 W&B Report)	27,034	519.4
Passenger 1	195	377.0
Passenger 2	195	377.0
Passenger 3	195	426.5
Passenger 4	195	430.5
Luggage	120	603.8
Zero-Fuel Weight (ZFW) Total	27,934	516.5
Left Fuel Tank (estimated distribution)	1280	483.5
Right Fuel Tank (estimated distribution)	1280	483.5
Center Fuel Tank (estimated distribution)	800	460.9
Fuel Weight	3,360	478.1
Gross Weight	31,294	512.4 (26.3% MAC)

Table 2. Weight and balance estimate for N605TR prepared by Bombardier.

³ See https://en.wikipedia.org/wiki/Bombardier_Challenger_600_series.

⁴ See <https://www.geaviation.com/sites/default/files/datasheet-CF34-3.pdf>.

II. Accident site and surveillance video

Accident site location

According to the preliminary report for this accident (Reference 2),

The accident site was located on a hillside between a golf course fairway and a residential street. The airplane was consumed by postcrash fire. A debris path, which measured about 225 ft long and 85 ft wide was marked by several broken trees and was oriented on an easterly heading. The initial point of impact was identified by a severed tree that stood about 70 ft tall, located about 120 ft west of the main wreckage. Portions of the right and left wings and control surfaces were found fragmented along the debris path. Additional airframe fragments were collocated with the main wreckage, which was comprised of both engines, the empennage, and fuselage remnants.

Reference 2 documents the location of the main wreckage as:

Latitude: 39.325433° N
Longitude: 120.16291° W

Per *Google Earth*, the elevation of these coordinates is 5,940 ft. MSL. Relative to the KTRK runway 11 threshold (elevation 5,901 ft. MSL), these coordinates are:

0.0351 nm (213 ft.) north of the KTRK runway 11 threshold
0.4735 nm (2,877 ft.) west of the KTRK runway 11 threshold

A *Google Earth* satellite view of the accident location, depicting the final portion of N605TR's flight path and part of runway 11, is presented in Figure 7.

Surveillance video

Reference 2 notes that “three surveillance videos captured the accident flight’s final movements.” Selected cropped and enlarged still frames from one of these videos, recorded by a surveillance camera located at the Truckee-Tahoe Lumber Co. Headquarters,⁵ are presented in Figure 3. The complete video, with filename “TTLCO-version2-2021-07-26_17-18-07.mp4,” is available in the public docket for this accident.

III. Surveillance data

N605TR's flight track was recorded by the Automatic Dependent Surveillance – Broadcast (ADS-B) system. ADS-B capability enables aircraft to broadcast their three-dimensional position (latitude, longitude, and altitude) to other ADS-B equipped aircraft and to ADS-B ground stations. ADS-B latitude and longitude are determined using Global Navigation Satellite System (GNSS) signals, including those from Global Positioning System (GPS) satellites, and altitudes determined both barometrically and by GNSS are included in ADS-B messages. The GNSS positions are very accurate compared to radar data; radar range uncertainty alone (without even considering azimuth uncertainty) is about $\pm 1/16$ nm, or

⁵ The address of this location is 11001 Soaring Way, Truckee, CA 96161.

± 380 ft., and GNSS positions are generally accurate to within 60 ft. (see Reference 3). Furthermore, ADS-B data is available at a higher frequency (typically 1 sample/second) than radar data (at best, 1 sample every 4.5 seconds). Consequently, only ADS-B surveillance data for N605TR are considered in this *Study*. The ADS-B positions are used to confirm the latitude and longitude recorded on the FDR, and in the computation of kinematically consistent airplane positions through mathematical integration of the load factors (accelerations) recorded by the FDR, as described in Section D-V.

The recorded ADS-B data includes the following parameters:

- UTC time of the ADS-B report, in hours, minutes, and seconds. PDT = UTC – 7 hours.
- Aircraft identifying information.
- Latitude and longitude, to a resolution of 0.01 arc-seconds (≈ 1 ft.)
- Pressure altitude in feet, to the nearest 25 ft. (an uncertainty band of ± 12.5 ft.)
- Geometric (GNSS) altitude in feet, to the nearest 25 ft.
- North-south and east-west components of ground speed, to a resolution of 1 kt.
- Rate of climb, to a resolution of 1 ft./min.
- Numerous parameters documenting the quality and accuracy of each reported GNSS position.

The sample rate of this data varies between 1 and 2 samples per second, but during the approach and circling maneuver is a consistent 2 samples / sec (2 Hz).

The ADS-B data is presented along with recorded flight data in subsequent sections of this *Study* (see Figures 5 – 11). The position of the airplane is described by its north and east coordinates relative to the KTRK runway 11 threshold; latitude and longitude are converted into these coordinates using the WGS84 ellipsoid model of the earth, and the coordinates of the runway 11 threshold:

39° 19' 29.4519" N latitude / 120° 09' 09.8729" W longitude / elevation 5,901 ft. MSL

IV. Recorded flight data

FDR and CVR data description

The aircraft cockpit voice recorder (CVR) and flight data recorder (FDR) were recovered and sent to the NTSB Recorders Laboratory in Washington, DC for readout.

Descriptions of the FDR and CVR and the recorder readout processes can be found in References 4 and 5, respectively. The FDR readout results in tabulated and plotted values of the recorded flight parameters versus time. The CVR readout results in a transcript of the CVR events, a partial list of which is presented in Table 3. The paraphrased version of the selected CVR events listed in Table 3 are also presented along with other information in various Figures throughout this *Study*. For the complete transcript and CVR report, see Reference 5.

ADS-B time (PDT)	Selected CVR items full transcript text	Paraphrased text on plots
13:04:54.13	[ZOA-E] N605TR cleared to the ALVVA intersection ... hold north on the 340 bearing ... uh turns and leg length at your discretion ... expect further clearance 2030 time now 2005 and a quarter.	[ZOA-E] cleared ALVVA and hold
13:05:56.32	[HOT-2] I'm gonna start the turn for ya 'cause we're missing it.	[HOT-2] starting turn
13:09:39.83	[ZOA-E] N605TR descend and maintain 14000 expect the approach shortly.	[ZOA-E] descend 14000
13:11:24.82	[RDO-2] 605TR is established in the hold.	[RDO-2] hold established
13:11:44.62	[ZOA-E] N5TR cleared direct AWEGA cross AWEGA at or above 12000 cleared R-NAV runway 20 approach Truckee airport.	[ZOA-E] cleared AWEGA
13:13:26.13	[HOT-2] gotta get this thing slowed down.	[HOT-2] comment about speed
13:13:55.02	[HOT-2] slope is available.	[HOT-2] glideslope available
13:14:08.32	[ZOA-F] N5TR I'm not sure if you're still here radar service terminated contact Truckee tower 120.57.	[ZOA-F] contact tower
13:14:16.62	[HOT-1] thank you...flaps twenty.	[HOT-1] request flaps 20
13:14:32.43	[HOT-2] path is captured.	[HOT-2] path captured
13:14:36.13	[RDO-2] tower N605TR is with you LUMMO inbound and we are going to have to circle the runway one one for runway length.	[RDO-2] LUMMO inbound
13:15:05.22	[HOT-2] how 'bout gear down flaps 30 before landing checklist.	[HOT-2] suggested gear down, flaps 30
13:15:07.12	[CAM] [increase in ambient noise consistent with gear down]	[CAM] [noise consistent with gear down]
13:15:45.72	[CAM] twenty five hundred. [electronic voice]	[CAM] [2500]
13:16:18.03	[CAM] approaching minimums. [electronic voice]	[CAM] [approaching minimums]
13:16:22.02	[CAM] minimums. [electronic voice]	[CAM] [minimums]
13:16:27.92	[RDO-2] 605TR is making the right hand turn we've got runway one one in sight.	[RDO-2] Turning, runway in sight
13:16:50.93	[CAM] [sound similar to cavalry charge]	[CAM] [cavalry charge]
13:16:55.12	[HOT-2] I'm gonna get your speed under control for you.	[HOT-2] Comment about speed
13:17:00.02	[HOT-2] yep you can start descending.	[HOT-2] start descending
13:17:43.02	[CAM] one thousand. [electronic voice]	[CAM] [1000]
13:17:48.03	[HOT-2] let me see the airplane for a second.	[HOT-2] Comment about control
13:17:56.32	[HOT-2] we're gonna go through it and come back okay?	[HOT-2] Comment about plan
13:18:03.03	[HOT-2] yes yes it's here but we are very high.	[HOT-2] Comment about altitude
13:18:05.23	[CAM] sink rate. [electronic voice]	[CAM] [sink rate]
13:18:05.82	[CAM] [sounds similar to stick shaker activation] / pull up. [electronic voice]	[CAM] [stick shaker & pull up]
13:18:08.23	[HOT-2] let me have the airplane.	[HOT-2] Comment about control
13:18:12.92	[CAM] [sounds consistent with impact]	[CAM] [impact]

Table 3. Full CVR transcript text corresponding to paraphrased text on plots in this *Study*. Audio sources are: [CAM] = Cockpit Area Microphone; [HOT1] = Captain's microphone; [HOT2] = First Officer's microphone; [RDO-2] = First Officer's radio transmission; [ZOA] = Oakland Center controller. Note that times are in ADS-B time, which are related to the FDR times provided in the CVR transcript (Reference 5) as described below. The items contained in this table are only a selected subset of the items contained in the complete CVR transcript over the time period shown; see Reference 5 for the complete transcript, including many items that appear in-between those included here.

Correlation of FDR, CVR, and ADS-B Times

The FDR, CVR, and ADS-B system record their information with respect to time, but these recorded times are not necessarily synchronized. To use these data sources together, their times must be synchronized to a single reference time. The reference time used in this *Study* is the ADS-B time, converted into PDT.

Time on the FDR is measured in terms of the Subframe Reference Number (SRN), with one SRN equivalent to one second of time. The Vehicle Recorders specialist provided the FDR data with the SRN synchronized to the UTC time parameters recorded on the FDR, such that the SRN represents the elapsed seconds since midnight PDT:

$$(\text{Seconds elapsed since midnight PDT, per FDR UTC parameters}) = (\text{FDR SRN}) \quad [1]$$

Equivalently,

$$00:00:00 \text{ PDT FDR time} = 0.0 \text{ SRN} \quad [2]$$

The correlation between the FDR and CVR times is described in Reference 5. The CVR transcript provided in Reference 5 uses the FDR PDT time.

The FDR time is aligned with the ADS-B time using the latitude and longitude parameters recorded on the FDR and in the ADS-B data. To align the FDR latitude and longitude with the ADS-B latitude and longitude, 1.625 seconds were added to the FDR times. Consequently,

$$(\text{ADS-B time in PDT}) = (\text{FDR time in PDT}) + 1.625 \text{ seconds} \quad [3]$$

Several of the plots in this *Study* portray selected CVR content. For example, plots of data vs. time include CVR content overlaid on vertical lines that intersect the x axis of the plot at the times that the content was recorded. The content portrayed on the plots is not the verbatim CVR transcript text, but rather a paraphrase or shorthand code for this text. The full CVR transcript text associated with each paraphrase or code is shown in Table 3.

V. Performance Calculations based on FDR Data

Overview

The FDR records many, but not all, performance parameters of interest. Many additional parameters can be derived from the FDR parameters; however, the FDR parameters themselves can suffer from inherent measurement errors⁶ and must be corrected before being used in these calculations.

⁶ "Measurement error" in this context means the difference between the actual true value of the property being measured and the measured or recorded value. It does not necessarily imply defects or malfunctions in the measurement and recording equipment itself.

This section describes the corrections applied to the FDR data, and the calculations used to derive additional performance parameters from the corrected data. The airplane weight and CG used in these calculations are 31,294 lb. and 26.3% MAC, respectively (see Table 2). Further details about the derivation of the equations and calculation methods used in this *Study* can be found in Appendix A of Reference 6.

The corrected and additional performance parameters derived from the FDR data include:

- Position of the airplane relative to the KTRK runway 11 threshold.
- True airspeed and altitude.
- Load factors corrected for accelerometer bias.
- Kinematically consistent positions and velocities from accelerometer integration.
- Wind speed and direction based on the accelerometer integration and true airspeed and heading data.
- Angle of attack and sideslip angle based on the accelerometer integration and smoothed winds.

The results of these corrections and derivations for the period from the airplane's descent through 7,400 ft. MSL to the end of the FDR data are presented in Figures 5 – 20.⁷

True airspeed calculation

True airspeed equals Mach number multiplied by the speed of sound; the speed of sound is a function of the static temperature. Static temperature is obtained from total temperature and Mach number.

Mach number can be computed from calibrated airspeed and static pressure. Calibrated airspeed and total temperature are recorded directly by the FDR, and the static pressure can be determined from the pressure altitude recorded by the FDR (which is based on the standard sea-level pressure of 29.92 "Hg).

Figure 12b shows the results of the true airspeed calculation, compared with the indicated (calibrated) airspeed recorded by the FDR. The computed true airspeed is depicted as the solid green line, and reflects the oscillations in the FDR calibrated airspeed on which it is based. The dashed green line shows the true airspeed computed from ground speed and estimated smooth winds (this calculation is described below). Figure 7 also shows the ground speed recorded by the FDR, and the ground speed computed from integration of the accelerometer data (this calculation is also described below); the integrated ground speed differs from the FDR ground speed in places because it is forced to be kinematically consistent with the ADS-B latitude and longitude positions (the recorded ground speed is not necessarily kinematically consistent with the ADS-B or FDR latitude and longitude).

⁷ Several Figures in this *Study* have an "a" and a "b" version, which present the same information but at different scales, or with different background images. When the *Study* refers to a Figure with two or more versions without specifying the version, all versions are meant to be included in the reference.

The true airspeed is generally within 5 to 10 knots of the ground speed, indicating relatively light winds (the wind calculation is described below, and Figure 15 compares the computed winds with the winds recorded on the FDR). The KTRK METAR observations surrounding the time of the incident (including winds) are presented in Table 4.

Parameter / Report	KTRK METAR 12:45 PDT	KTRK METAR 13:50 PDT
Sky condition	2,300 ft. broken	2,300 ft. broken
Visibility	4 statute miles	4 statute miles
Winds	090° @ 5 kt.	280° @ 11 kt. gusting to 16 kt.
Temperature / Dew Point	32°C / 6°C	33°C / 8°C
Altimeter setting	30.14 "Hg	30.13 "Hg
Precipitation	-	-
Remarks	Prevailing visibility 3 sm, variable between 0.5 and 5 sm in smoke	Prevailing visibility 3 sm, variable between 0.5 and 5 sm in smoke, *** Aircraft mishap ***

Table 4. METAR weather observations at KTRK surrounding the time of the incident. Wind directions are relative to true north. sm = statute miles.

The 12:51 PDT broadcast KTRK Automated Weather Observation System (AWOS) report, which the CVR indicated was received by the First Officer, stated:

Truckee Tahoe airport automated weather observation one niner five one zulu weather: Wind 080° at 5, visibility 7, clear below 12,000, temperature 32°C, dew point 5°, altimeter 30.14. Remarks: Density altitude 8,900. Truckee traffic be advised actual visibility may be different than what is shown on AWOS due to heavy smoke in the area. Conditions are not monitored from 21:00 to 07:00 local ... Truckee.

The dashed green line in Figure 12 shows the true airspeed computed from the integrated ground speed and a smooth approximation to the computed winds. The result matches the true airspeed computed from the FDR calibrated airspeed within about 4 knots prior to 13:17:05, and within about 2 knots after that time.

Pressure-based true altitude and density altitude calculations

The altitude recorded by the FDR is pressure altitude; i.e., it is the altitude in the standard atmosphere corresponding to the pressure sensed at the airplane's static pressure ports. The altitude in the actual atmosphere corresponding to the local static pressure generally does not equal the pressure altitude, and it is insufficient to simply adjust the pressure altitude for the local sea level pressure because, in general, the lapse rate of pressure with altitude does not match the lapse rate in the standard atmosphere.

To estimate the actual altitude of N605TR, the change in altitude corresponding to a change in static pressure is calculated by solving the hydrostatic equation continuously (the hydrostatic equation describes the pressure increment across a differential element of air required to balance the weight of the element). With static pressure and the static temperature values from the speed calculations, the density and weight of the air elements can be calculated.

The solution of the hydrostatic equation is shown in Figures 9 and 10 as the blue line labeled “Corrected barometric altitude.” This result is modified near the end of the data to smooth through oscillations and better match the altitude defined by the radio altitude plus the terrain elevation, so as to provide a better “target” altitude for the accelerometer integration calculation described below. Accounting for the higher-than-standard temperature of the day changes the rate of change of pressure with true altitude slightly, compared to the rate of change of pressure with pressure altitude.⁸

The indicated altitude shown on the airplane’s altimeters is obtained by adjusting the FDR pressure altitude to account for the 30.13” Hg altimeter setting reported in the 13:50 METAR (see Table 4). Note that the indicated altitude plotted in Figure 10b (magenta line) deviates from the hydrostatically derived altitude (blue line) as altitude increases; this deviation results from the nonstandard lapse rate of pressure with altitude.

The density altitude is the altitude in the standard atmosphere corresponding to the actual air density at each point in the flight. Because of the hotter-than-standard day, the density altitude during the approach was about 2,700 ft. higher than the true MSL altitude.

True altitude based on radio altimeter and terrain elevation data

The green line in Figures 9 and 10 labeled “Radio altitude + terrain elevation” is the altitude that results from adding the height of the airplane’s main gear tires above the ground (measured by the radio altimeter) to the elevation of the terrain underneath the airplane. The terrain elevation is determined by using the ADS-B latitude and longitude data to define the airplane’s track over the ground, and then by obtaining the terrain elevation underneath the airplane’s track from Shuttle Radar Topography Mission (SRTM) elevation data provided by the United States Geological Survey (USGS). The USGS provides SRTM digital elevation data with a resolution of 1 arc-second (about 100 ft.) for the United States and 3 arc-seconds (300 ft.) for global coverage⁹. The resolution of the terrain data used in this *Study* is 1 arc-second.

Note that the “Radio altitude + terrain elevation” (green line) matches the “Corrected barometric altitude” (blue line) relatively well, particularly at the lower altitudes, but at times exceeds the “Corrected barometric altitude” by 50 to 100 ft. The waviness in the green line results from undulations in the terrain (see the terrain profile in Figure 10).

The oscillations in the radio altitude data, resulting from undulations in the terrain or other terrain features (such as buildings), do not indicate variations in the airplane’s MSL altitude; the blue barometric-based line is a better indicator of *changes* in altitude. However, the green line in Figure 10 serves to set the proper ending altitude of the blue line. Described another way, the blue line is the result of an integration of changes in altitude, and the green line provides the “constant of integration” in this calculation that sets the “absolute level” of the blue line.

⁸ The standard-day temperature at the field elevation of 5,900 ft. is 3.3° C (38.0° F); at 33° C (91.4° F), the temperature was 29.7° C (53.4° F) higher than standard.

⁹ See <http://viewer.nationalmap.gov/viewer/>.

However, the “Corrected barometric altitude” (blue line) constructed in this way might not be entirely kinematically consistent with the load factor data recorded on the FDR. In addition, while the FDR ground speed parameter is relatively accurate, it may not be entirely kinematically consistent with the FDR load factor data or the FDR and ADS-B position data. “Kinematically consistent” means that the mathematical relationships between acceleration (measured by load factor parameters), speed (measured by the ground speed and heading parameters), and position (measured by the FDR and ADS-B position parameters) hold in the three dimensions of the airplane’s motion. In practice, the FDR parameters as recorded are only approximately kinematically consistent, as a result of inherent measurement errors and uncertainties.

In light of these errors and uncertainties, a better, kinematically consistent solution for the airplane’s altitude, position, and speed throughout the approach and landing can be obtained by integrating the load factor data recorded on the FDR. This calculation is described below.

Accelerometer data corrections and integration

The red line in Figures 9 and 10 labeled “Altitude from accelerometer integration” is the altitude that results from integrating¹⁰ the FDR load factor data twice to derive aircraft position. The positions, speeds, and accelerations defined by the integrated flight path are known to be kinematically consistent, unlike other measures of these quantities recorded on the FDR.

A kinematically consistent and accurate estimate of the flight path of the airplane during relatively short intervals (about 30 to 60 seconds) can be obtained by integrating the accelerations recorded at the CG of the airplane. In general, the accelerometers are not located exactly on the CG, and so the accelerations at the CG must be computed by adjusting the FDR-recorded load factors for the effects of angular rates and accelerations. In the present case, the angular rates and accelerations are sufficiently small that this correction is negligible.

However, accelerometers generally contain small offsets, or “biases,” that produce large errors in speed and position if not removed prior to integration.¹¹ In addition, the initial values of speed, rate of climb, and track angle are required during the integration process (these are essentially the “constants of integration” when integrating acceleration to get speeds). The constants of integration and the values of the accelerometer biases can be estimated by selecting them such that the aircraft position that results from the integration agrees with known “target” positions determined from another source.

The accelerometer biases are not necessarily constant over an entire flight, but can drift over time. It is for this reason that integrating the accelerometers works best over relatively

¹⁰ In the following discussion, “integrating” the load factor data refers to mathematical integration with respect to time, per the theorems of Calculus.

¹¹ For details about the equations to be integrated and the bias correction technique described in this *Study*, see Appendix A of Reference 6.

short intervals, during which the accelerometer biases are approximately constant. In this case, the accelerometers are integrated over the 116 second period from 13:16:17 to 13:18:13 (from the point the airplane was descending through 7,400 ft. MSL to the end of the data). This period covers N605TR's circling maneuver from the end of the KTRK RNAV (GPS) RWY 20 approach (see the approach plate in Figure 4) to impact with the ground (see Figures 5 and 6). The "target" positions for the accelerometer integration are defined by the ADS-B latitude and longitude coordinates¹² converted to north and east coordinates, and the blue "Corrected barometric altitude" line shown in Figures 9 and 10.

The beginning and end times, constants of integration, and accelerometer biases for the accelerometer integration are shown in Table 5. The constants of integration are expressed as increments, or biases, on the initial ground speed, track, and rate of climb that would be computed using the "target" trajectory.

Start time (PDT)	End time (PDT)	Speed bias, knots	Track bias, degrees	Rate of climb bias, ft/min	n_x bias, G's	n_y bias, G's	nlf bias, G's
13:16:16.66	13:18:13.28	-1.63	0.49	350	-0.001846	0.037125	0.034773

Table 5. Constants of integration and accelerometer biases for the accelerometer integration.

The n_y and nlf biases shown in Table 5 are relatively large, but are confirmed by the values of n_y and nlf recorded by the FDR while the airplane was at rest on approximately level ground (at very small pitch and roll angles). The NTSB asked Bombardier whether the magnitude of these biases are unusual, and Bombardier replied¹³ that

On the CH605 the accelerations recorded in the FDR are from a tri-axial dedicated accelerometer in the landing gear bay. Offsets are expected, this arrangement is not as precise as IRS accelerations recorded on newer aircraft ...

The offsets on [airplane serial number] 5715 appear to be larger than we see on other aircraft of the same type, but it would be hard to say why or even if this is "abnormal". As this is a dedicated accelerometer for the FDR and not otherwise used, there's no monitoring of the output and such deviations would not be identified in service.

Accelerometer integration results

The airplane position and altitude resulting from the integrated trajectory are shown in Figures 5, 6, 9, and 10 as the red lines with the "Accelerometer integration" label. The ground speed and rate of climb resulting from the integrated trajectory are plotted as red lines in Figure 12.

The corrected load factors are compared to the load factors recorded by the FDR in Figure 14. Figures 5 and 6 indicate that the path over the ground resulting from the accelerometer

¹² ADS-B latitude and longitude are used in these calculations instead of the FDR latitude and longitude because the ADS-B data are recorded at a higher resolution than the FDR data.

¹³ In an email dated 10/22/2021.

integration is in generally good agreement with both the ADS-B position data, and is therefore a satisfactory solution.

Flight path angle (γ) calculation

The flight path angle is defined by

$$\gamma = \sin^{-1} \left(\frac{\dot{h}}{V} \right) \quad [4]$$

where γ is the flight path angle, \dot{h} is the rate of climb, and V is speed. Using true airspeed gives γ relative to the airmass, and using ground speed gives γ relative to the Earth. If \dot{h} and V from the pressure-based altitude¹⁴ and true airspeed calculations described above are used in Equation [4], the resulting γ is very noisy (i.e., it contains unrealistic “spikes” and oscillations). A better (smoother) calculation of γ results from using \dot{h} and V from integrated accelerometer data. The γ relative to the Earth using \dot{h} and ground speed from the accelerometer integration is shown as the blue line in the top plot of Figure 13. Because the winds in this case are relatively light, the true airspeed and ground speed are within about 5 knots of each other throughout the circling maneuver, and consequently the γ relative to the airmass (computed using the true airspeed based on the integrated ground speed and smoothed winds) is very close to the γ relative to the Earth. The \dot{h} used in these calculations is shown as the red line in the bottom plot of Figure 12.

Wind calculations

Airspeed, ground speed, and wind are related as follows:

$$\vec{V}_W = \vec{V}_G - \vec{V} \quad [5]$$

where \vec{V} is the airspeed vector, \vec{V}_G is the ground speed vector and \vec{V}_W is the wind vector. The components of \vec{V}_G in body axes result from the integration of the accelerometer data described above. The components of the airspeed \vec{V} in body axes, as indicated by Figure 17, are related to the angle of attack α and sideslip angle β as follows:

$$u = V \cos(\beta) \cos(\alpha) \quad [6a]$$

$$v = V \sin(\beta) \quad [6b]$$

$$w = V \cos(\beta) \sin(\alpha) \quad [6c]$$

As a first approximation, $\beta \cong 0$ and, for shallow roll angles, $\alpha \cong \theta - \gamma$, where θ is the pitch angle recorded on the FDR. Once the components of \vec{V}_W in the airplane body axes are computed using Equations [6a-c], they can be transformed into Earth axes using the known θ , roll (ϕ), and true heading (ψ). The results of the wind calculations are shown in Figure 15.

¹⁴ This is the altitude labeled “Corrected barometric altitude” in Figures 9 and 10.

The computed winds are plotted as a function of altitude in Figure 16. The thick blue lines through the data are approximations to the computed wind speed and direction, and can be used in Equation [5] along with the integrated ground speed and rate of climb to compute a smooth, “inertial” true airspeed. The components of this inertial airspeed along each of the airplane’s axes can then be used to compute smooth “inertial” α and β values, as described below. The total “inertial” airspeed computed as described here is plotted as the dashed green line in Figure 12b.

Inertial angle of attack (α) and sideslip angle (β) calculations

As illustrated in Figure 17, the angle of attack (α) is the angle the projection of the airspeed vector onto the airplane’s plane of symmetry makes with the airplane’s x-axis. The sideslip angle (β) is the angle that the airspeed vector makes with the airplane’s plane of symmetry. These angles can be calculated from the components of airspeed along each of the airplane’s axes (given by Equations [6a-c]):

$$\alpha = \tan^{-1} \left(\frac{w}{u} \right) \quad [7]$$

$$\beta = \sin^{-1} \left(\frac{v}{V} \right) \quad [8]$$

The “inertial” α and β computed using Equations [7] and [8] are plotted as the magenta lines in the top and middle plots of Figure 13, respectively. The inertial α is also compared to the α computed from the angle of attack vane data recorded on the FDR in the top plots of Figures 13 and 21 (Figure 21 will be discussed further in Section D-VI). In these plots, α is labeled as α_F (α of the fuselage) in order to distinguish it from α_V (α measured by the airplane’s angle of attack vanes). The relationship between α_V and α_F , and the performance of the SPS, is discussed in Section D-VI.

VI. Additional aircraft performance considerations

Introduction

The nature of the airplane’s loss of control at approximately 13:18:11 – an apparent asymmetrical stall following the activation of the stick shaker and stick pusher – merits further consideration of the flight condition at which the stall occurred, and the performance of the Stall Protection System (SPS) preceding the stall. Furthermore, the effect of the deployment of the spoilers at 13:18:01 on the airplane’s lift curve and consequent load factor capability is of interest, as is a comparison of the overall performance of the airplane (as recorded by the FDR data) with its expected performance (as defined by Bombardier’s engineering simulation model of the CL-605). These items are addressed in this Section of the *Study*.

The CL-605 Stall Protection System (SPS)

The CL-605 SPS is described in an internal Bombardier memorandum dated January 2008, provided to the NTSB in Reference 7. The subject of the memorandum is the “CL-604 Stall Protection System (SPS),”¹⁵ and its introduction states:

The CL-604 Stall Protection System (SPS) comprises a dual channel analogue Stall Protection Computer (SPC), two AOA [α] vanes ... mounted on the left and right forward fuselage sides, two dedicated lateral accelerometers (for sideslip compensation), a shaker motor on each control column and a pusher motor connected to the right side elevator control system There is an SPS disconnect button on each control column.

Implemented within the SPC are algorithms, which define the AOA firing angles for the “auto-ignition,” “stick shaker” and “stick pusher.” The CL-604 SPC algorithms are functions of altitude and flap angle. The shaker, pusher, and associated aural and visual warnings are disabled with a valid weight on wheels (WOW) signal.

The SPS pusher firing angles were set to lower AOA than the AOA for natural aerodynamic stall and as such the SPS can be described as a “pre-stall” pusher system.

The section of the memorandum titled “VS1G – Reduced Operating Reference Speed Certification,” provides additional details about the design of the CL-605 SPS:

The CL-604 was certified, through a finding of equivalent safety, to use reduced operating reference speed factors based on V_{S1G} . Transport Canada Issue Paper F-1, which describes an acceptable means for certification of reduced operating reference speed factors, contains additional requirements for airplanes that incorporate a stick pusher to define the stall. Based on the requirements of Issue Paper F-1 the CL-604 SPS was designed to operate and perform its intended function under normally expected operating conditions, which include:

- a) Allowable leading edge damage
- b) Wing leading edge contamination from dirt and insects
- c) Wing contamination from ice accumulation
- d) Wing contamination from application of anti-icing/de-icing fluids.

The design case that defined the SPS pusher firing angles was with the wing leading edge contaminated with insects. The SPS pusher firing angles were set to provide an adequate margin between the pusher and the natural stall, i.e. the pusher was set to activate at an AOA lower than the natural stall with the wing leading edge contaminated with insects.

The CL-604 natural stall characteristics that drive the need for the stick pusher are described in Appendix B.

Subsequent sections of the memorandum provide details about the implementation of the SPS, and how the SPS firing angles are calculated. In this *Study*, the recorded FDR data are used to compute the expected stick shaker and stick pusher activation times per the criteria defined in the January 2008 Bombardier memorandum, and the results compared with the actual shaker and pusher activation times recorded on the FDR. The results indicate that, considering uncertainties associated with the limited sample rate of the FDR

¹⁵ The memorandum refers to the “CL-604” SPS; the CL-605 SPS is identical.

data, the recorded activation times of the shaker and pusher are consistent with the criteria defined in the memorandum. The details of these calculations will now be presented.

Figure 18 diagrams the SPC shaker and pusher activation logic. The nominal shaker and pusher firing angles are programmed into the SPC as a function of altitude and flap setting, and are then adjusted to account for the rate of change of angle of attack. The SPS works with the α measured by the AOA vanes (α_V). The α of the fuselage (α_F) is related to α_V as follows:

$$\alpha_F = (a)\alpha_V + b \quad [9]$$

Where a and b vary with flap setting.¹⁶ As described in the SPS memorandum,

The raw or measured vane signal is filtered to avoid nuisance shaker or pusher activation due to air turbulence. The measured stall vane angle is filtered by a low pass filter This filtered AOA is output to the FDR and is the input to the sideslip compensation calculation.

The filtered α_V data recorded on the FDR are plotted in Figure 21. Note that the left α_V is consistently higher than the right α_V . Bombardier commented on this difference in an email to the NTSB dated 8/20/2021, stating:

We observe a difference (a “split”) between the recorded LH and RH AoA vane data of approximately 0.5 to 0.75 degrees in the cruise portion of the accident flight. While some difference is expected, a value of 0.25 would be more typical and 0.5 might be the “normally expected maximum.” There appears to be an increased AoA split towards the end of the flight, perhaps reaching of the order of 1.5 degrees (observed from a cross-plot of AoA data towards the end of the flight). But it should be noted that comparing the split during the approach segments of the flight is made more difficult by the apparent turbulence (seen as the increased noise on the Ny and Nz traces, which is consistent with lower altitude flight) and the aircraft maneuvering, both of which create a more dynamic vane AoA signal; in addition, with the LH and RH vane data recorded asynchronously, making a direct comparison when the vanes are moving more rapidly is harder. Similar AoA split behavior and trends do seem to be present during the flight immediately prior as well.

...

Our assessment is that, despite any splits in AoA, from whatever cause (simple AoA to AoA variability can cause splits), the pusher did fire well before any natural stall in the first stall warning event, and the system did recover the aircraft, indicating that any effect of a split in delaying pusher response was not large or significant to the extent of affecting recovery capability, and that for the second stall warning event, the apparent resistance to the pusher by the crew occurred prior to the natural stall, again suggesting that the pusher did function as intended before the natural stall. However, an AoA split would reduce the margin between pusher activation and natural stall, even if this reduction were not in the end deemed critical.

To further assess the split between the left and right α_V readings, for this *Study* the “inertial” α_F computed as described above and plotted as the magenta line in Figure 13 is transformed into an inertial α_V using Equation [9], and plotted as the black line in the top plot of Figure 21. Note that in the period before the initial activation of the stick pusher, the inertial α_V is closer to the right α_V than to the left α_V , suggesting that the left α_V is reading

¹⁶ The values of a and b are Bombardier proprietary information.

erroneously high (for whatever reason), rather than that the right α_V is reading erroneously low. In any case, this result and the additional evaluation of the SPS performance discussed below are consistent with Bombardier's conclusion that "the pusher did fire well before any natural stall in the first stall warning event, and the system did recover the aircraft, indicating that any effect of a split in delaying pusher response was not large or significant."

In the CL-605 SPC, the filtered α_V parameters are adjusted to account for the effect of sideslip angle on the measurement of α at the vanes. Per the SPS memorandum,

The SPC compensates the measured AOA for the cross-flow induced effects on the windward and leeward AOA vanes in sideslip. The cross-flow of air on the forward fuselage due to sideslip causes the left and right stall-vanes to deflect differently. Sideslip (β) compensation in the SPC is based on the measured lateral acceleration (N_y - lateral acceleration is provided by a dedicated accelerometer as a programmed substitute for sideslip), for all flap positions, to minimize the split between the two stall vanes. The stall vane correction has been "capped" for lateral accelerations beyond the normally expected operational range.

The filtered α_V signals compensated for β , using the corrected n_y plotted in Figure 14, are plotted in top plot of Figure 21 as the thick red (left α_V) and green (right α_V) lines. When the left or right α_V depicted by these lines increases above the shaker and pusher α_V firing thresholds, the logic for activating these stall protection systems (on that side) is satisfied.

However, the shaker and pusher firing thresholds are not necessarily the nominal thresholds defined by altitude and flap position. As noted above, the actual thresholds are the nominal thresholds adjusted to account for the rate of change of angle of attack; this adjustment is called the "SPS phase advance" in the SPS memorandum:

To protect the aircraft from inertial overshoots during accelerated stall entries at low speed the SPC incorporates an AOA phase advance function This function reduces the shaker and pusher AOA firing angles in proportion to the rate of increase of AOA, up to a pre-set maximum (cap). ...

The SPS memorandum defines the magnitude of the phase advance term ($\Delta\alpha_V$) that reduces the shaker and pusher firing angles as a function of $\dot{\alpha}_V$, the rate of change of α_V . However, $\dot{\alpha}_V$ is capped (limited); this limit "prevents nuisance shaker/pusher activation by eliminating large phase advance that would be generated by rapid stall vane excursions due to turbulence."

The SPS $\dot{\alpha}_V$ term is computed using a transfer function, and is not simply the time derivative of α_V ; it acts more like a lag filter on this derivative. This can be seen in the second plot in Figure 21, which compares the time derivative of the inertial α_V described above with the $\dot{\alpha}_V$ obtained by applying the SPS $\dot{\alpha}_V$ transfer function ("rate filter") to the inertial α_V . The $\dot{\alpha}_V$ obtained by applying the rate filter to the left and right α_V signals (corrected for n_y) are also shown in the second plot of Figure 21.

The third plot in Figure 21 shows the left and right $\Delta\alpha_V$ resulting from the left and right $\dot{\alpha}_V$. Note that because the $\dot{\alpha}_V$ terms are capped, the $\Delta\alpha_V$ terms are also capped (at about 2.1°). The final left and right α_V shaker and pusher firing angles (or thresholds), obtained by

subtracting $\Delta\alpha_V$ from the nominal firing angles, are plotted in the top plot of Figure 21. When the left and right corrected α_V values exceed these thresholds, the corresponding shaker or pusher is activated. The times at which the left and right shaker and pusher thresholds are exceeded and the corresponding devices are activated are shown in the fourth and fifth plots in Figure 21, and compared with the left and right shaker and pusher discrete parameters recorded on the FDR.

The computed firing times are consistent with the FDR discretized (that is, they show the devices activating in between the samples defining the corresponding discrete parameter change of state), except for the first right shaker activation. The calculated first right shaker activation occurs about 0.7 seconds before the last “inactive” sample of the FDR right shaker discrete (though it coincides nicely with the sound of the stick shaker recorded on the CVR). This discrepancy might be the result of a slightly high $\Delta\alpha_V$ applied to the right shaker firing angle, stemming from a high right α_V that is computed based on a cubic fit to the right α_V data (which are sampled at 1 Hz). In other words, the relatively low sample rate of the α_V data introduces uncertainties in the calculation of the α_V and $\Delta\alpha_V$ terms that might make the computed right shaker activate at a slightly earlier time than would have been computed with higher fidelity data. In the larger picture, the computed shaker and pusher activation times showed good agreement with the recorded changes of state in the FDR shaker and pusher discrete parameters, indicating that on the accident flight, the performance of the SPS was consistent with the specifications in the SPS memorandum.

While the left and right *shakers* will be deactivated as soon as the corresponding α_V decreases below its activation threshold, the deactivation of the *pushers* is not so simple. As stated in the SPS memorandum,

Cancellation of the stick pusher occurs at a lower AOA than the tabulated stick pusher firing angle (hysteresis) to ensure that the push is of sufficient duration. However, to minimize negative “g,” in for example recovery from high speed or high altitude pusher stall recovery, there is a phase advance term applied to the basic stick pusher cancellation hysteresis term. The phase advance reduces the basic cancellation hysteresis term as a function of the AOA rate on recovery

The SPS memorandum defines the magnitude of the pusher hysteresis term as a function of α_V and altitude. The computed deactivation times of the pusher plotted in the fifth (bottom) plot of Figure 21 account for this hysteresis term.

The thick gray lines in the fourth and fifth plots of Figure 21 depict the effect of the “combined” left and right shaker and pusher activations. As described in the SPS memorandum section titled “SPS Activation,”

Consider that the aircraft is slowing down and the AOA is increasing towards the stall:

If the signal from one of the AOA vanes exceeds the programmed “auto-ignition” firing angle, it will cause the activation of both engine auto-ignition systems. At a higher AOA, and if the signal from one of the AOA vanes exceeds the programmed “shaker” firing angle, it will cause the activation of the stick shaker motor on that side, and if the autopilot is selected it will be automatically dis-engaged at this time. Both the pilot and co-pilot’s sticks will shake because they are mechanically connected. The stick shaker provides a tactile and audible response.

If both AOA vanes exceed the “shaker” firing angle, both stick shaker motors will be activated.

At even higher AOA, and if the signal from one of the AOA vanes exceeds the programmed “pusher” firing angle, it will trigger the “stall” aural warning and the flashing red “STALL” warning lights.

If both vane AOA's exceed the “pusher” firing angle the stick pusher motor will be activated. The stick pusher motor will apply an approximately 80 lbs forward force to the control columns. The motor will cease to be active, and the 80 lbs push force removed, once the AOA of the aircraft reduces below a preset value below the pusher threshold.

In Figure 21, the thick gray line in the fourth plot shows the activation of *either* the left or right shaker signals, which (because the columns are connected) will shake both the left and right control columns. The thick gray line in the fifth plot shows the activation of *both* the left and right pusher signals, since both signals must be active for the pusher motor to activate.

The effect of spoiler deployment on normal load factor capability

The natural stall of N605TR can be identified at 13:18:11, when the normal load factor (*nlf*) drops suddenly from 1.62 G's to 1.29 G's over 1/8 of a second (see Figure 14b). At the same time, the roll rate increased dramatically to the left, and the airplane rolled from -27° to -147° in 2.3 seconds, consistent with the left wing stalling before the right wing. The airspeed at 13:18:11 was about 127 KCAS. However, at about 13:18:06, before this stall and loss of control, the left α_v was high enough to activate the left stick shaker. At this time, the airspeed was 130 kt., the roll angle (ϕ) was -36°, and the *nlf* was 1.23 G's. It is of interest to determine if stick shaker activation would normally be expected in this flight condition. As will be shown below, shaker activation would *not* normally be expected in these circumstances, but the deployment of the flight spoilers at 13:18:01 (see Figure 19), as the airplane was crossing the extended KTRK runway 11 centerline, reduced the lift (and therefore *nlf*) capability of the airplane, contributing to the shaker activation at 13:18:06.

The CL-605 Flight Crew Operating Manual (FCOM) (Reference 9), Volume 1, Chapter 4: “Normal Procedures,” “Approach and Landing,” Section F: “Circling Approach,” outlines the circling approach procedure as follows:

Circling Approach

When performing a circling approach, maintain the airplane configuration from the final approach fix (FAF) onwards (flaps 30° and landing gear down). At the circling MDA with the field in sight, maneuver to establish a downwind leg parallel to the runway at a distance of approximately 1 1/2 miles.

At the established downwind:

- (1) Circling MDA Maintain
- (2) Flaps..... 30 degrees
- (3) Airspeed Flaps 30° speed
+ 10 KIAS

When abeam the runway threshold:

(4) Chronometer Start Time for 15 to 30 seconds,
plus or minus wind correction.

After the desired timing has elapsed, start the turn towards the base leg:

(5) Descent Initiate

Approaching 400 feet, start turn towards final, and when landing is assured:

(6) Flaps 45 degrees

(7) Airspeed $V_{REF} + WIND$ Wind correction is half steady
state crosswind plus all gust
(regardless of direction).
Maximum correction is
+ 20 KIAS.

The FCOM circling approach procedure calls for maintaining 30° of flaps from the final approach fix until 400 feet above the runway, and turning from base to final. Flaps 45° is selected once the turn to final is initiated. Further, while the flaps are at 30°, the airspeed should be maintained at the “Flaps 30° speed + 10 knots,” and then decreased to the “ $V_{REF} + WIND$ ” speed once Flaps 45° are selected.

Of note, the “Flaps 30 speed” is not defined in the FCOM (see further discussion below). In addition, on the accident flight the flaps were set to 45° at 13:16:29, while the airplane was descending through 7,200 ft. MSL (1,300 ft. above runway 11) at the start of the circling maneuver from the runway 20 approach towards runway 11; that is, well before the turn from base to final, as specified in the FCOM procedure. However, as noted by Bombardier (see below), performing the circling maneuver at Flaps 45° is not prohibited and is in fact a common practice.

The FCOM procedure calls for a downwind leg “parallel to the runway.” For KTRK runway 11 (bearing 120° true), this would mean a heading on downwind of 300° true. As shown in Figures 6 and 13, N605TR’s true heading during its “downwind” leg peaked at 266° at 13:17:20, 34° to the left of runway 11’s reciprocal heading. The “base” leg was similarly not “square” to the runway, and the airplane crossed the runway 11 extended centerline at about 13:18:01, 0.84 nm from the threshold, and heading 169° true, 49° to the right of the runway heading. As the airplane crossed the extended centerline, it was about 200 ft. above a 3° glidepath towards a touchdown point 1,000 ft. past the runway threshold (see Figure 9), and the spoilers were deployed to 40° (see Figure 19).¹⁷ Following the FCOM procedure, and assuming an airspeed of 130 kt., a downwind-to-base turn initiated 15 to 30 seconds past the runway threshold would put the airplane on final, aligned with the runway, about 0.5 to 1 nm from the threshold.

The NTSB asked Bombardier about the definition of the “Flaps 30 speed.” In response, Bombardier stated that:

¹⁷ KTRK runway 11 does not have an instrument landing system (ILS) or any visual glidepath indicators, such as a Precision Approach Path Indicator (PAPI) or Visual Approach Slope Indicator (VASI).

The procedures shown in the Normal Procedures chapter of the Flight Crew Operating Manual (FCOM) are intended to be detailed procedures for conducting a normal flight with all airplane systems operational. However, it is recognized that a given operator may choose to deviate from the manufacturer's normal procedures in order to take into account circumstances specific to their operation. This is acceptable provided that the airplane is operated at all times within the approved flight envelope. Thus a given crew may choose to conduct a circling approach in a flaps 45 configuration rather than as described in the circling procedure in the FCOM, if circumstances dictate it. Some of the normal procedures in the FCOM refer to "flaps 30 speed." This is an artifact of older Challenger models (600/601) in which both flaps 20 and flaps 30 were approved approach climb configurations, and thus approach climb speeds were defined in the AFM for both. Beginning with the Challenger 604, flaps 30 was removed as an approved approach climb configuration, and approach climb speed data for flaps 30 were removed; however, the reference to flaps 30 remained in the normal procedures in the FCOM. In the absence of the approach climb speed data for flaps 30 in the AFM, the only remaining guidance for a flaps 30 approach speed is the speed additive defined in the FLAPS FAIL procedure; this value is consistent with what is taught in training for the approaches that call out the flaps 30 speed reference. Bombardier will review the FCOM normal procedures which refer to flaps 30 speed and adjust them as required to be more consistent with the AFM.¹⁸

The CL-605 Quick Reference Handbook (QRH) (Reference 8) indicates that at the estimated accident weight of 31,294 lb., the flaps 45° landing reference speed (V_{REF}) is 124 knots. The wind reports received by the accident crew included the 12:51 PDT ATOS report of wind from 080° at 5 knots, and a 13:16:30 report from the KTRK tower of "wind calm." Hence, the WIND additive of "half the steady state crosswind" specified in the FCOM circling procedure would have been about 1.3 kt. for runway 11, if the 080° at 5 kt. were used, or 0 kt. if "calm" winds were used. Consequently, in this case the final flaps 45° airspeed specified by the FCOM circling approach procedure would have been about 124 kt. If 10 kt. were added to this speed for maneuvering, the appropriate flaps 45° speed during the circling maneuver would have been about 134 kt. As shown in Figure 12, the calibrated airspeed during the last minute of the flight varied between 120 kt. and 137 kt., and was about 130 kt. ($V_{REF} + 6$ kt.) at 13:18:05.8, the time the sound of the stick shaker was recorded on the CVR. As noted, the nlf at this time was 1.23 G's. It seems surprising that this relatively modest nlf would trigger the stick shaker at $V_{REF} + 6$ kt. However, the activation of the stick shaker at this time can be understood by considering the effect of spoiler deployment on the airplane's lift curve (the lift coefficient (C_L) as a function of α).

The lift coefficient is defined as

$$C_L \equiv \frac{L}{(1/2)\rho V^2 S} \quad [10]$$

Where:

L = Lift force
 ρ = Air density
 V = True airspeed
 S = Wing area

The load factor nlf is the ratio of the lift force to the airplane's weight; consequently,

¹⁸ Email from the Bombardier party coordinator to the NTSB performance specialist, dated 2/10/2022.

$$nlf = \frac{L}{W} = \frac{(C_L)\rho V^2 S}{2W} \quad [11]$$

The C_L in a given airplane configuration (flap setting) is primarily a function of α , as shown by the lift curve sketched in Figure 22a. During the approximately linear portion of the lift curve prior to the stall,

$$C_L \cong \left(\frac{\partial C_L}{\partial \alpha} \right) (\alpha - \alpha_0) \quad [12]$$

The maximum C_L , achieved just prior to stall, is depicted in Figure 22a as C_{Lmax} and occurs at the stall angle of attack (α_{max}). On the CL-605, the stick pusher activates before the natural stall at α_{max} , at α_{push} ; and the “stall” on this airplane is defined as the pusher activation. The stick shaker warns of approaching stall at α_{ss} , and the C_L at the shaker activation is C_{LSS} . Normal operations take place below α_{ss} and C_{LSS} ; the α_{op} and C_{Lop} in Figure 22a illustrate one possible operating point.

Figure 22b shows the effect of deploying the spoilers on the lift curve. The entire curve shifts downwards, much like extending flaps makes the lift curve shift upwards. Note that the angles of attack that characterize the stall and stall protection system – α_{ss} , α_{push} , and α_{max} – remain the same, but the corresponding lift coefficients have decreased by ΔC_{Lsp} . Defining C'_L as the C_L with spoilers deployed, we can write

$$C'_L \cong \left(\frac{\partial C_L}{\partial \alpha} \right) (\alpha - \alpha_0) - \Delta C_{Lsp} \quad [13]$$

Note that if the spoilers are deployed while at the operating point depicted in Figure 22a, the lift coefficient will drop by ΔC_{Lsp} , and to recover the lift (make $C'_{Lop} = C_{Lop}$), α will have to increase by

$$\Delta \alpha = \frac{\Delta C_{Lsp}}{(\partial C_L / \partial \alpha)} \quad [14]$$

Which will bring α that much closer to α_{ss} . Furthermore, the C_L at stick shaker activation with the spoilers deployed, C'_{LSS} , will be

$$C'_{LSS} = C_{LSS} - \Delta C_{Lsp} \quad [15]$$

Similarly, at pusher activation with the spoilers deployed,

$$C'_{Lpush} = C_{Lpush} - \Delta C_{Lsp} \quad [16]$$

The load factors at shaker and pusher activation will consequently also be reduced. With the spoilers stowed, the load factors at shaker and pusher activation are:

$$nlf_{ss} = \frac{L_{ss}}{W} = \frac{(C_{Lss})\rho V^2 S}{2W} \quad [17]$$

$$nlf_{push} = \frac{L_{push}}{W} = \frac{(C_{Lpush})\rho V^2 S}{2W} \quad [18]$$

With the spoilers deployed, the load factors at shaker and pusher activation are:

$$nlf'_{ss} = \frac{L'_{ss}}{W} = \frac{(C_{Lss} - \Delta C_{Lsp})\rho V^2 S}{2W} \quad [19]$$

$$nlf'_{push} = \frac{L'_{push}}{W} = \frac{(C_{Lpush} - \Delta C_{Lsp})\rho V^2 S}{2W} \quad [20]$$

nlf_{ss} , nlf_{push} , nlf'_{ss} , and nlf'_{push} at flaps 45, 6,300 ft. MSL, and a gross weight of 31,294 lb. are plotted as a function of calibrated airspeed in Figure 23. The combination of nlf and calibrated airspeed during N605TR's circling maneuver is also plotted in Figure 23 as the multi-colored line; the time corresponding to each point on the line is depicted by the color scale. Flight events, such as the spoiler deployment and shaker and pusher activation times, are also noted at corresponding points on the line. Note in Figure 23 that at 130 KCAS, spoiler deployment results in about a 0.31 G reduction in nlf at shaker and pusher activation. On the accident flight, the stick shaker activated at 130 KCAS and an nlf of 1.23 G, exactly at the spoilers-deployed shaker boundary shown in Figure 23. If the spoilers had been stowed, at 130 KCAS the stick shaker would not have activated until an nlf of 1.54 G's. Since rolling the airplane into a turn requires increasing the nlf to maintain lift (see Figure 24), the deployment of the spoilers during the circling maneuver resulted in a reduction in maneuvering capability. Notably, the FCOM contains this statement concerning the use of the flight spoilers:

Flight below an altitude of 300 feet AGL with flight spoilers extended is prohibited.

To ensure adequate maneuver margins, flight spoilers must not be extended in flight at airspeeds below the recommended approach speed plus 10 KIAS

Figure 24 depicts the maximum level-turn bank angle that could be achieved over a range of airspeeds at the stick shaker and pusher boundaries, with the spoilers stowed and deployed, under the accident conditions. Note that at 130 KCAS, the level-turn bank angle at the shaker boundary is about 49° with the spoilers stowed, but decreases to about 35° with the spoilers deployed.

During the circling maneuver, the spoilers were extended at 13:18:01, at a radio altitude of about 650 ft. and an indicated altitude of 6,400 ft., about 500 ft. above the runway elevation (see Figure 9). The radio altitude decreased to 300 ft. at about 13:18:09, after the stick shaker had already activated. The calibrated airspeed at 13:18:01 was about 137 kt. (above the $V_{REF} + 10$ of 134 kt.), but slowed to 130 kt. at shaker activation. However, using a V_{REF} of 118 kt. (the reference speed called out by the First Officer on the CVR, which was likely based on an erroneously light basic weight programmed into the FMS), $V_{REF} + 10$ would have been 128 kt. The airspeed remained above this speed from the deployment of the spoilers to the activation of the stick shaker. At a gross weight of 28,300 lb. (about 3,000 lb. lighter than the estimated actual weight), at 130 kt. and with the spoilers deployed, the stick shaker would have activated at an nlf of about 1.35 G's, corresponding to a level turn at a 42° roll angle.

Flight control inputs following stick shaker and pusher activation

Figure 19 shows the flight control positions recorded on the FDR. As shown in Figure 21, the first activation of the stick pusher occurred at about 13:18:06.6, within about a second of the first activation of the stick shaker. Immediately after the activation of the pusher, the elevators moved about 16° over 1.3 seconds in the trailing-edge-down (TED) direction, reaching 10° TED at 13:18:07.9. This movement was likely the result of the 80 lb. forward force exerted on the control column by the pusher. The airplane θ , α , and nlf all decreased in response to this elevator movement (see Figures 13 & 14), and the shaker and pusher both deactivated temporarily. However, between 13:18:07.9 and 13:18:09.2 (1.3 seconds), the elevators moved from 10° TED to about 18° trailing-edge-up (TEU) (a change of 28° TEU). This movement was most likely the result of a reaction by the Pilot Flying (PF) against the forward column movement caused by the pusher. As result of this TEU elevator movement, the θ , α , and nlf all increased again. The stick shaker and pusher re-activated at about 13:18:10.0 and 13:18:10.3, respectively. However, this time the final TED elevator position in response to the pusher force was not as large as on the first occasion; the elevators moved from about 18° TEU to between about 1.3° TEU and 0.5° TEU between about 13:18:09.4 and 13:18:11.0 (over about 1.6 seconds). While the change in elevator position was about 1° greater than that following the first pusher activation, the resulting TED elevator position was not as large (about 0.5° TEU vs. 10° TED), possibly because the PF was resisting the pusher. The large TEU elevator movement that started at 13:18:07.9 caused a nose-up pitch rate that propelled α above the natural stall at about 13:18:11.0, as evidenced by the sharp drop in nlf and the large roll rate to the left that started at about that time. At 13:18:11.0, the elevators had only just reached the approximately neutral position following the second activation of the pusher.

The CL-605 natural stall characteristics that drive the need for the stick pusher are described in Appendix B, along with Bombardier's own analysis of the final seconds of the flight.

Figure 20 plots the engine N1 speeds recorded on the FDR, along with estimated, "scaled" throttle lever angles¹⁹ (TLA) that Bombardier computed could produce the N1 values recorded on the FDR (throttle position was not recorded). Note that the throttles were advanced substantially shortly after the first stick shaker activation; this, together with the adjustment of the speed bug to 138 kt. about this time (see Figure 12), suggests that at least one of the pilots might have intended to abandon the approach and execute a go-around. However, it is difficult to determine which pilot took these actions. The CVR indicates that during the approach, the Captain was the PF and the FO was the Pilot Monitoring (PM); however, at 13:17:48, the CVR records the FO requesting control of the airplane from the Captain. Hence, in the final moments it is unclear which pilot was manipulating the controls, or whether both pilots were attempting to control the airplane independently.

¹⁹ Per Bombardier, the estimated TLAs are not the actual positions of the TLAs, but are "scaled to the peak go-around N1 for [the] conditions." The estimated TLAs indicate the approximate time that the throttles were advanced following the first stick shaker activation.

Simulation model comparison of circling maneuver performed by Bombardier

Bombardier performed a simulation model comparison of the last two minutes of the flight using their CL-605 engineering simulator. The memorandum transmitting the simulation results to the NTSB (Reference 10) describes the simulation model comparison as follows:

The Bombardier Challenger 600 Series Six Degree of Freedom Simulation Model is used as a supporting tool in Bombardier's responses provided herein. The aerodynamic model is a high-fidelity flight test validated model that has demonstrated representative flight characteristics across the full flight envelope.

Flight Control and Engine Inputs

The simulation model is a surface driven model, where the control surface positions (elevators, stabilizer, rudder, ailerons, spoilers, landing gear, flaps) are direct inputs to the model. There is no detailed Systems model available, where column/wheel/pedal/TLA can be driven or derived. Engine thrust is calculated through an N1-thrust engine flight test validated model. The simulation model is driven with N1 flight test time histories, and the engine part of the simulation model provides the thrust output.

The inputs to the simulation model were derived from FDR data. The FDR control surface sampling rates vary between 1 and 4 Hz. These sampling frequency ranges are considered low for model matching purposes. As a result, "math pilots" are used to control pitch, roll and yaw. Math pilots are PID controllers that allow the simulation to track the aircraft attitudes closely. Control surface offsets are applied to the primary control surfaces in order to reduce or zero-out the error in the variable being tracked. For example, a PID controller in the pitch axis will calculate elevator offsets that are applied to the FDR elevator time history in order to closely match the simulator pitch angle to the FDR pitch angle. The error that the PID controller is trying to zero-out is $\theta_{\text{error}} = \theta_{\text{FDR}} - \theta_{\text{SIM}}$. In the roll and yaw axes, the same process is followed with aileron and rudder to match roll and heading angles respectively. Generally, when working with FDR data, the use of math pilot PID controllers is necessary to balance out errors caused by lower data fidelity and varying sampling frequencies from one parameter to another. Note that the raw FDR data was linearly interpolated between samples in order to obtain continuous signal time histories with reduced time step responses. ...

Simulation Initial Conditions

The simulation analysis consists of the last two minutes of the flight. ... All initial conditions were determined from FDR data, except for the mass properties. The weight, CG and inertias were estimated based on [the December 2007 Weight and Balance report], as well as the FDR recorded fuel on-board and stabilizer to trim in the approach condition. ... the estimated 4-passenger weight configuration at $t_{\text{sim}} = 0\text{s}$ is displayed in [Table 2]. ...

Note that the fuel weight distribution between tanks was estimated. The simulation model was iteratively trimmed in the approach condition at varying CGs, and the model's resulting stabilizer angle was compared to the FDR value. The iterative approach was considered complete when the stabilizer angle difference between simulation and FDR stabilizer was less than 0.3 degrees. For reference, the stabilizer tolerances used in developing an aerodynamic model are +/- 0.5 degrees. The resulting CG (26.3% MAC) was then used to determine the fuel tank distribution for $t_{\text{sim}} = 0\text{s}$. There is no fuel burn, fuel migration or fuel slosh modelling within the simulation, thus the mass properties ... are kept constant for the full duration of the simulation replay. The simulation was initialized at the FDR derived airspeed, pressure altitude, terrain elevation and outside air temperature.

The results of the simulation are presented along with FDR and other computed parameters in the Figures throughout this *Study*. As shown in these Figures, the simulation agrees very well with the airplane position, speeds, and attitude recorded by or derived from the FDR data. Significantly, the simulation stick shaker and stick pusher times agree within a fraction of a second with the computed shaker and pusher activation times plotted in Figure 21.

The simulation north/east coordinates and ground speed differ slightly from those based on the FDR, as shown in Figures 5b, 6b, and 12b. This is consistent with the simulation assuming calm winds, but with computed actual winds from the southeast at about 10 knots (see Figures 15 and 16).

The generally excellent agreement between the engineering simulation and the computed performance based on FDR data indicates that the airplane was responding to throttle and flight control inputs as expected, and is further evidence that the Stall Protection System was performing as designed.

E. CONCLUSIONS

The material in this *Study* supports a number of observations and conclusions regarding the performance of N605TR during its circling approach to KTRK runway 11. Section C of this *Study* summarizes the motion of the airplane during the circling maneuver. As N605TR was circling to land on runway 11 after approaching KTRK on the RNAV runway 20 instrument approach, α exceeded the stall α . The left wing stalled, and the airplane abruptly rolled to the left past 140° and impacted the ground. This asymmetric stall and abrupt roll is consistent with the known natural stall characteristics of the CL-605, which is why the airplane is equipped with a stick pusher system (“pusher”) that activates before the natural stall occurs.

The FDR data indicates that prior to the natural stall, the stick shaker and stick pusher both activated twice. A comparison of the performance of the Stall Protection System (SPS) based on FDR data with the SPS design as described in documents provided by Bombardier indicates that the SPS performed as designed, and in fact the stick pusher arrested the increase in α and averted the natural stall during the first activation by moving the elevators to the 10° TED position. However, following this elevator TED movement, the elevators moved to about the 18° TEU position, most likely as the result of a reaction by the PF against the pusher force. This TEU elevator movement propelled the α above the natural stall, resulting in the abrupt roll, loss of control, and impact with the ground.

Bombardier performed a simulation model comparison of the last two minutes of the flight using their CL-605 engineering simulator. The generally excellent agreement between the engineering simulation and the computed performance based on FDR data indicates that the airplane was responding to throttle and flight control inputs as expected, and is further evidence that the SPS was performing as designed.

During the circling maneuver, N605TR did not achieve a “downwind” leg parallel to runway 11, and the “base” leg of the approach was not perpendicular to runway 11. This contributed to the airplane crossing the extended centerline of runway 11 only 0.85 nm from the threshold, while heading 49° to the right of the runway heading and above a 3° glide path to the runway. CVR evidence indicates that the crew were aware that they had overshot the centerline and were high, but intended to continue the landing by maneuvering back towards the centerline. As the airplane crossed the centerline, the flight spoilers were deployed to 40° and remained deployed until impact.

The deployment of the spoilers resulted in a noticeable reduction in maneuvering capability. The stick shaker activated at 130 KCAS and an *nlf* of 1.23 G, corresponding to a level turn bank angle of about 36°; if the spoilers had been stowed, at 130 KCAS the stick shaker would not have activated until an *nlf* of 1.54 G's, corresponding to a level turn bank angle of about 50°.

The V_{REF} speed annunciated by the First Officer on the CVR was 118 KCAS, which corresponds to a gross weight about 3,000 lb. lower than the estimated actual weight at the time of the accident. The erroneous V_{REF} was most likely the result of an incorrect empty weight programmed into the airplane's FMS; the correct V_{REF} corresponding to the estimated weight is 124 KCAS. However, because the airspeed at the time of the accident was about 130 KCAS, the deployment of the spoilers had a much more significant impact on the α margin to stall than the reduced V_{REF} speed resulting from the erroneous FMS weight.

The advancement of the throttles shortly after the first stick shaker activation, together with the adjustment of the speed bug to 138 kt. about this time, suggests that at least one of the pilots might have intended to abandon the approach and execute a go-around shortly before the stall and loss of control. However, it is difficult to determine which pilot took these actions. The CVR indicates that during the approach, the Captain was the PF and the FO was the PM; however, near the end of the flight, the CVR records the FO requesting control of the airplane from the Captain. It is unclear which pilot was manipulating the controls in the final moments of the flight, or whether both pilots were attempting to control the airplane independently.

John O'Callaghan
National Resource Specialist – Aircraft Performance
Office of Research and Engineering

F. REFERENCES

1. Bombardier Aerospace, *Challenger 605 Weight and Balance Manual*, document identification number CH 605 WBM, Revision 6, June 11, 2015.
2. National Transportation Safety Board, Office of Aviation Safety, *Preliminary Report: Bombardier INC CL-600-2B16, N605TR, Truckee, California, July 26, 2021, NTSB accident # WPR21FA286*. (Available through the NTSB CAROL search tool at <https://data.nts.gov/carol-main-public/landing-page>).
3. International Civil Aviation Organization (ICAO), *The Tenth Meeting of Automatic Dependent Surveillance – Broadcast (ADS-B) Study and Implementation Task Force (ADS-B SITF/10) Agenda Item 6: Review States' activities and interregional issues on trials and implementation of ADS-B and multilateration: ADS-B / GPS Accuracy (Presented by Australia)*. Singapore, 26-29 April 2011. Document available at https://www.icao.int/APAC/Meetings/2011_ADS_B_SITF10/IP10_AUS%20AL%206%20-%20GPS%20Accuracy.pdf.
4. National Transportation Safety Board, Office of Research and Engineering, *Flight Data Recorder Specialist's Factual Report, Bombardier INC CL-600-2B16, N605TR, Truckee, California, July 26, 2021, NTSB accident # WPR21FA286*. (Available through the NTSB CAROL search tool at <https://data.nts.gov/carol-main-public/landing-page>).
5. National Transportation Safety Board, Office of Research and Engineering, *Cockpit Voice Recorder Specialist's Factual Report, Bombardier INC CL-600-2B16, N605TR, Truckee, California, July 26, 2021, NTSB accident # WPR21FA286*. (Available through the NTSB CAROL search tool at <https://data.nts.gov/carol-main-public/landing-page>).
6. National Transportation Safety Board, Office of Research and Engineering, *Group Chairman's Aircraft Performance Study, American Airlines Flight 587, Airbus A300B4-605R, Belle Harbor, New York, November 12, 2001*, NTSB Accident Number DCA02MA001, Docket Item 188 (Washington, DC: NTSB, October 10, 2002). (Available through the NTSB CAROL search tool at <https://data.nts.gov/carol-main-public/landing-page>).
7. Bombardier Air Safety Investigation Office memorandum to the NTSB dated August 10, 2021: *Aerodynamic Data for Modeling - Challenger 605 N605TR (MSN 5715) - Impact with Terrain on Approach to Runway 11 at Truckee Tahoe Airport (KTRK) on July 26th, 2021* (Bombardier proprietary document.)
8. Bombardier Aerospace, *Challenger 605 Quick Reference Handbook (Imperial Version) Volume 1*, document identification number CH 605 QRH-I, Revision 59, June 02, 2021.
9. Bombardier Aerospace, *Challenger 605 Flight Crew Operating Manual Volume 1*, document identification number CH 605 FCOM, Revision 59, June 02, 2020.
10. Bombardier Air Safety Investigation Office memorandum to the NTSB dated February 18th, 2022: *Simulation Analysis - Challenger 605 N605TR (MSN 5715) - Impact with Terrain on Approach to Runway 11 at Truckee Tahoe Airport (KTRK) on July 26th, 2021*, Memorandum # ASIO-2022-ML-003 (Bombardier proprietary document).
11. National Transportation Safety Board, Office of Aviation Safety, *Systems Group Chairman Factual Report: Bombardier INC CL-600-2B16, N605TR, Truckee, California, July 26, 2021, NTSB accident # WPR21FA286*. (Available through the NTSB CAROL search tool at <https://data.nts.gov/carol-main-public/landing-page>).

G. GLOSSARY

Acronyms

ADS-B	Automatic Dependent Surveillance – Broadcast
AFM	Airplane Flight Manual
ASOS	Airport Surface Observation System
ATC	Air Traffic Control
ATIS	Automatic Terminal Information Service
CG	Center of Gravity
CVR	Cockpit Voice Recorder
FAA	Federal Aviation Administration
FCOM	Flight Crew Operating Manual
FDR	Flight Data Recorder
FMS	Flight Management System
FO	First Officer
GNSS	Global Navigation Satellite System
GPS	Global Positioning System
KTRK	Truckee-Tahoe Airport, Truckee, California
MAC	Mean Aerodynamic Chord
METAR	Meteorological Terminal Air Report
NTSB	National Transportation Safety Board
PDT	Pacific Daylight Time
PF	Pilot Flying
PM	Pilot Monitoring
QRG	Quick Reference Guide
SPC	Stall Protection Computer
SPS	Stall Protection System
SRN	Subframe Reference Number
SRTM	Shuttle Radar Topography Mission
TDZE	Touchdown Zone Elevation
TED	Trailing edge down
TEU	Trailing edge up
USGS	United States Geological Survey
UTC	Coordinated Universal Time

English symbols

C_L	Lift coefficient with spoilers stowed
C'_L	Lift coefficient with spoilers deployed
C_{Lop}	Operating lift coefficient
C_{Lmax}	Maximum lift coefficient (at stall)
C_{Lpush}	Lift coefficient at stick pusher activation, spoilers stowed
C'_{Lpush}	Lift coefficient at stick pusher activation, spoilers deployed
C_{Lss}	Lift coefficient at stick shaker activation, spoilers stowed
C'_{Lss}	Lift coefficient at stick shaker activation, spoilers deployed
ΔC_{Lsp}	Increment in lift coefficient due to spoiler deployment

h	Altitude
\dot{h}	Rate of climb
L	Lift force
nlf	Normal load factor
nlf_{push}	Normal load factor at stick pusher activation, spoilers stowed
nlf'_{push}	Normal load factor at stick pusher activation, spoilers deployed
nlf_{ss}	Normal load factor at stick shaker activation, spoilers stowed
nlf'_{ss}	Normal load factor at stick shaker activation, spoilers deployed
n_x	Longitudinal load factor
n_y	Lateral load factor
S	Wing reference area
T	Air temperature
u	Component of airspeed along body x-axis
v	Component of airspeed along body y-axis
V	Airplane speed (airspeed or ground speed depending on context)
\vec{V}	Airspeed vector
V_G	Ground speed
\vec{V}_G	Ground speed vector
V_{REF}	Landing reference speed
\vec{V}_W	Wind speed vector
w	Component of airspeed along body z-axis
W	Airplane weight

Greek symbols

α	Angle of attack
α_0	Zero-lift angle of attack
α_F	Fuselage angle of attack
α_{max}	Maximum (stall) angle of attack
α_{op}	Operating angle of attack
α_{push}	Angle of attack at stick pusher activation
α_{ss}	Angle of attack at stick shaker activation
α_V	Vane angle of attack
$\dot{\alpha}_V$	Rate of change of vane angle of attack computed by the SPS
$\Delta\alpha$	Required angle of attack increment due to spoiler deployment
$\Delta\alpha_V$	Stall Protection System phase advance term
β	Sideslip angle
γ	Flight path angle
θ	Pitch angle
ρ	Air density
ϕ	Roll angle
ψ_{DRIFT}	Drift angle
ψ_{THDG}	True heading angle
ψ_{TRRK}	True track angle

FIGURES

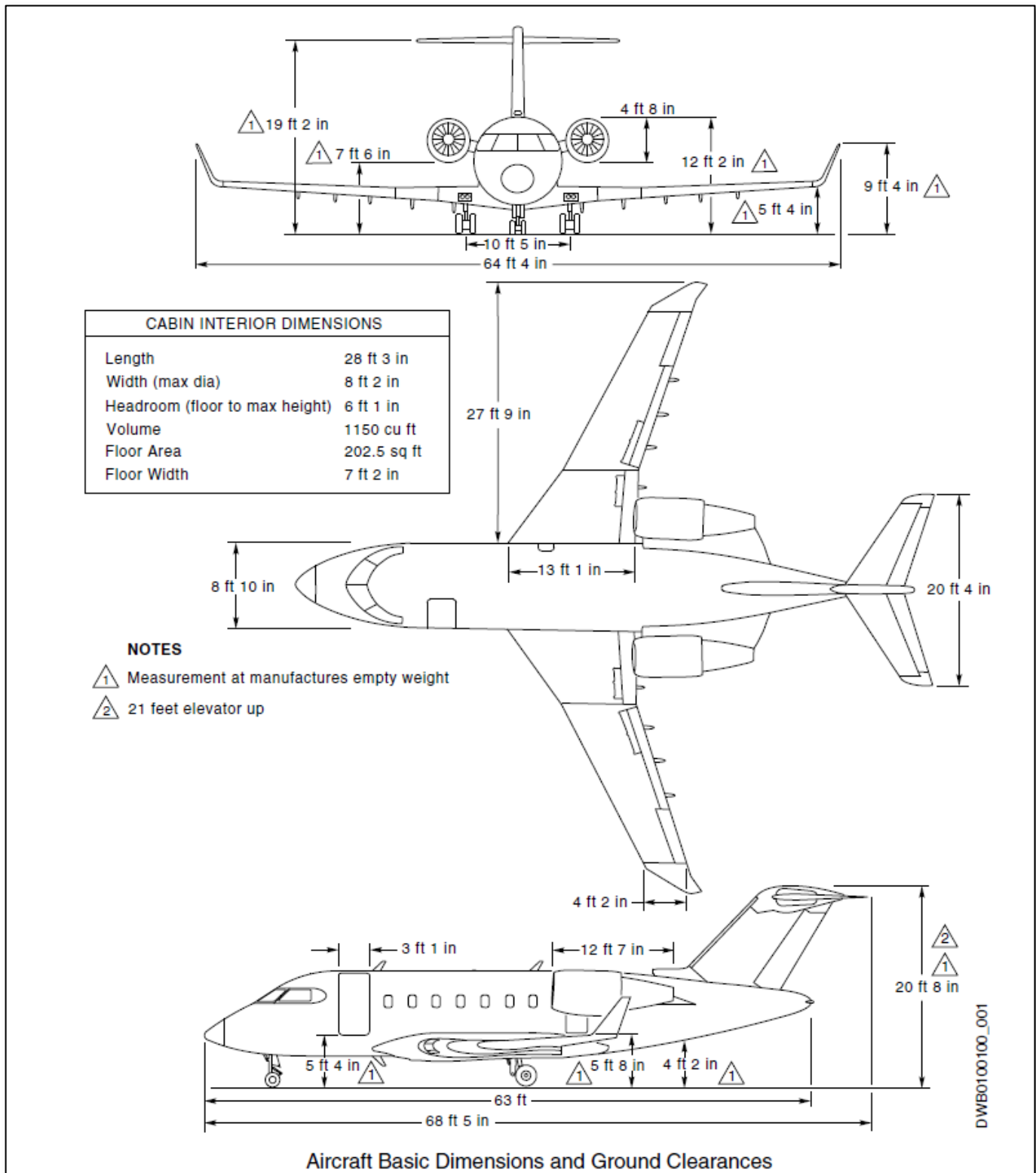


Figure 1. 3-view drawing of the Bombardier Challenger 605, from Reference 1.



Figure 2. Pre-accident photographs of N605TR. Images obtained from <https://www.aircraft.com/aircraft/199392929/n605tr-2008-bombardier-challenger-605>.



Frame # 001



Frame # 030



Frame # 093



Frame # 131



Frame # 150



Frame # 314

Figure 3. Selected cropped and enlarged frames from video with filename "TTLCO-version2-2021-07-26_17-18-07.mp4."

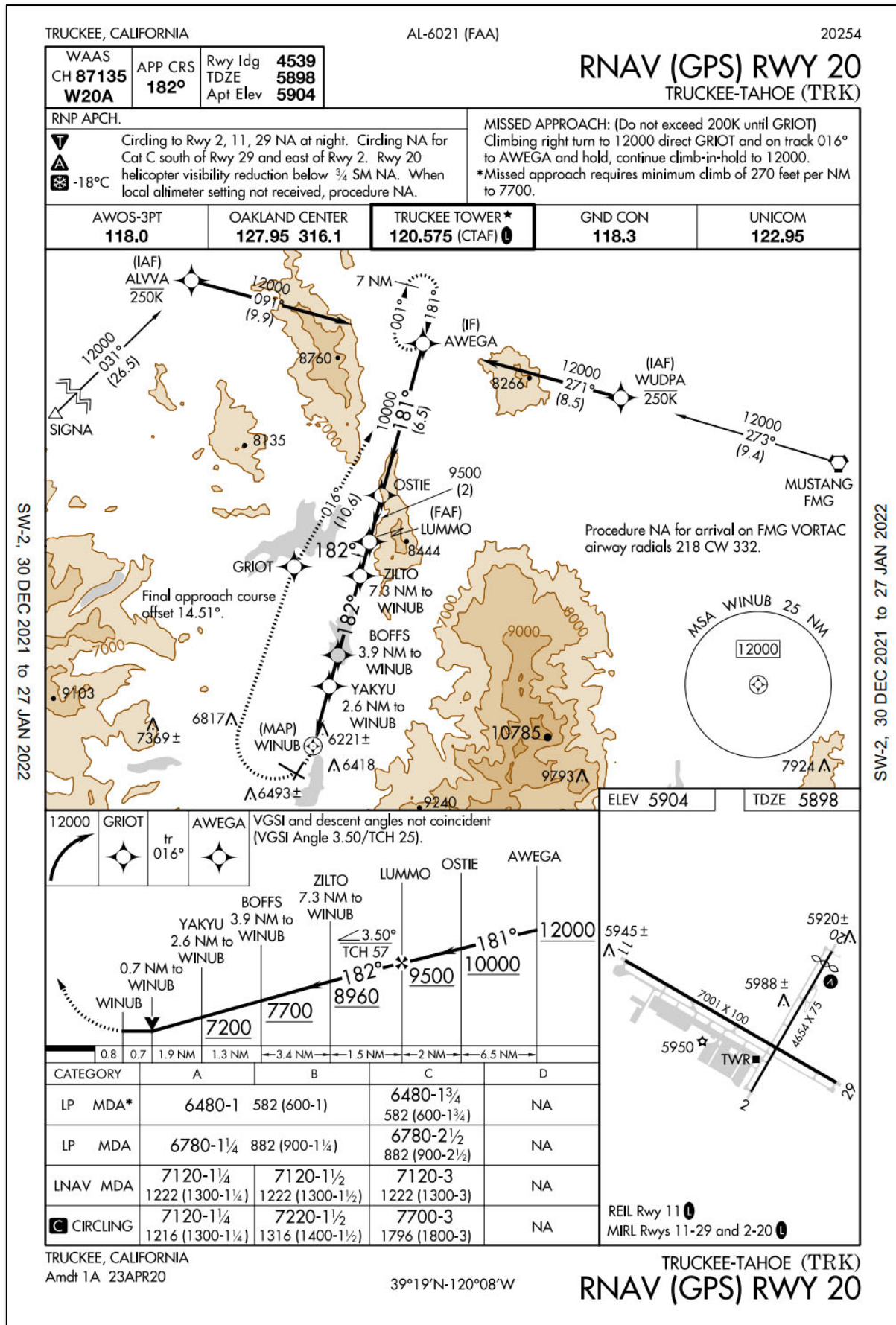


Figure 4. FAA National Aeronautical Charting Office (NACO) instrument approach plate for the KTRK RNAV (GPS) RWY 20 approach.

WPR21FA286: Bombardier CL-600-2B16, N605TR, Truckee, CA, 07/26/2021

Plan view of approach to KTRK (ADS-B data)

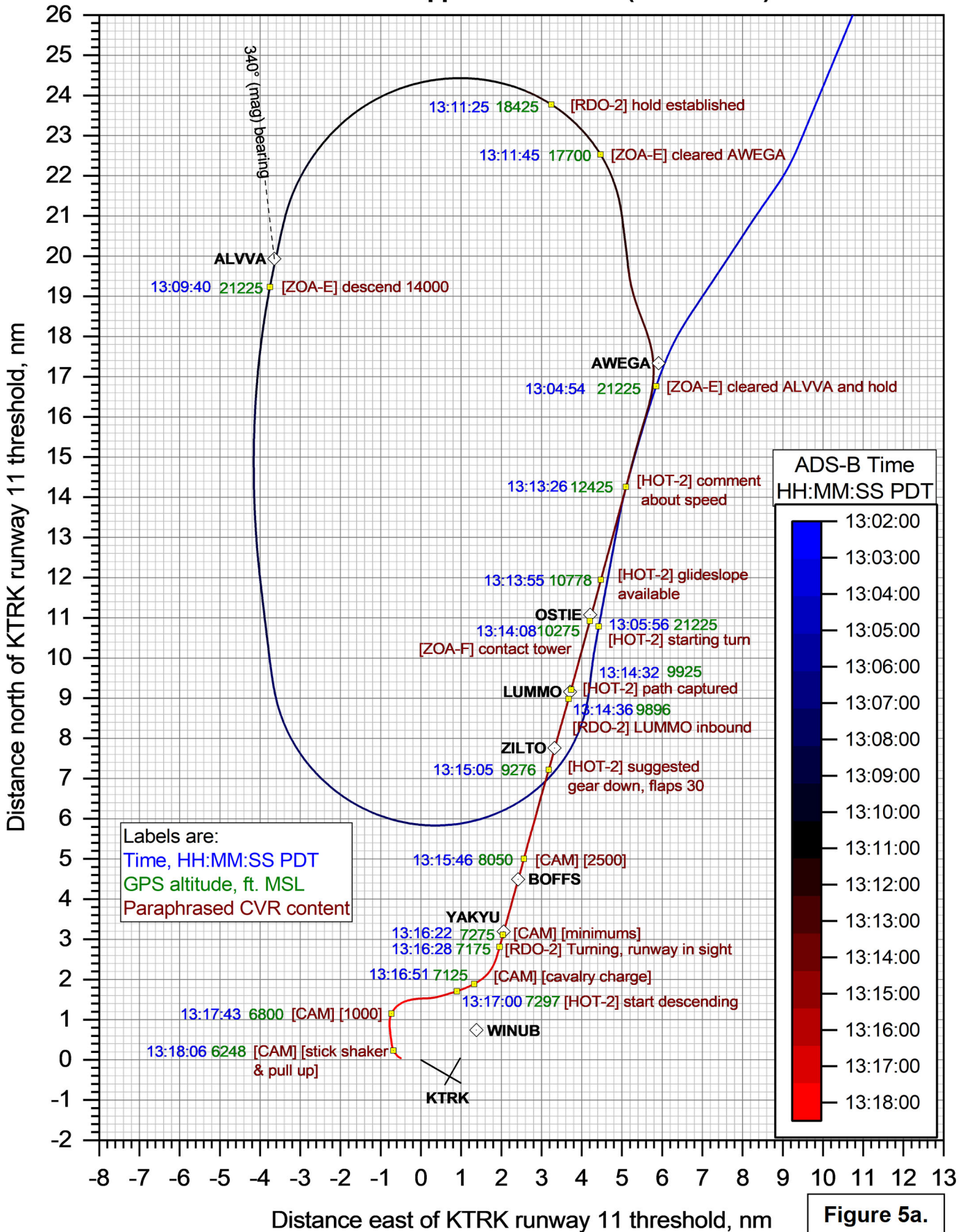


Figure 5a.

WPR21FA286: Bombardier CL-600-2B16, N605TR, Truckee, CA, 07/26/2021

Plan view of approach to KTRK (ADS-B data)

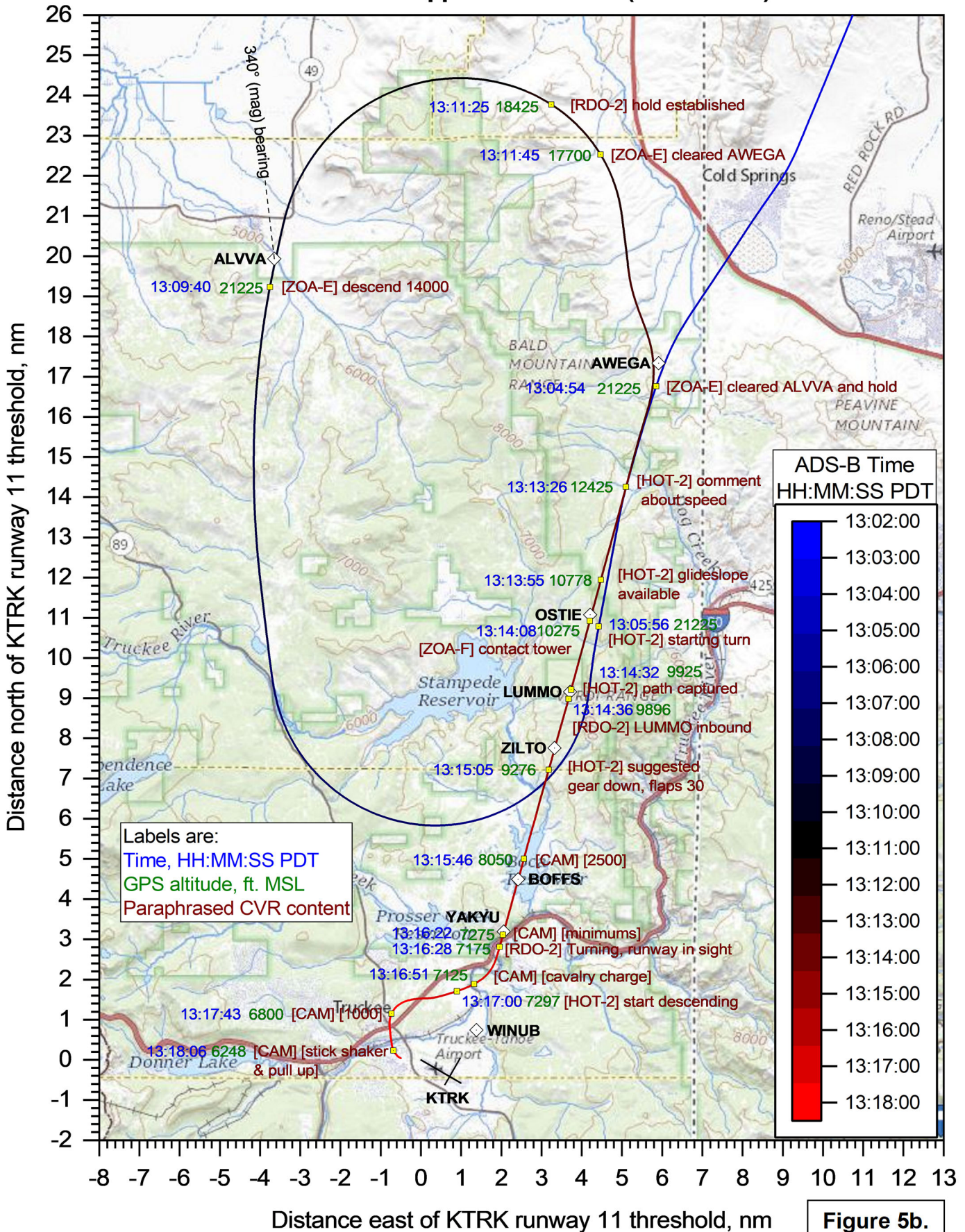


Figure 5b.

Plan view of approach to KTRK (detail)

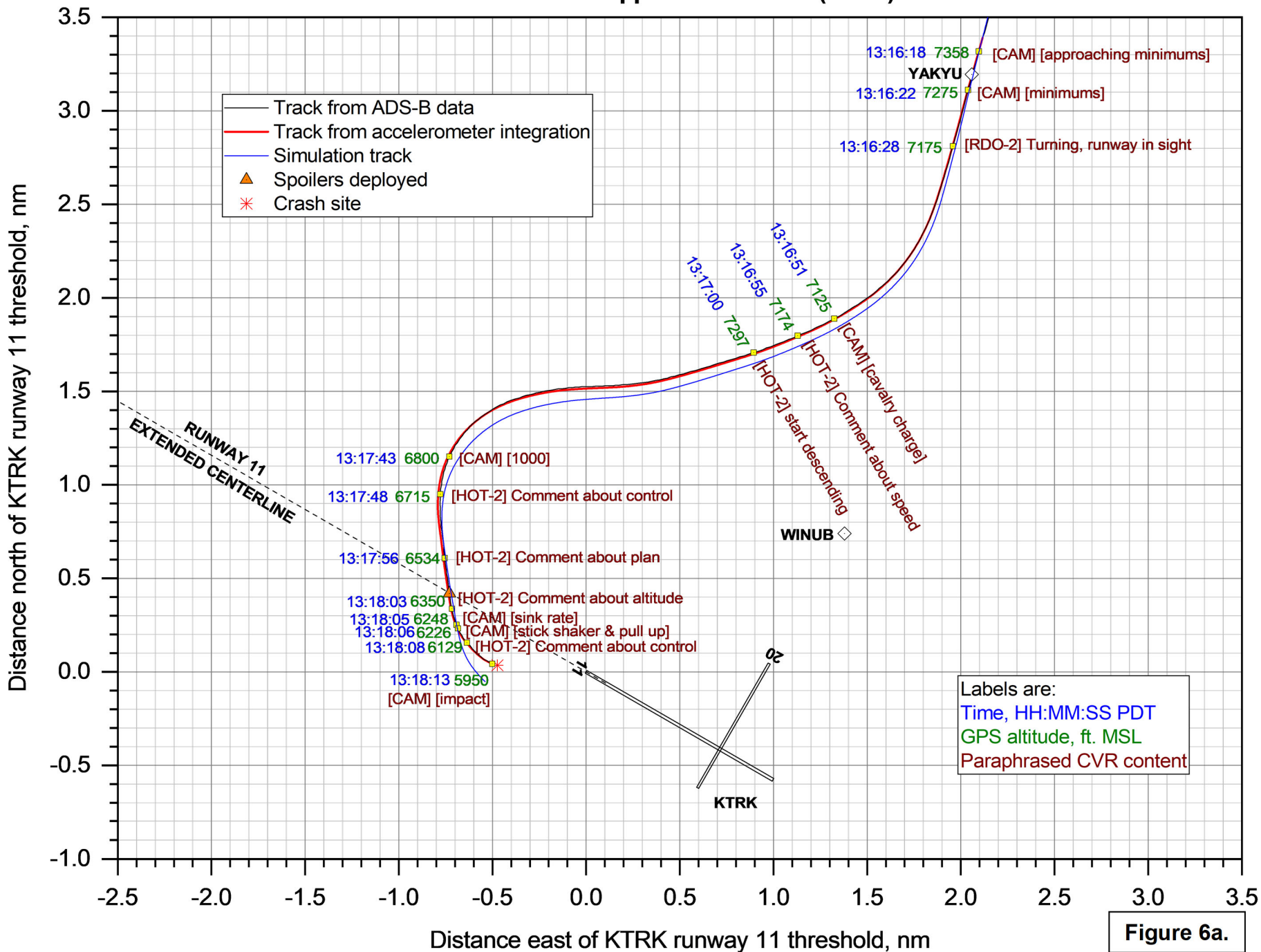


Figure 6a.

Plan view of approach to KTRK (detail)

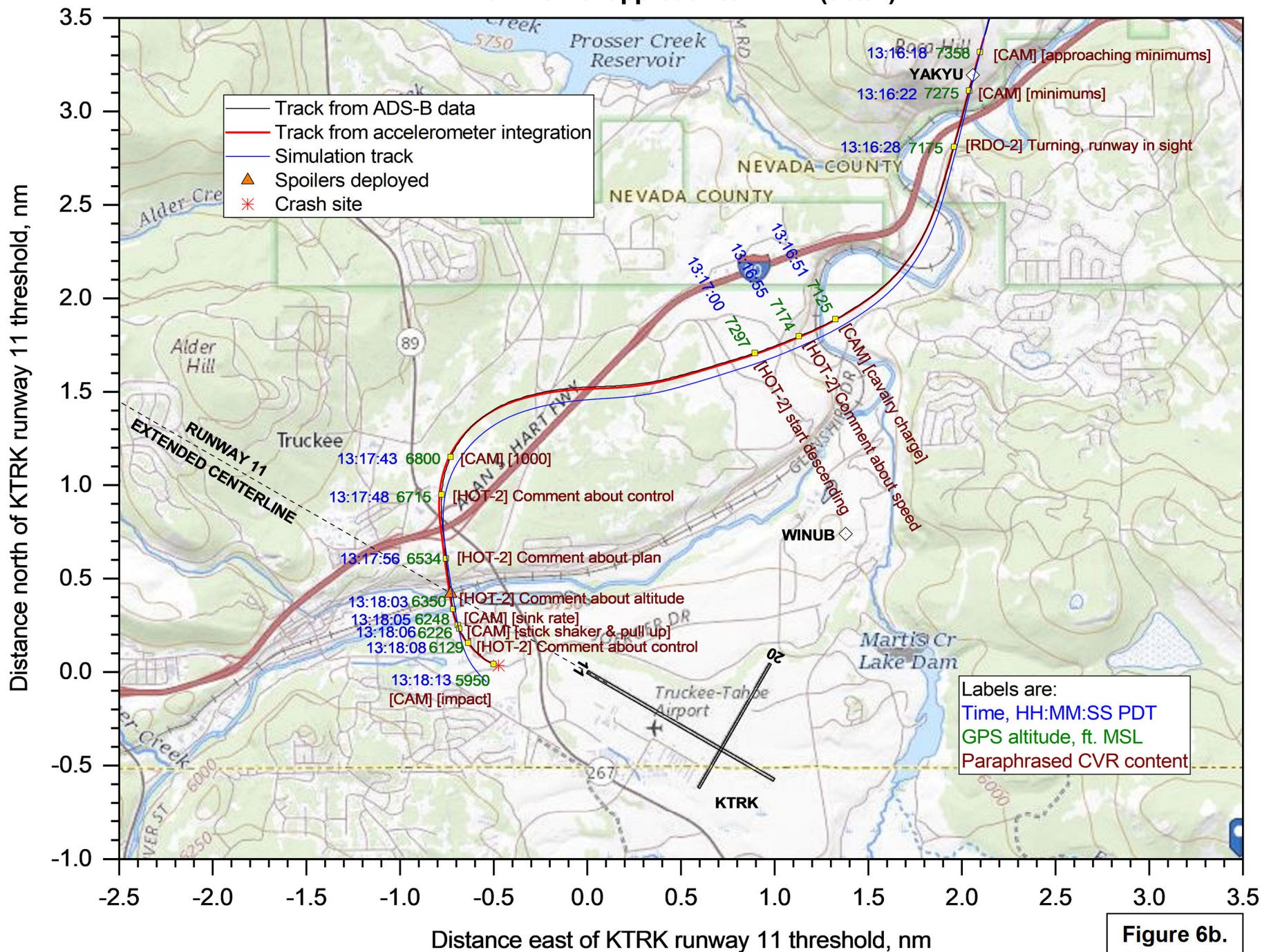


Figure 6b.



Figure 7. Final segment of N605TR's flight path and the accident site depicted over a *Google Earth* satellite image. Labels along the flight path indicate ADS-B time in PDT and altitude in feet MSL.

WPR21FA286: Bombardier CL-600-2B16, N605TR, Truckee, CA, 07/26/2021
Profile view of RNAV approach to KTRK RWY 20 (ADS-B data)

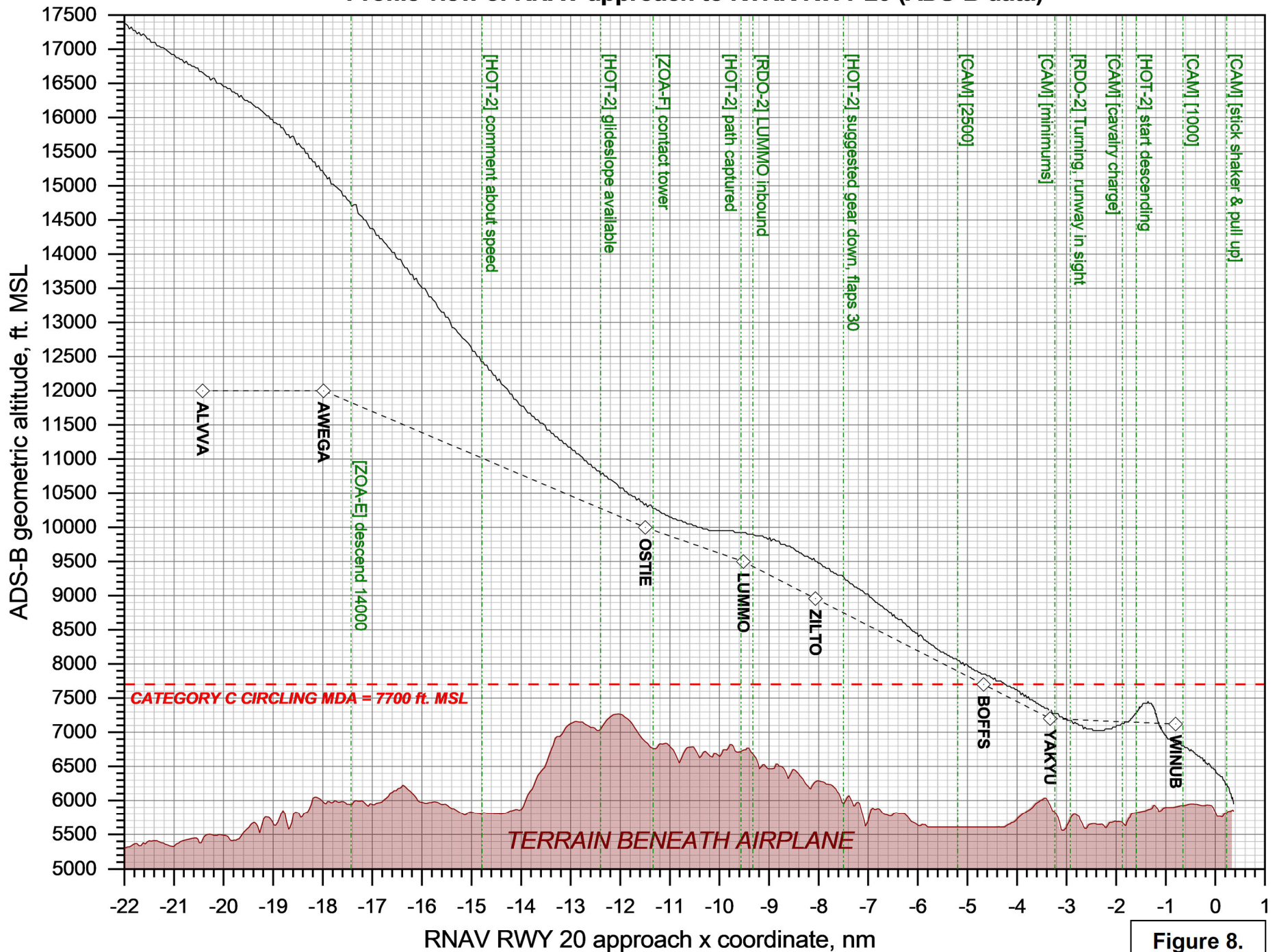


Figure 8.

Profile view of circling approach to KTRK RWY 11

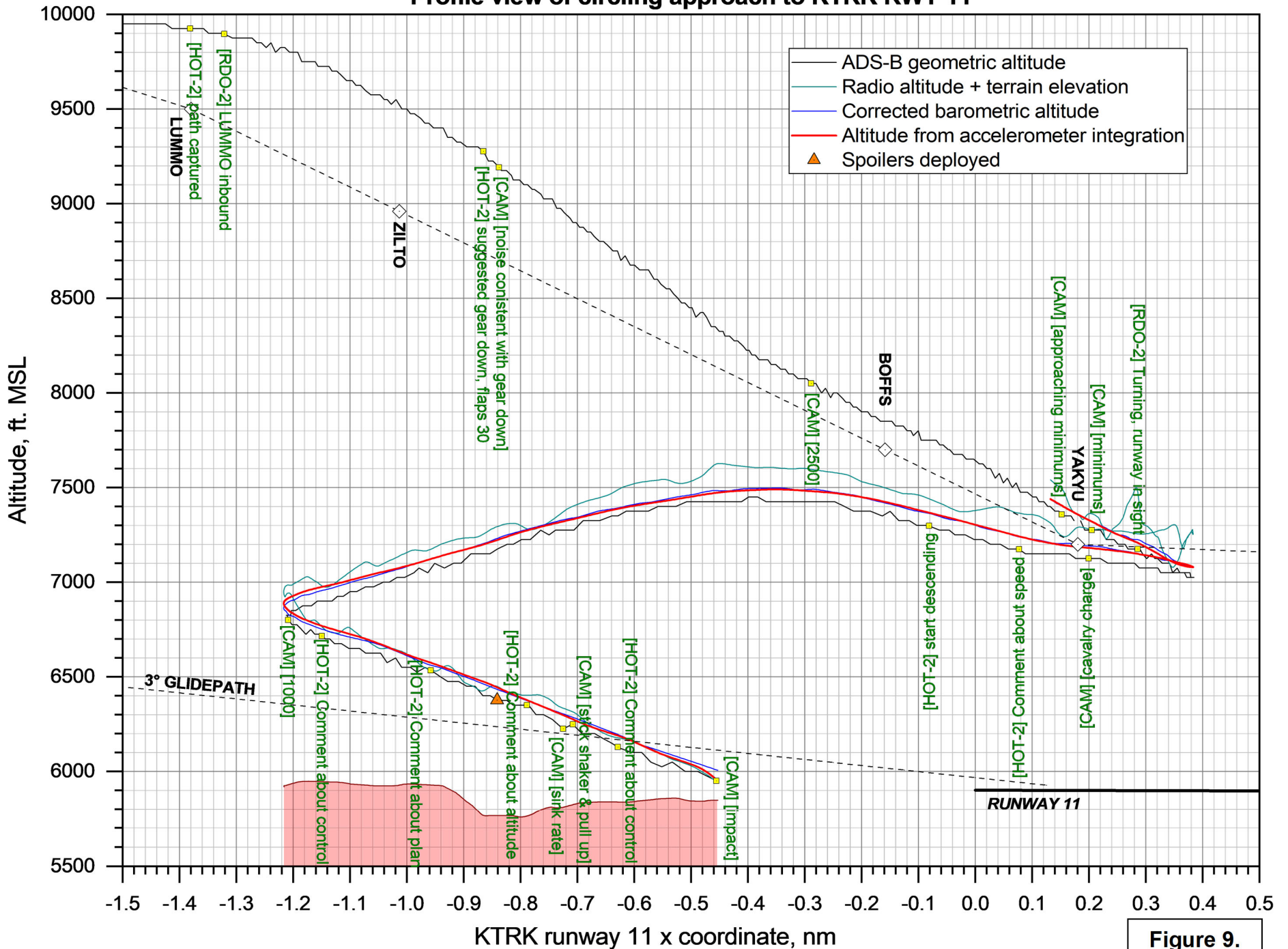


Figure 9.

Altitude vs. time

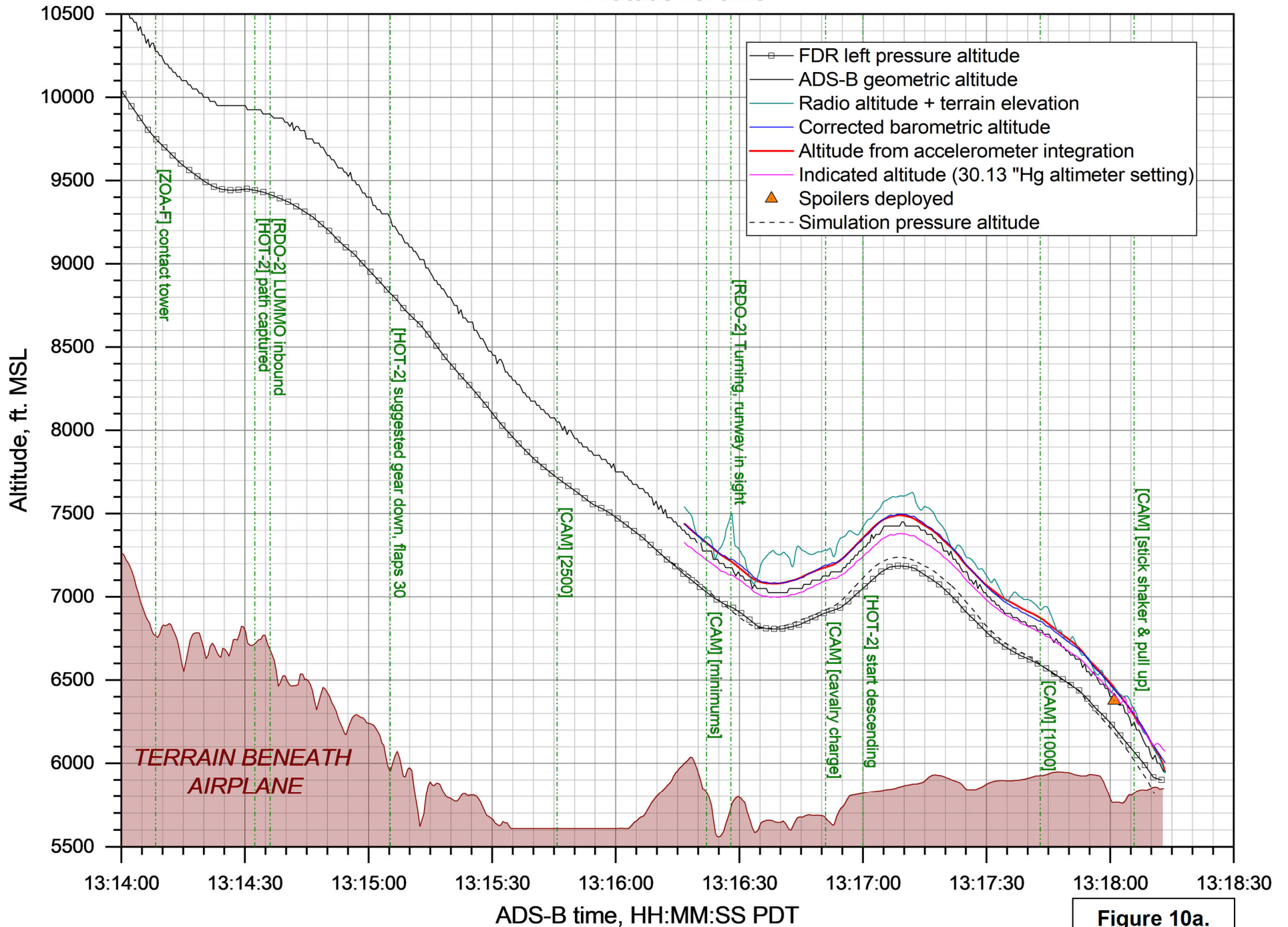


Figure 10a.

Altitude vs. time (detail)

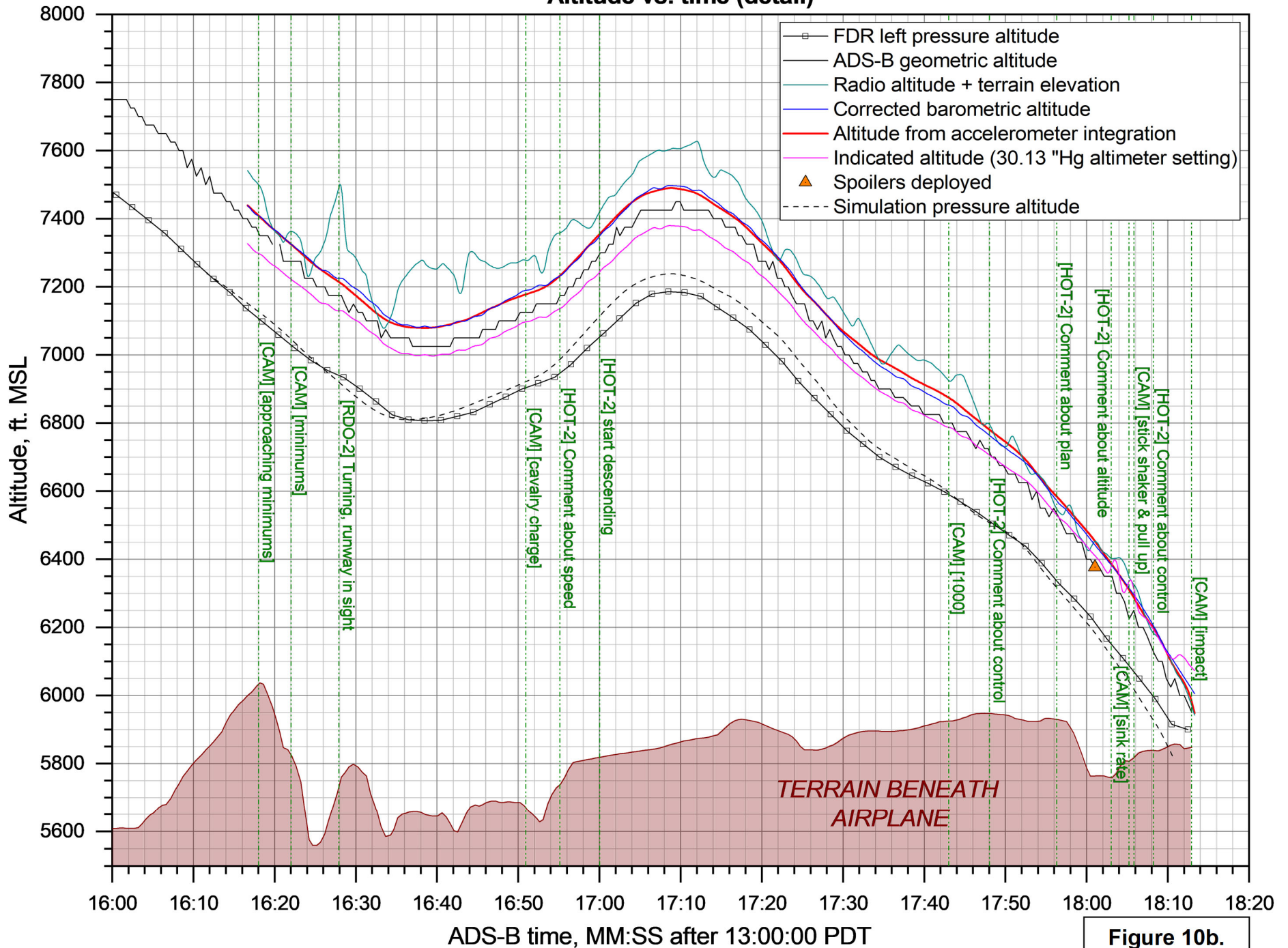


Figure 10b.

WPR21FA286: Bombardier CL-600-2B16, N605TR, Truckee, CA, 07/26/2021

North & east coordinates vs. time

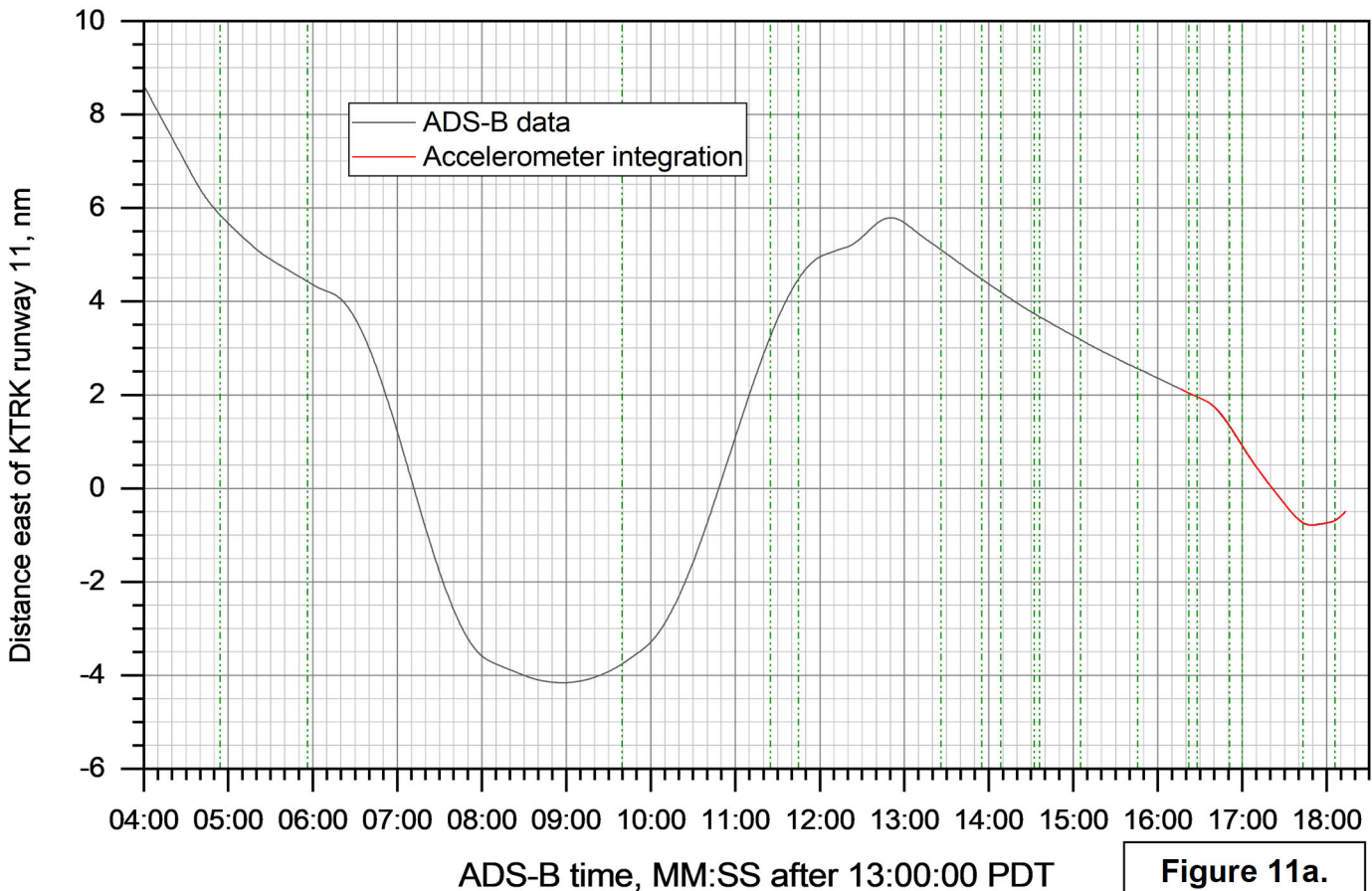
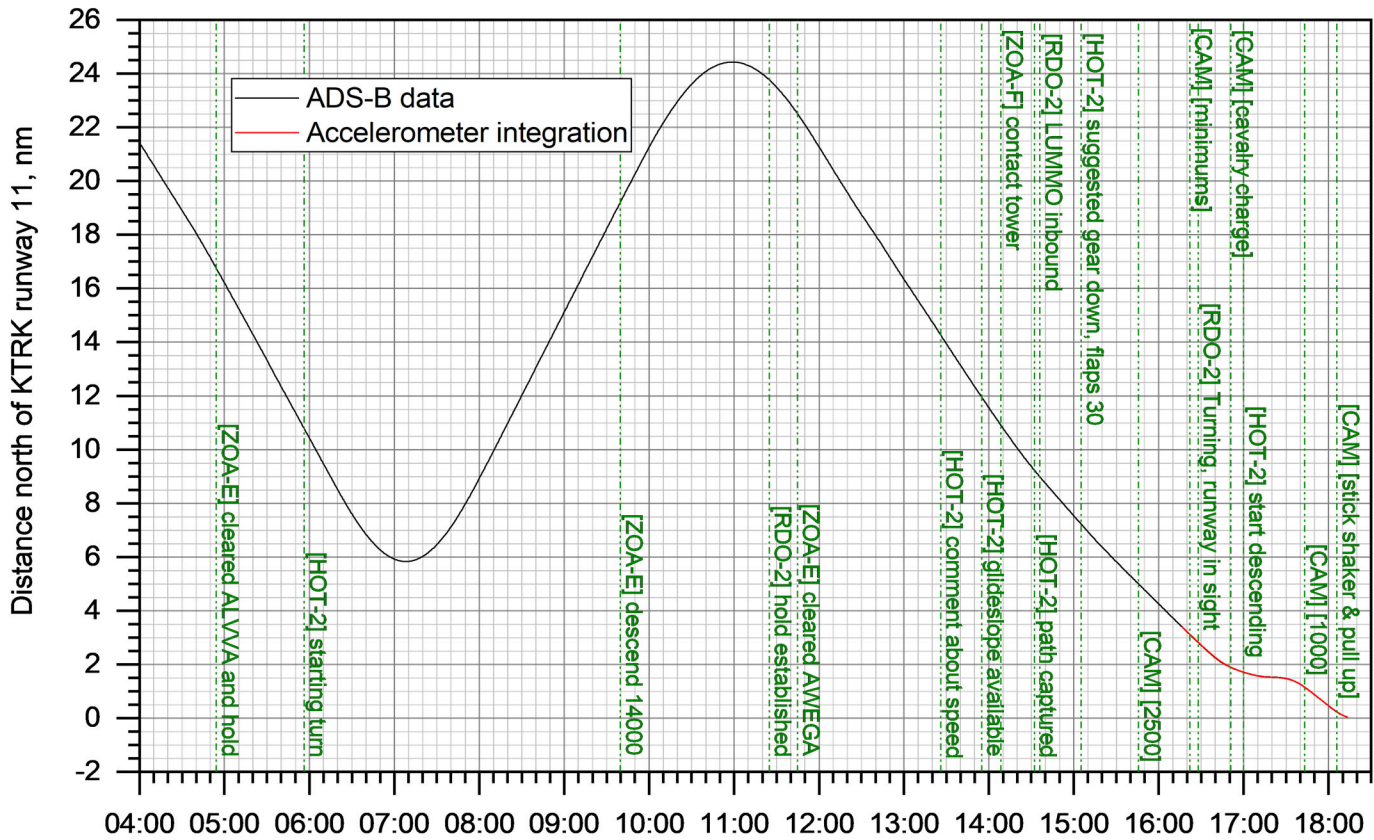


Figure 11a.

WPR21FA286: Bombardier CL-600-2B16, N605TR, Truckee, CA, 07/26/2021

North & east coordinates vs. time (detail)

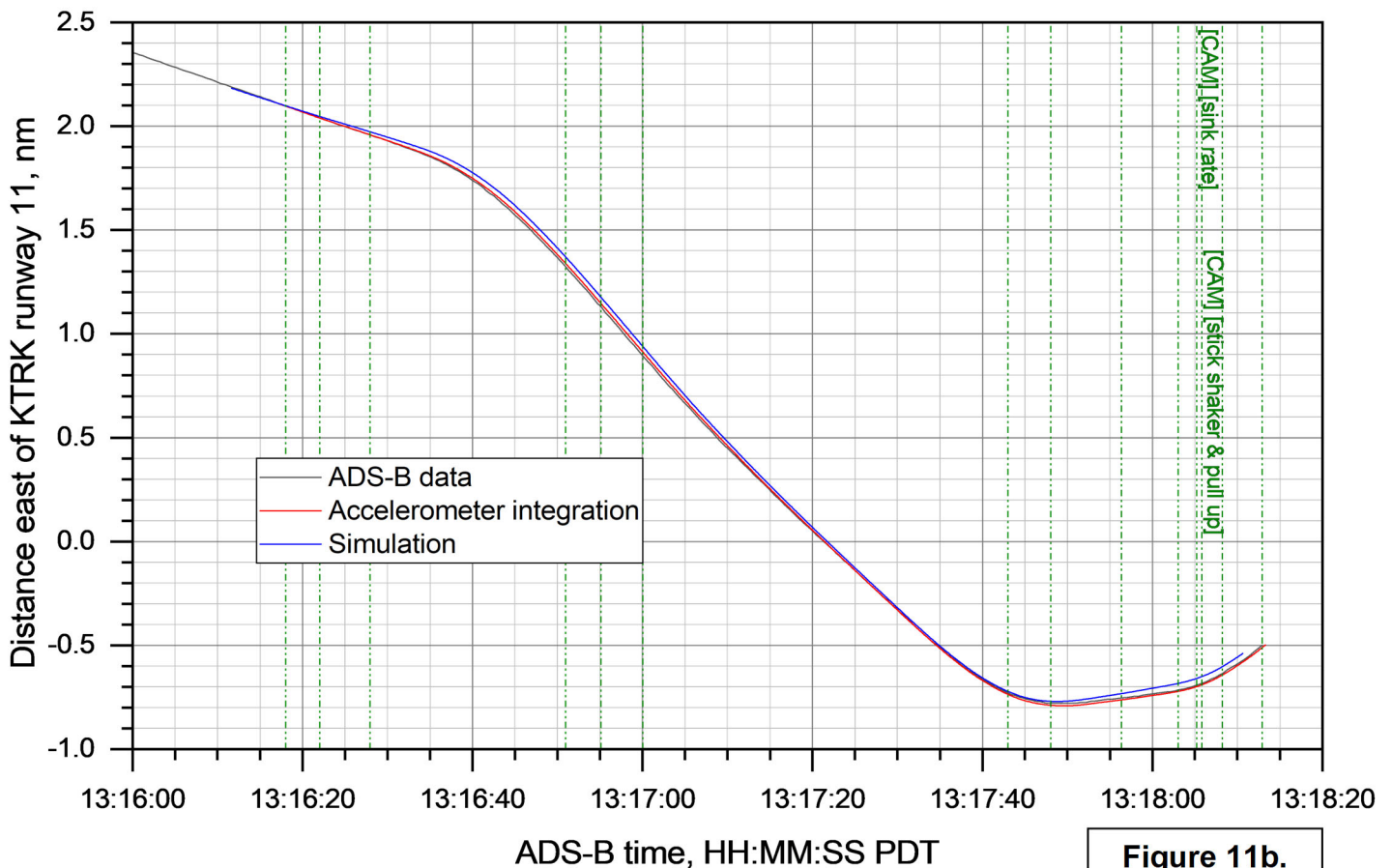
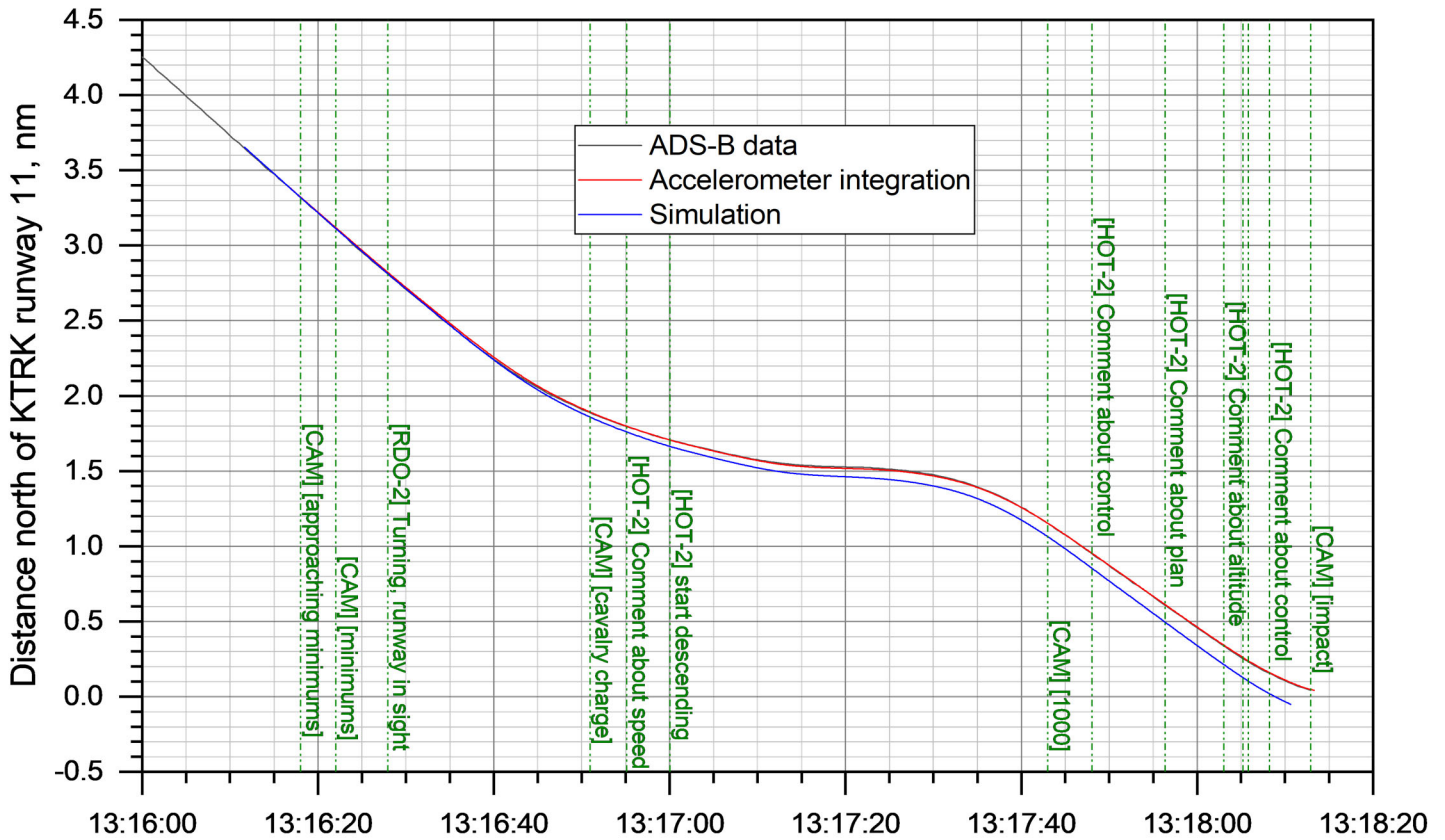
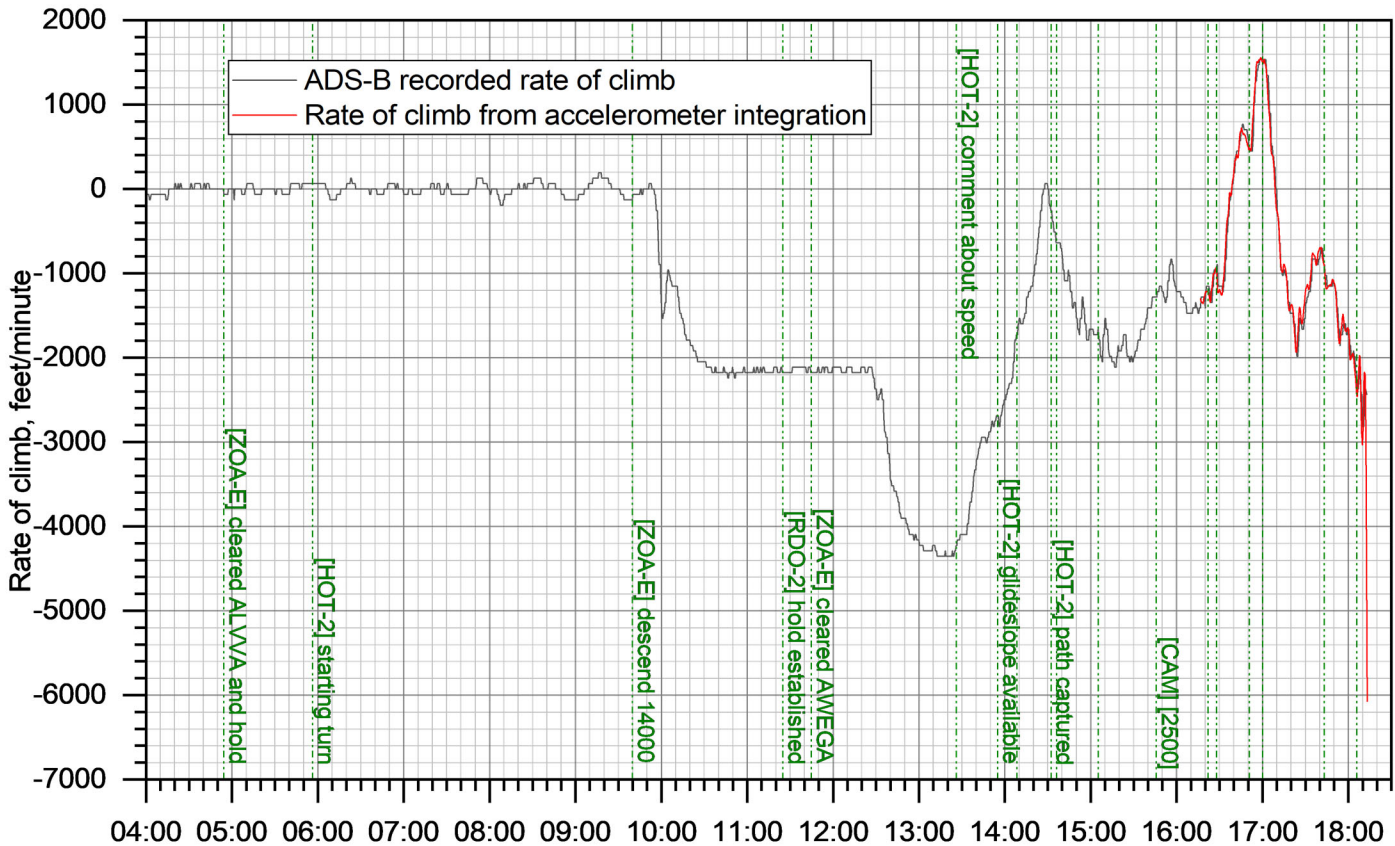
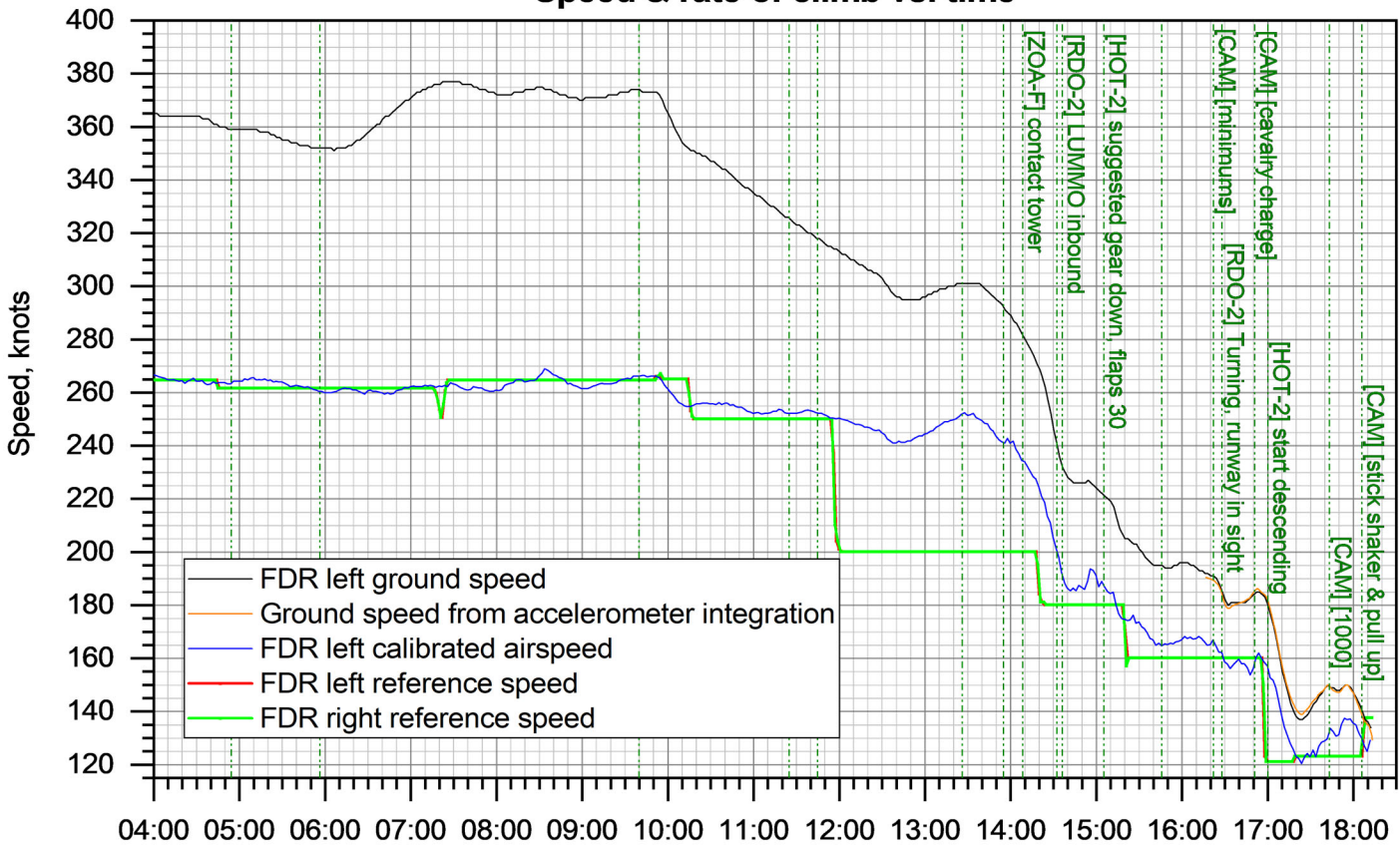


Figure 11b.

WPR21FA286: Bombardier CL-600-2B16, N605TR, Truckee, CA, 07/26/2021

Speed & rate of climb vs. time



ADS-B time, MM:SS after 13:00:00 PDT

Figure 12a.

WPR21FA286: Bombardier CL-600-2B16, N605TR, Truckee, CA, 07/26/2021

Speed & rate of climb vs. time (detail)

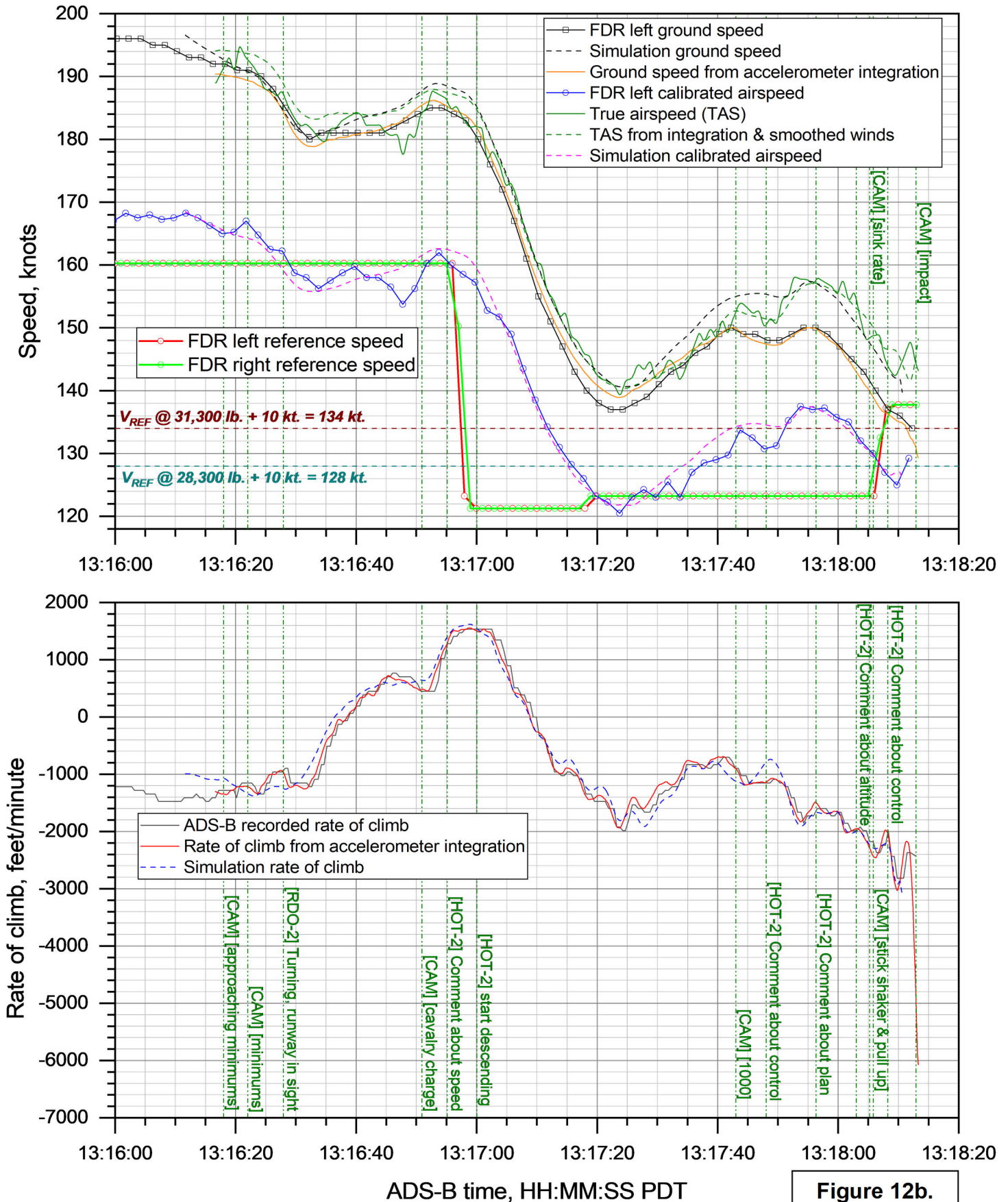


Figure 12b.

WPR21FA286: Bombardier CL-600-2B16, N605TR, Truckee, CA, 07/26/2021

Euler angles during circling maneuver

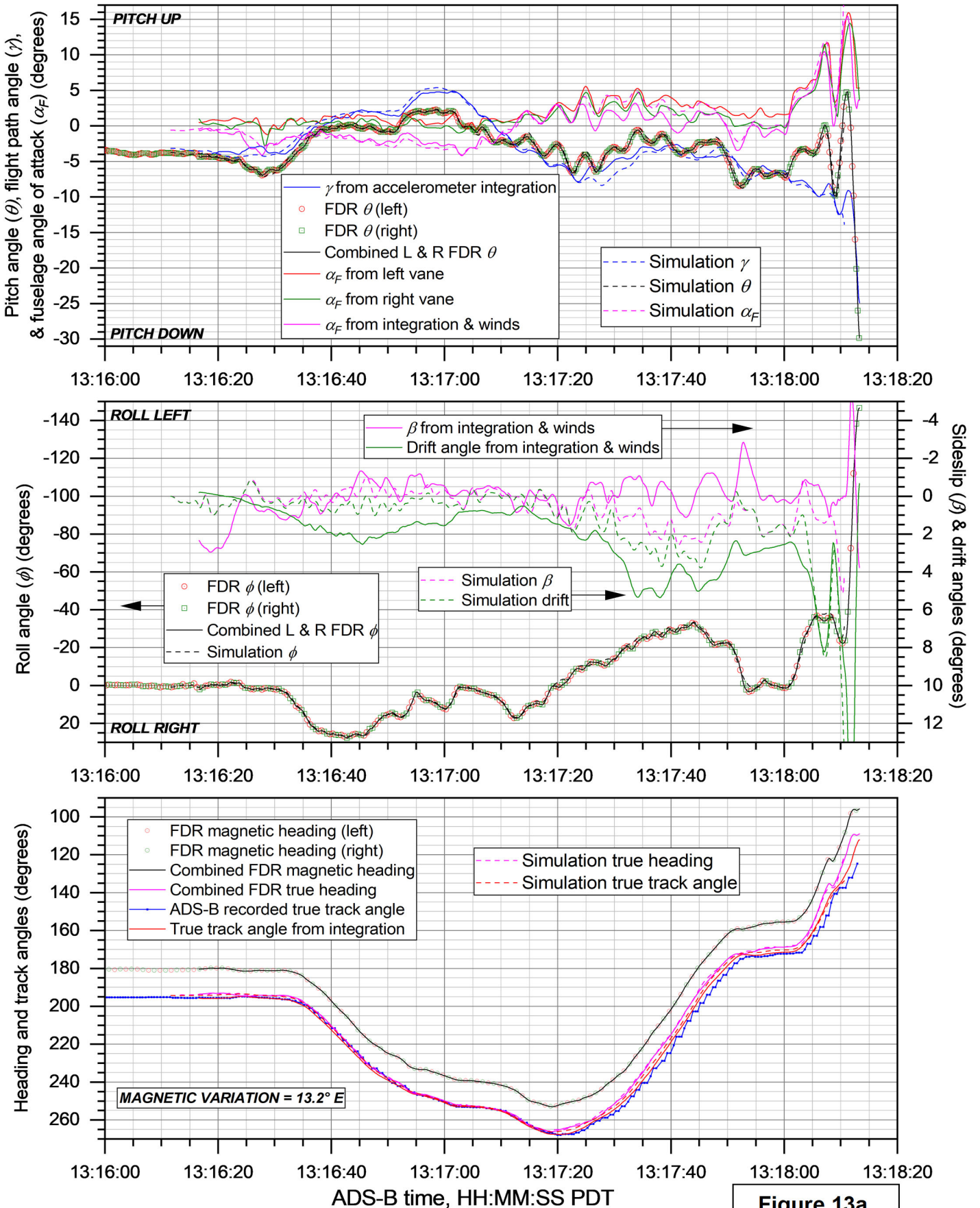


Figure 13a.

WPR21FA286: Bombardier CL-600-2B16, N605TR, Truckee, CA, 07/26/2021

Euler angles during circling maneuver (detail)

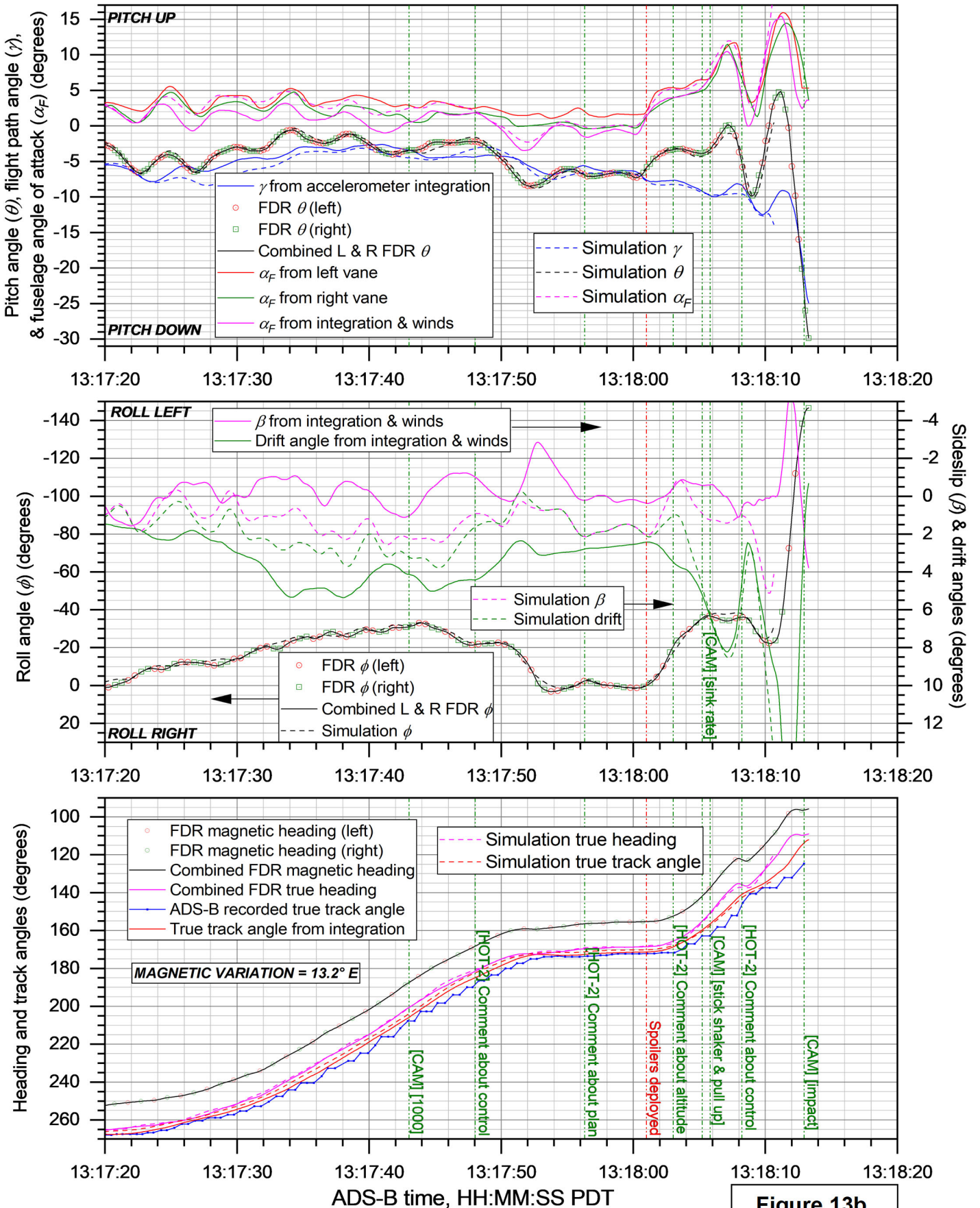


Figure 13b.

WPR21FA286: Bombardier CL-600-2B16, N605TR, Truckee, CA, 07/26/2021

Load factors during circling maneuver

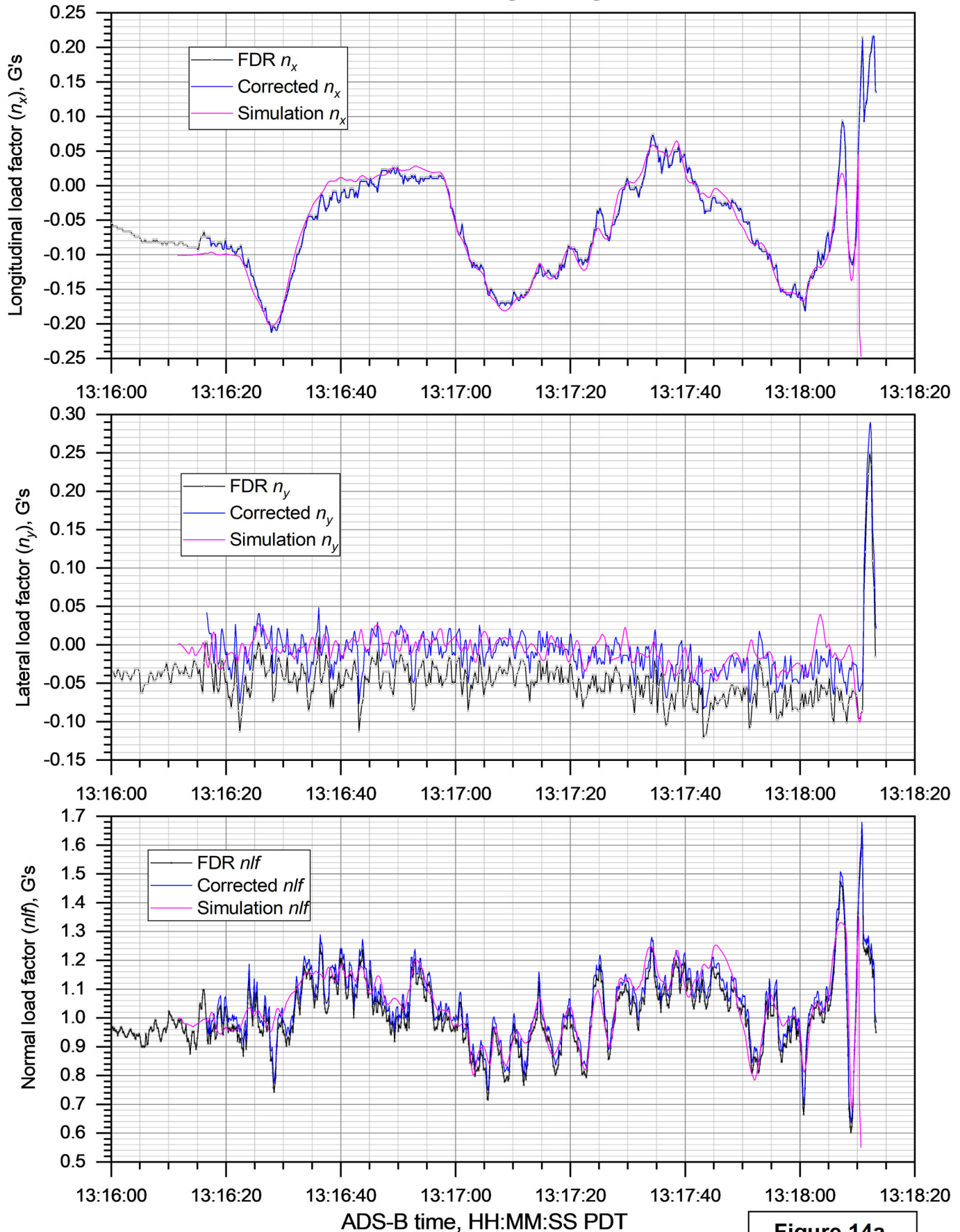


Figure 14a.

WPR21FA286: Bombardier CL-600-2B16, N605TR, Truckee, CA, 07/26/2021

Load factors during circling maneuver (detail)

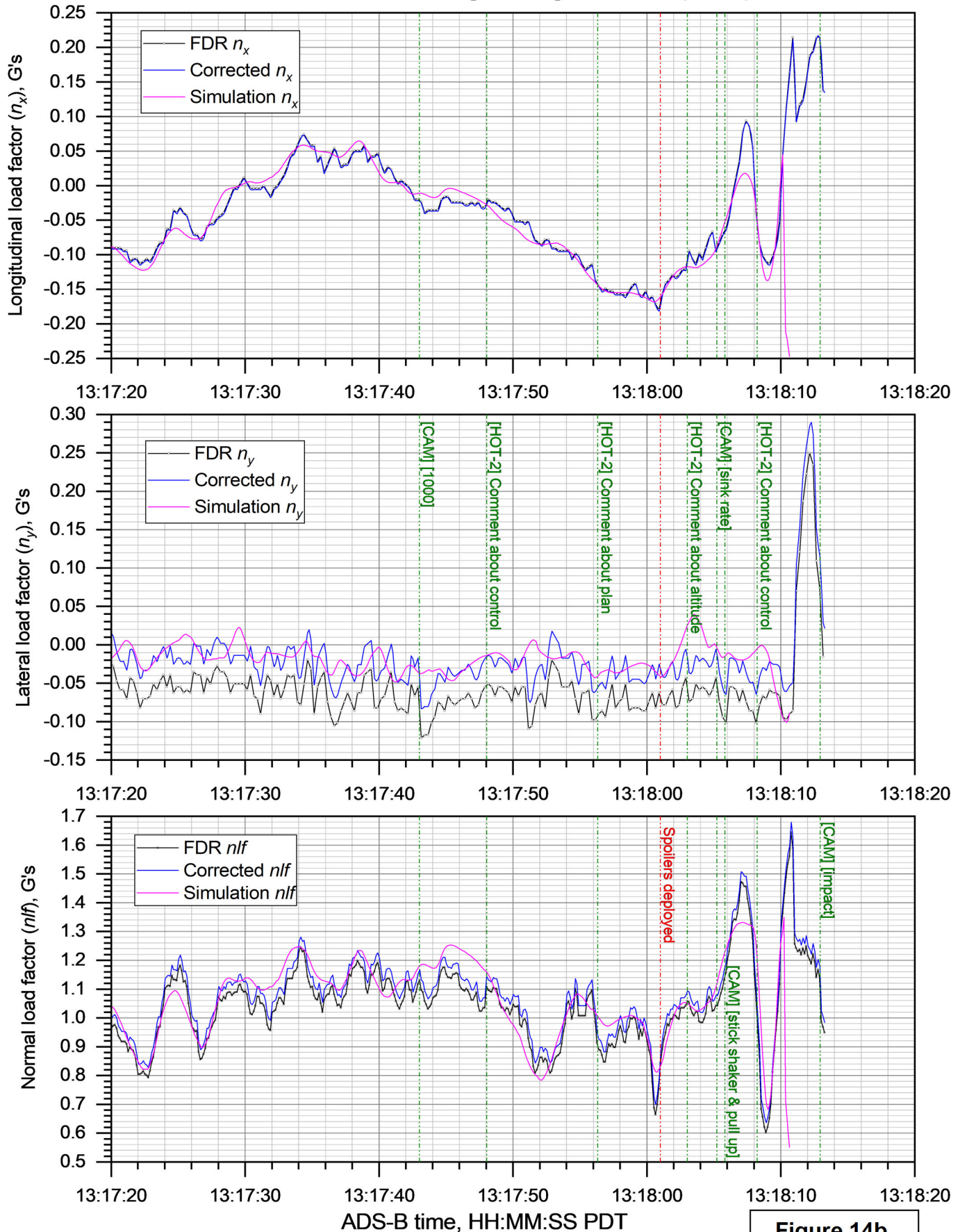


Figure 14b.

WPR21FA286: Bombardier CL-600-2B16, N605TR, Truckee, CA, 07/26/2021

Winds during circling maneuver

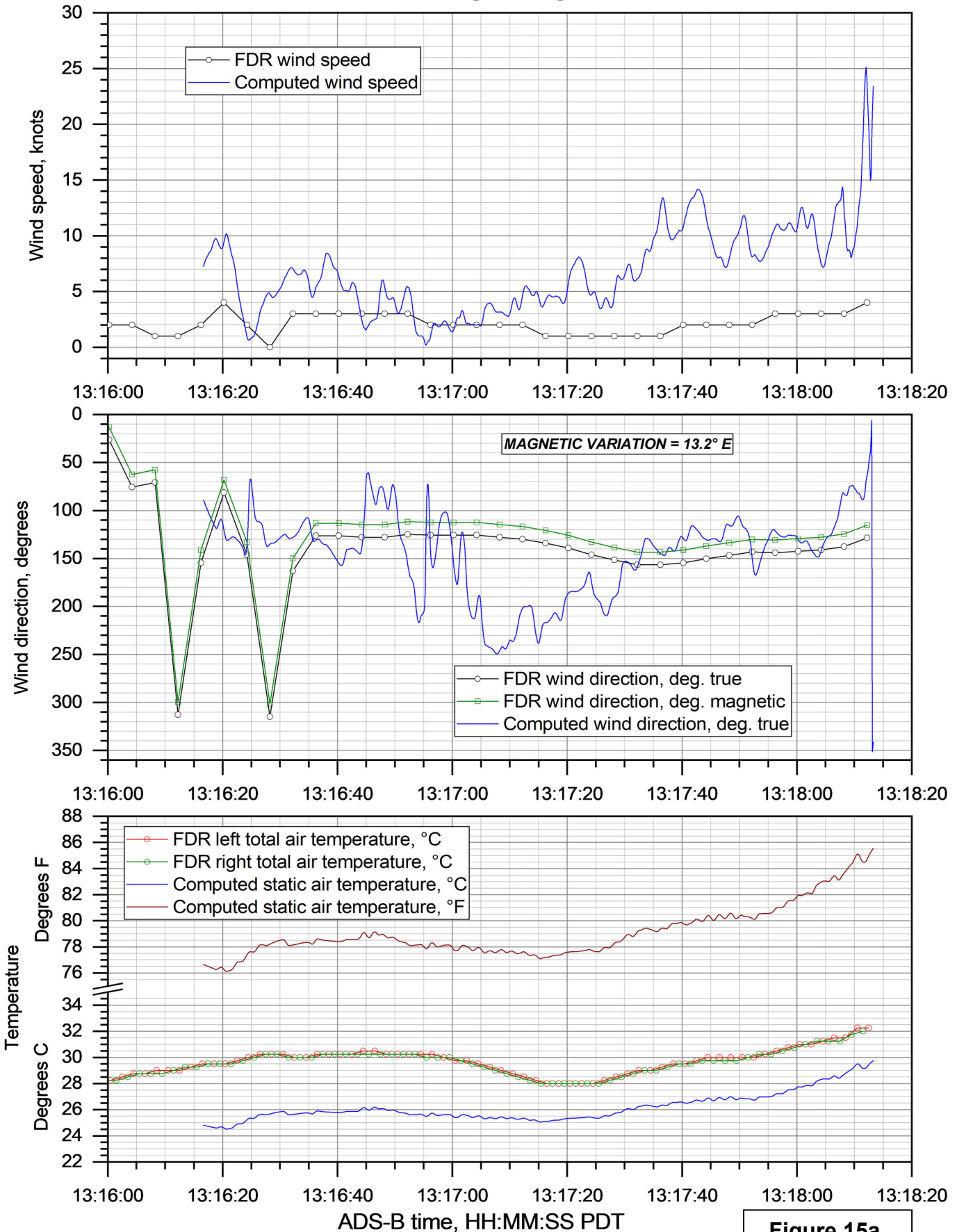


Figure 15a.

Assumed winds vs. altitude for inertial α and β calculations

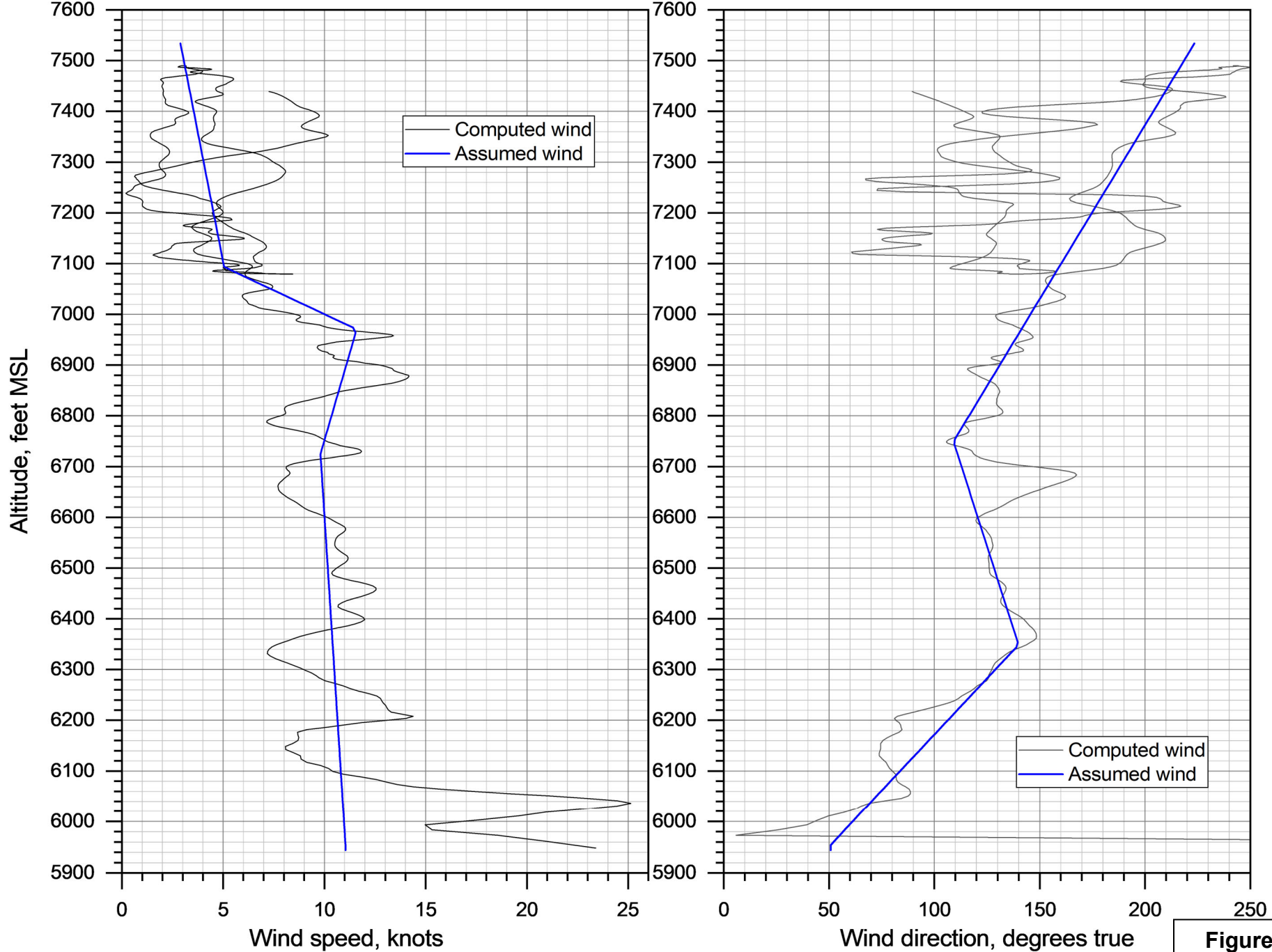


Figure 16.

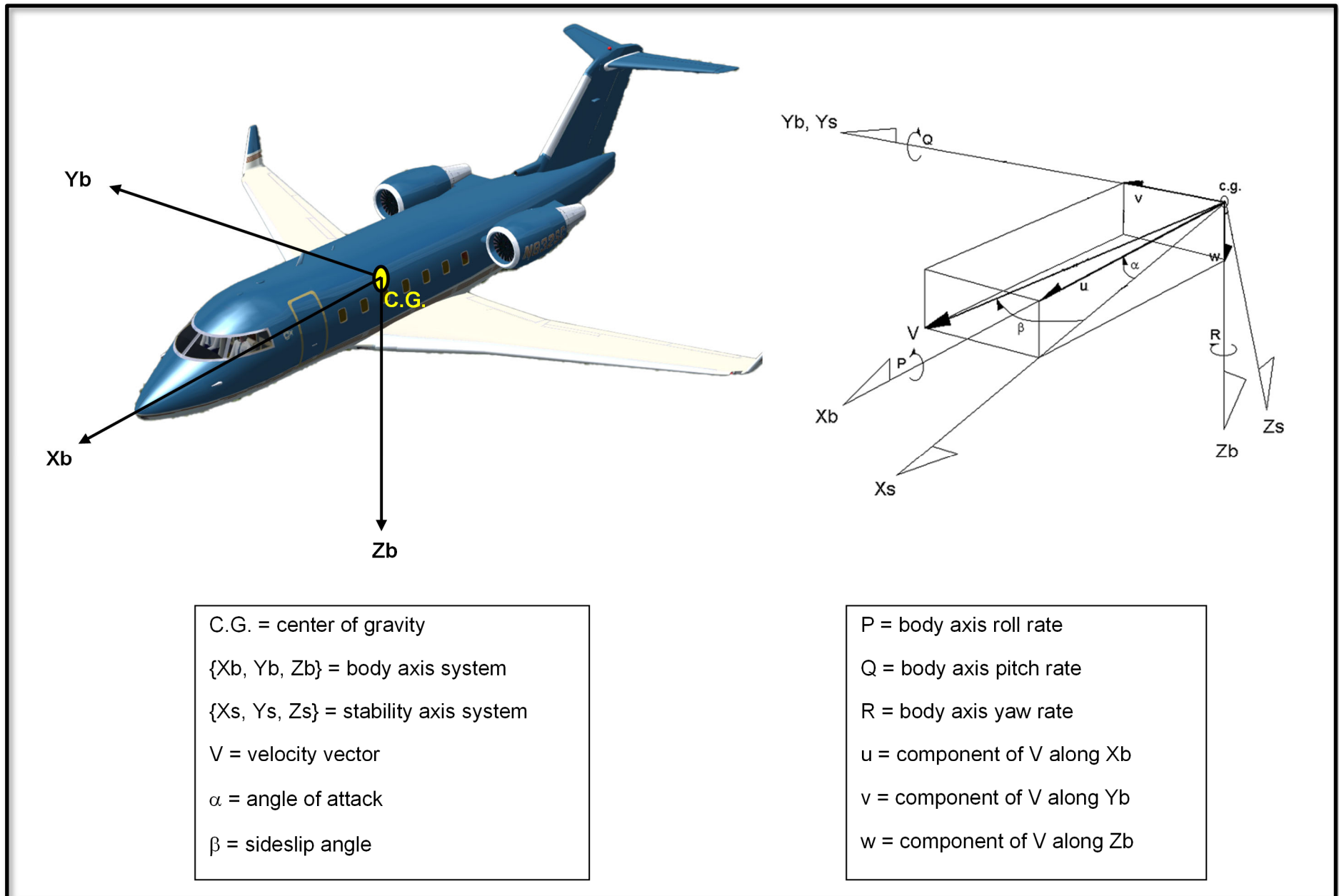


Figure 17. Airplane body axis system, body-axis components of linear and angular velocities, and definitions of α and β .

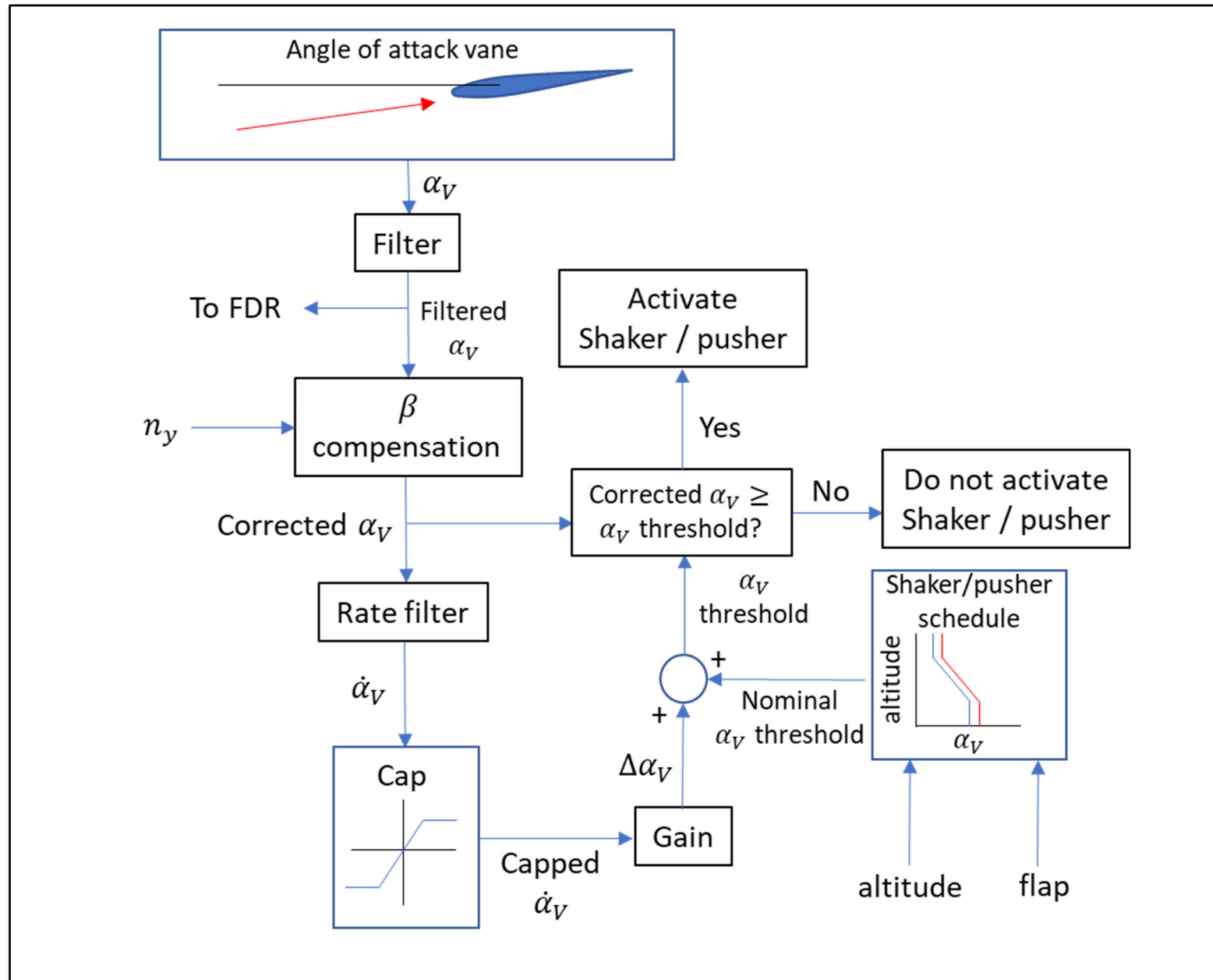


Figure 18. Diagram of SPC shaker / pusher activation logic (cancellation logic, including hysteresis, not shown).

WPR21FA286: Bombardier CL-600-2B16, N605TR, Truckee, CA, 07/26/2021 Flight control surfaces during circling maneuver

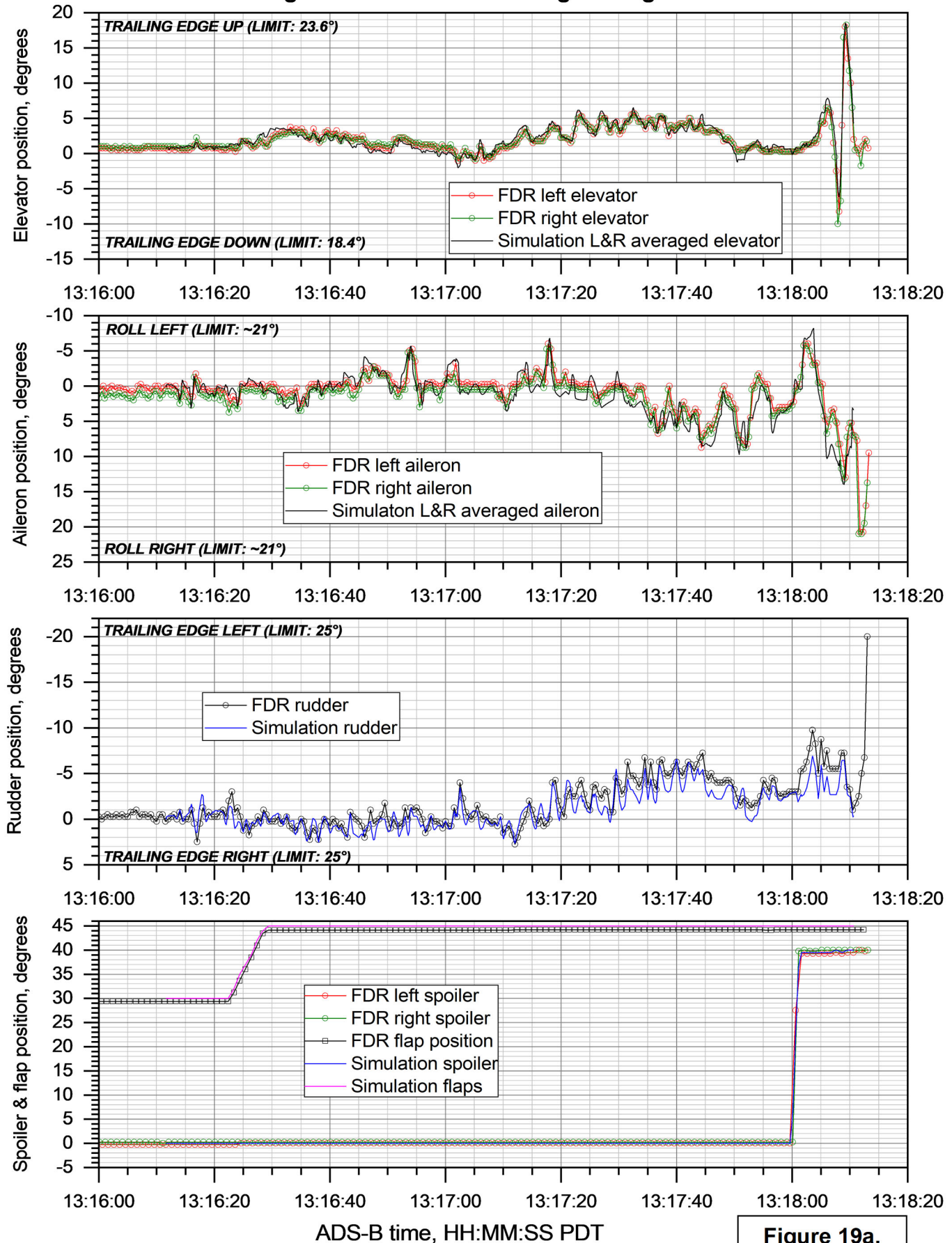


Figure 19a.

WPR21FA286: Bombardier CL-600-2B16, N605TR, Truckee, CA, 07/26/2021

Flight control surfaces during circling maneuver (detail)

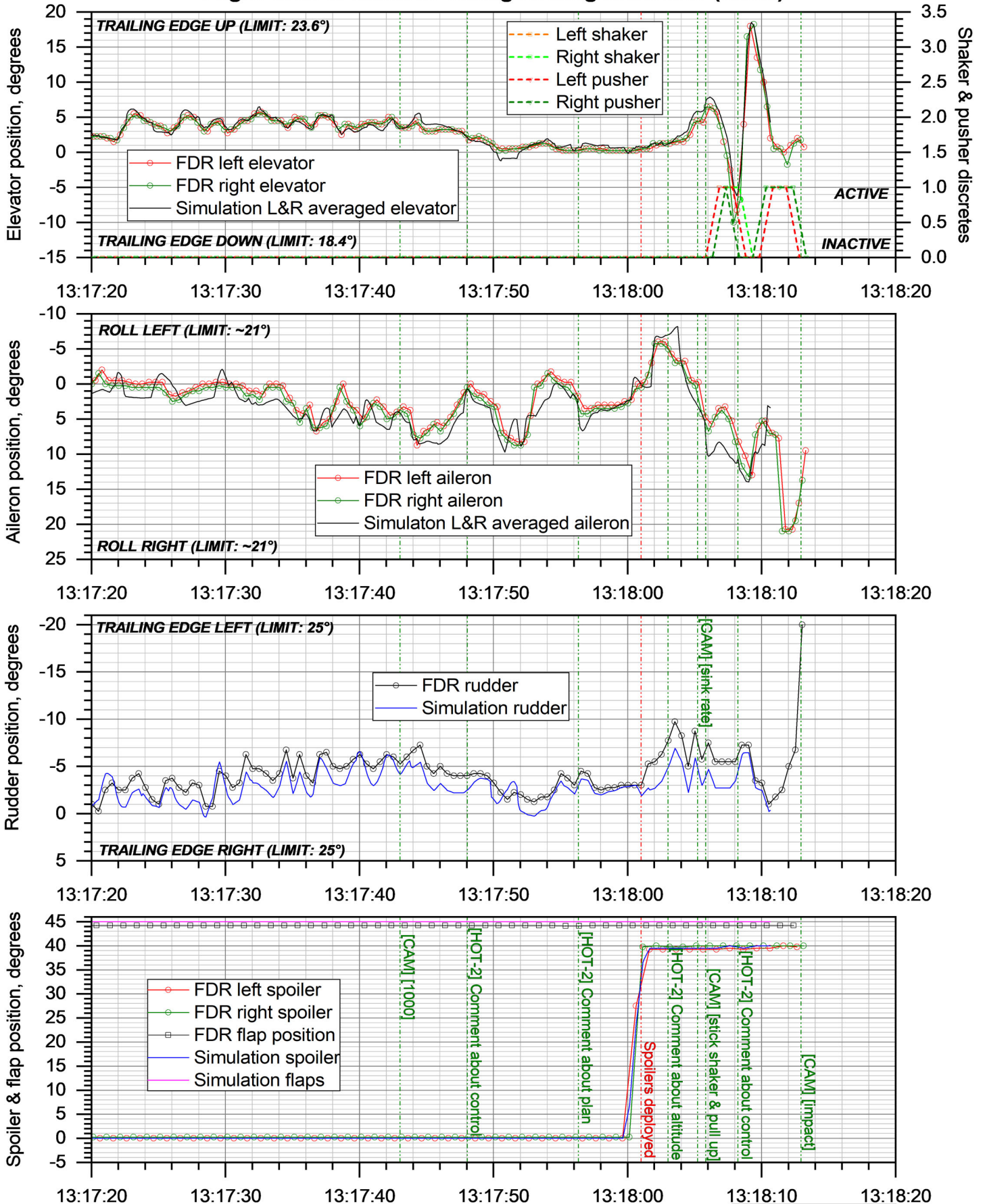


Figure 19b.

WPR21FA286: Bombardier CL-600-2B16, N605TR, Truckee, CA, 07/26/2021

Engine, autoflight, and gear parameters during circling maneuver

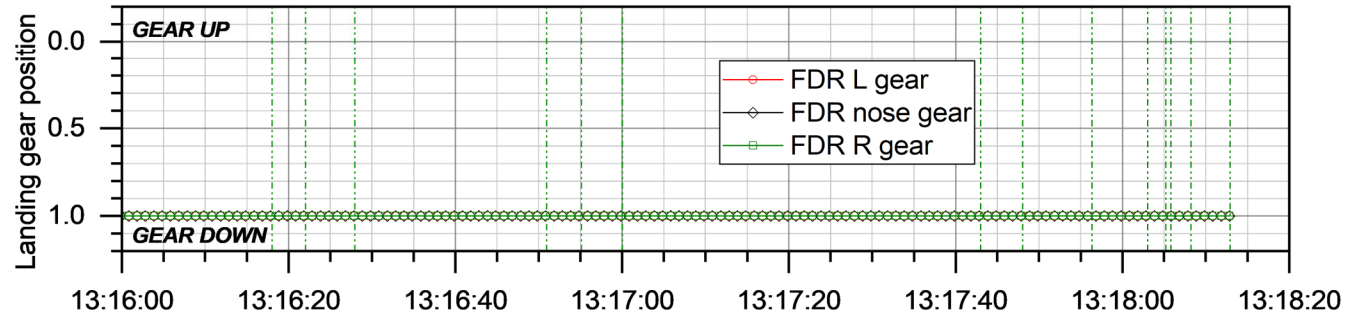
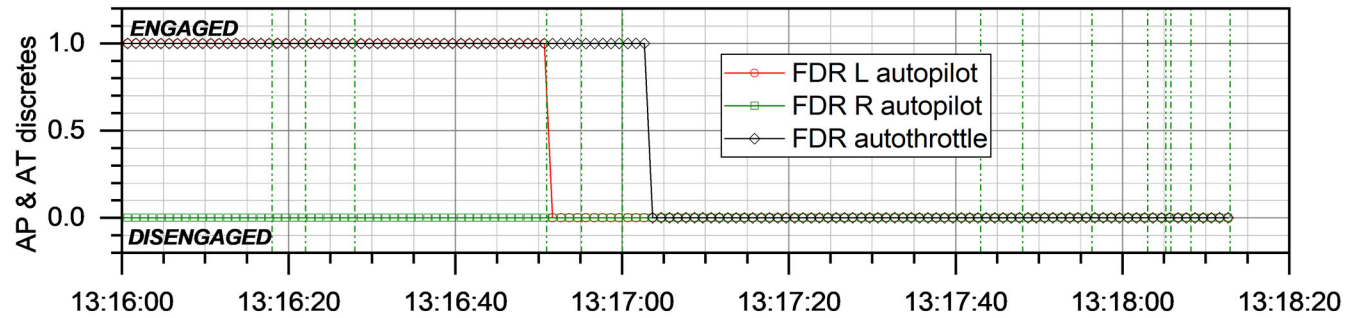
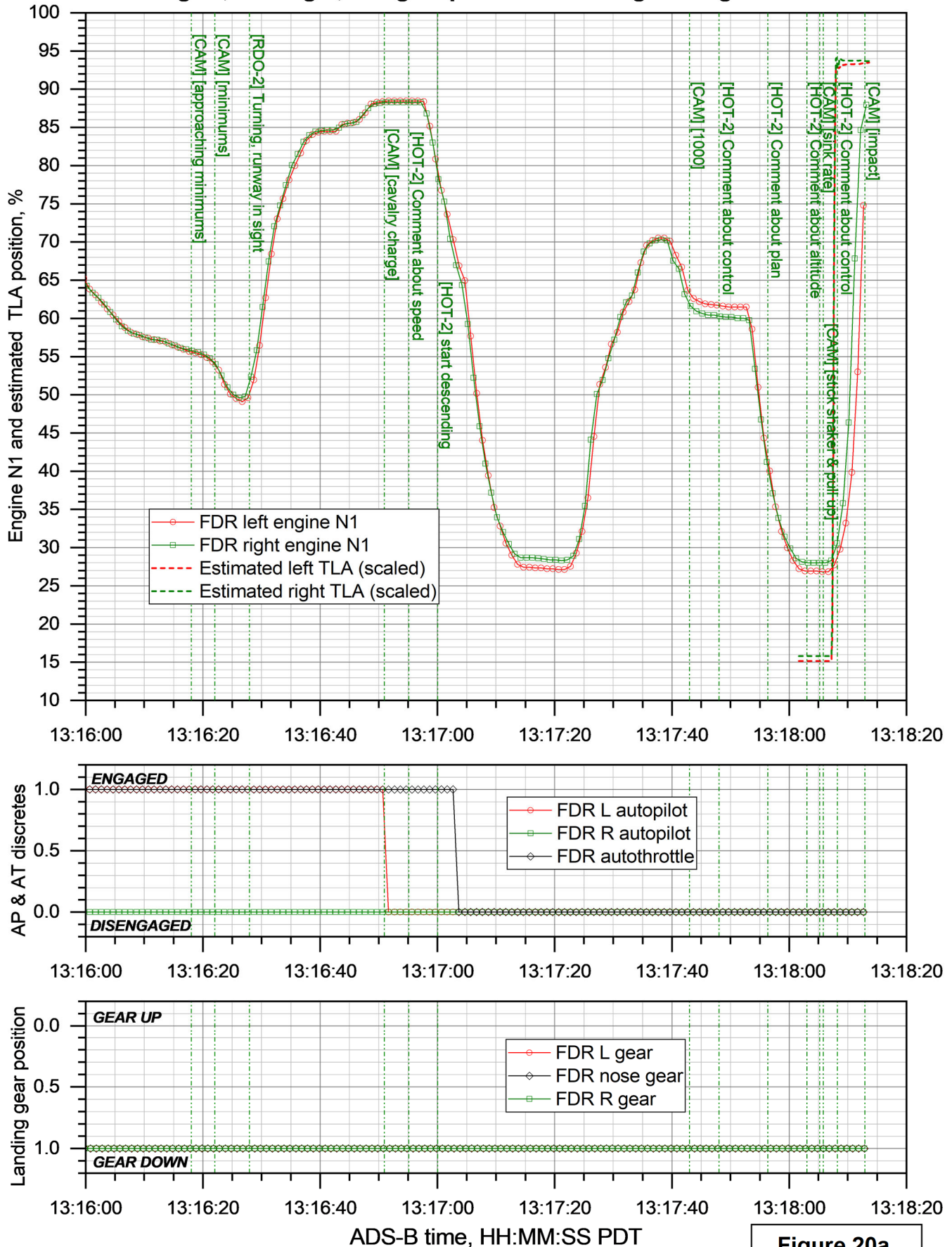


Figure 20a.

WPR21FA286: Bombardier CL-600-2B16, N605TR, Truckee, CA, 07/26/2021

Engine, autoflight, and gear parameters during circling maneuver (detail)

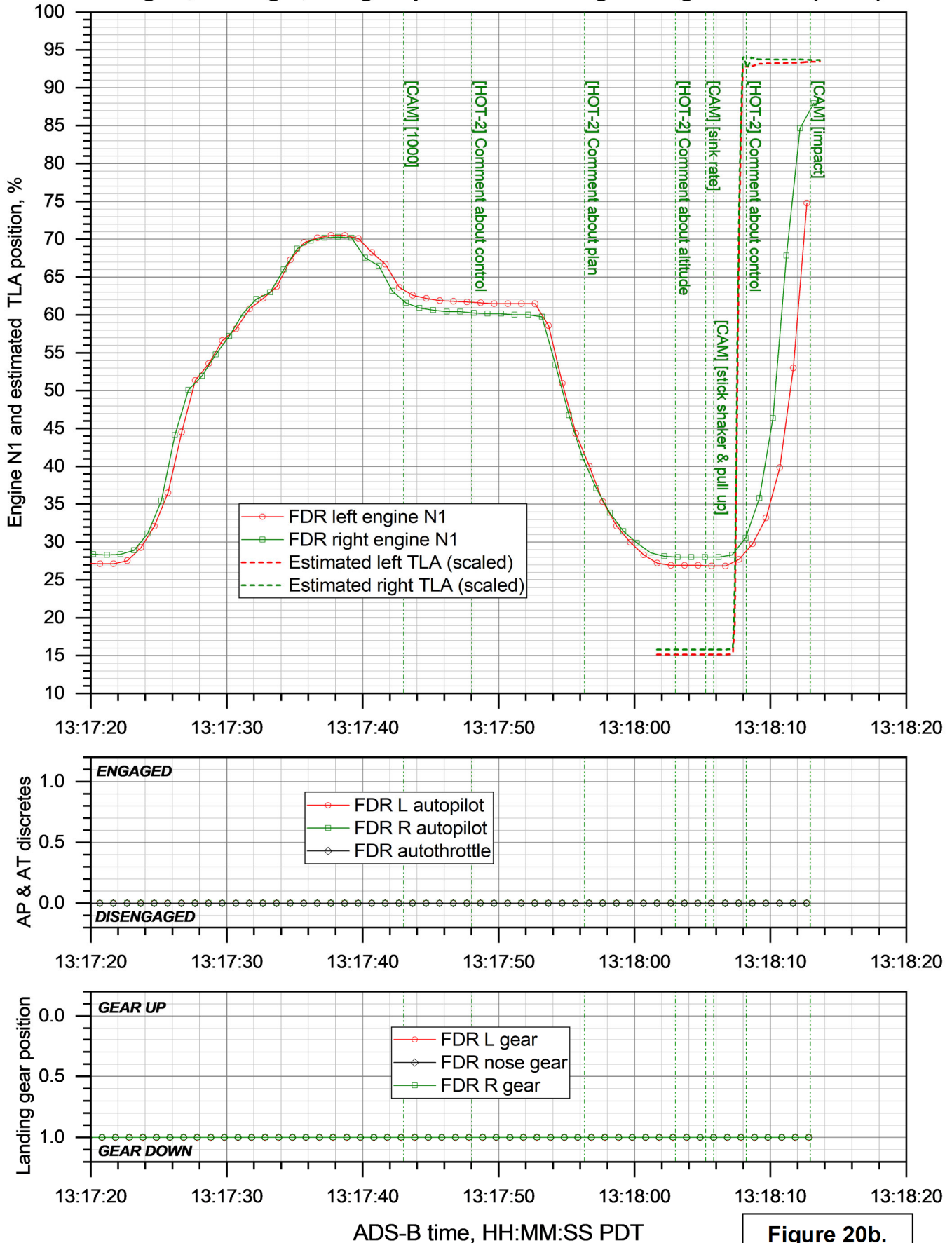


Figure 20b.

WPR21FA286: Bombardier CL-600-2B16, N605TR, Truckee, CA, 07/26/2021

Stall Protection System performance during final turn

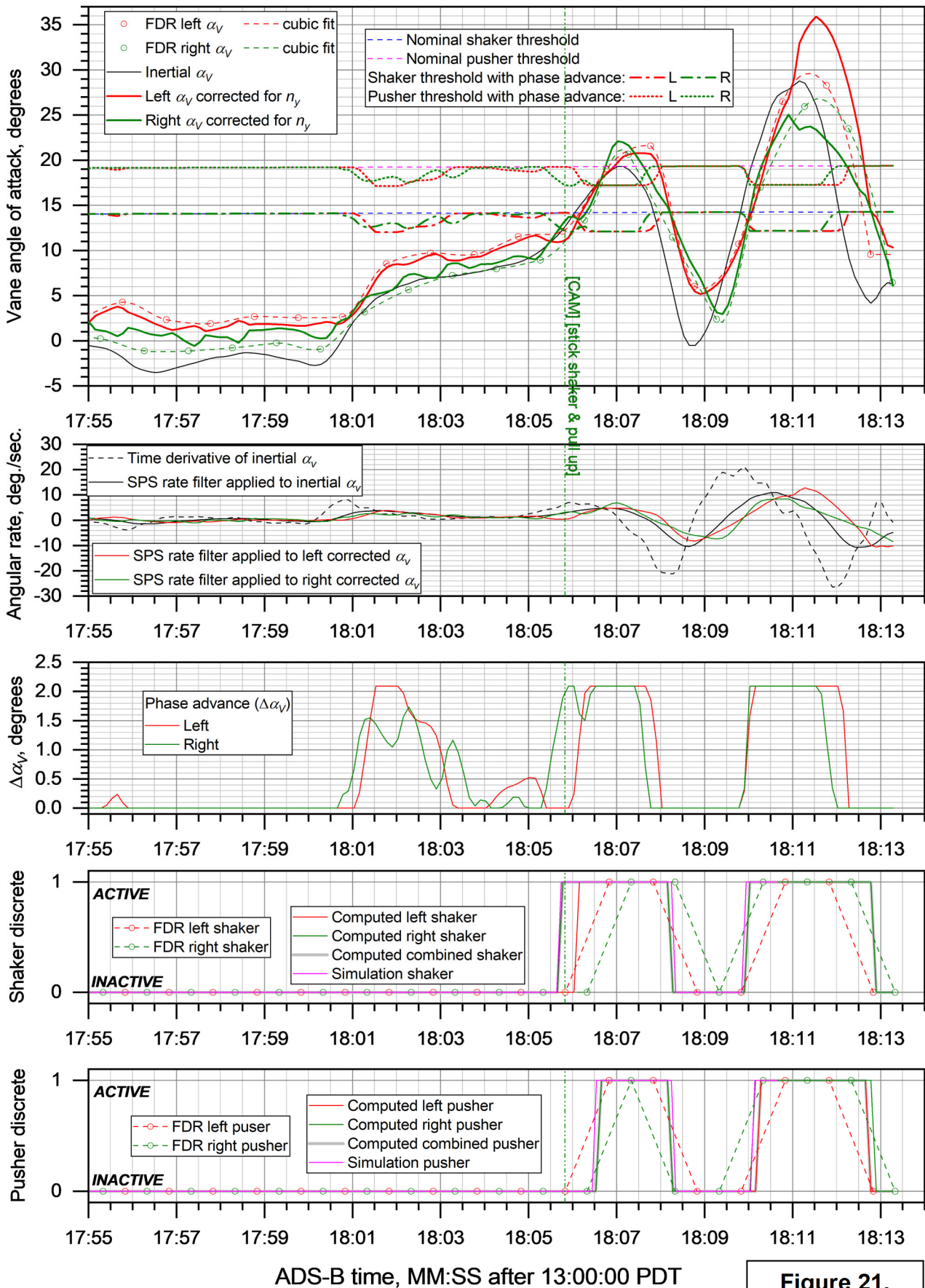


Figure 21.

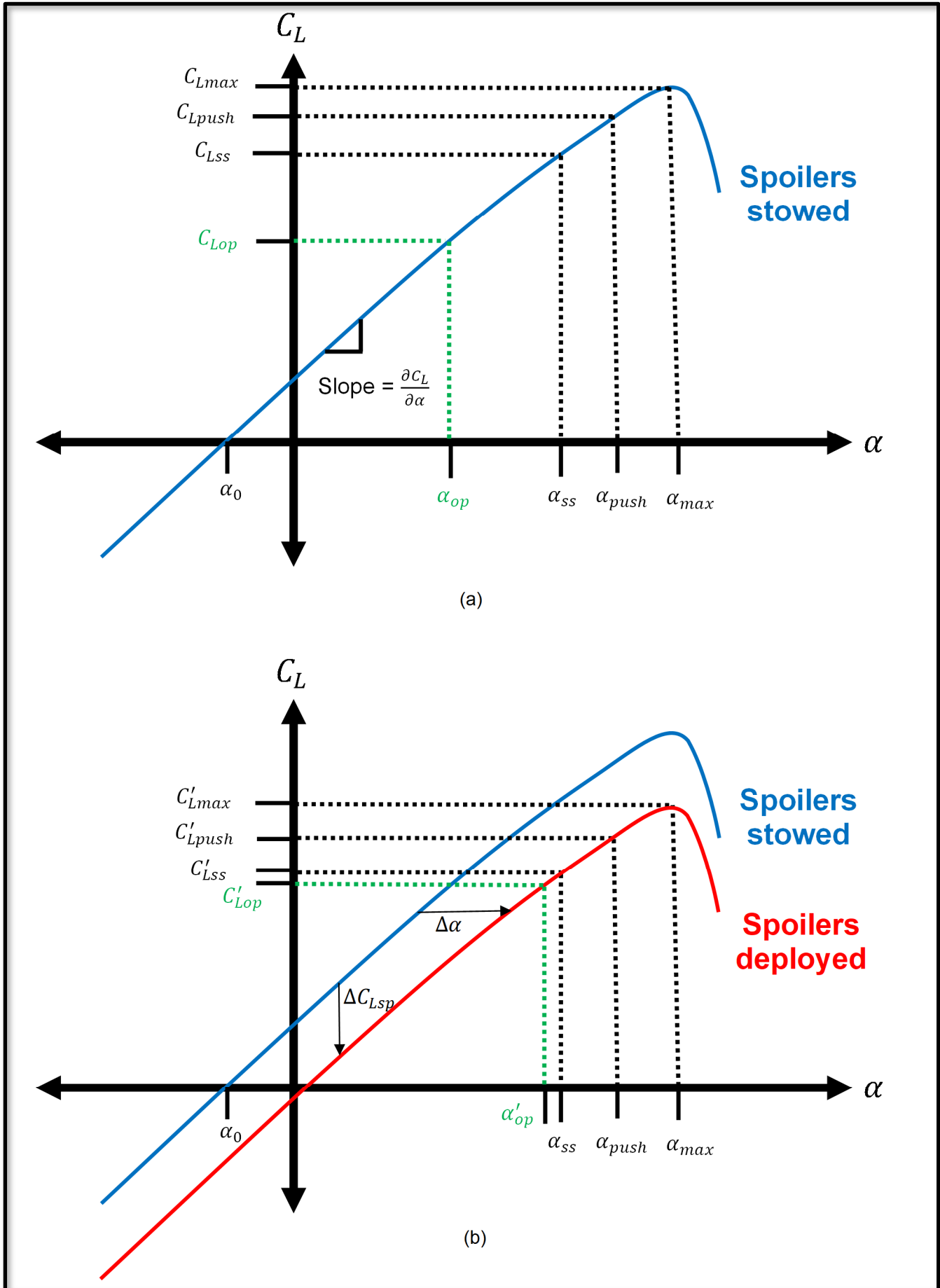


Figure 22. Effect of spoiler deployment on the airplane lift curve.

WPR21FA286: Bombardier CL-600-2B16, N605TR, Truckee, CA, 07/26/2021 Stall protection system load factor envelope @ flaps 45, 6300 ft. MSL, spoilers down & up

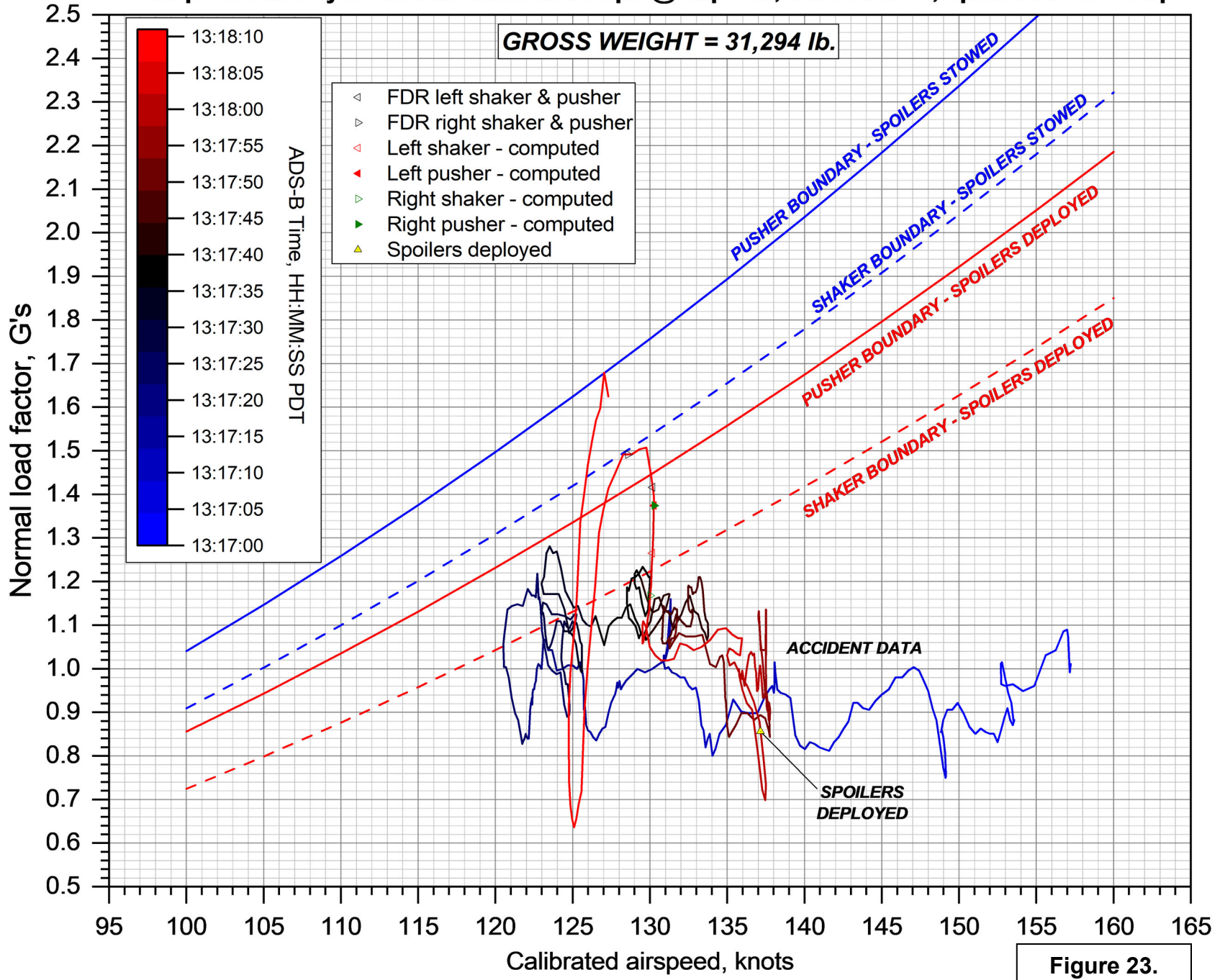
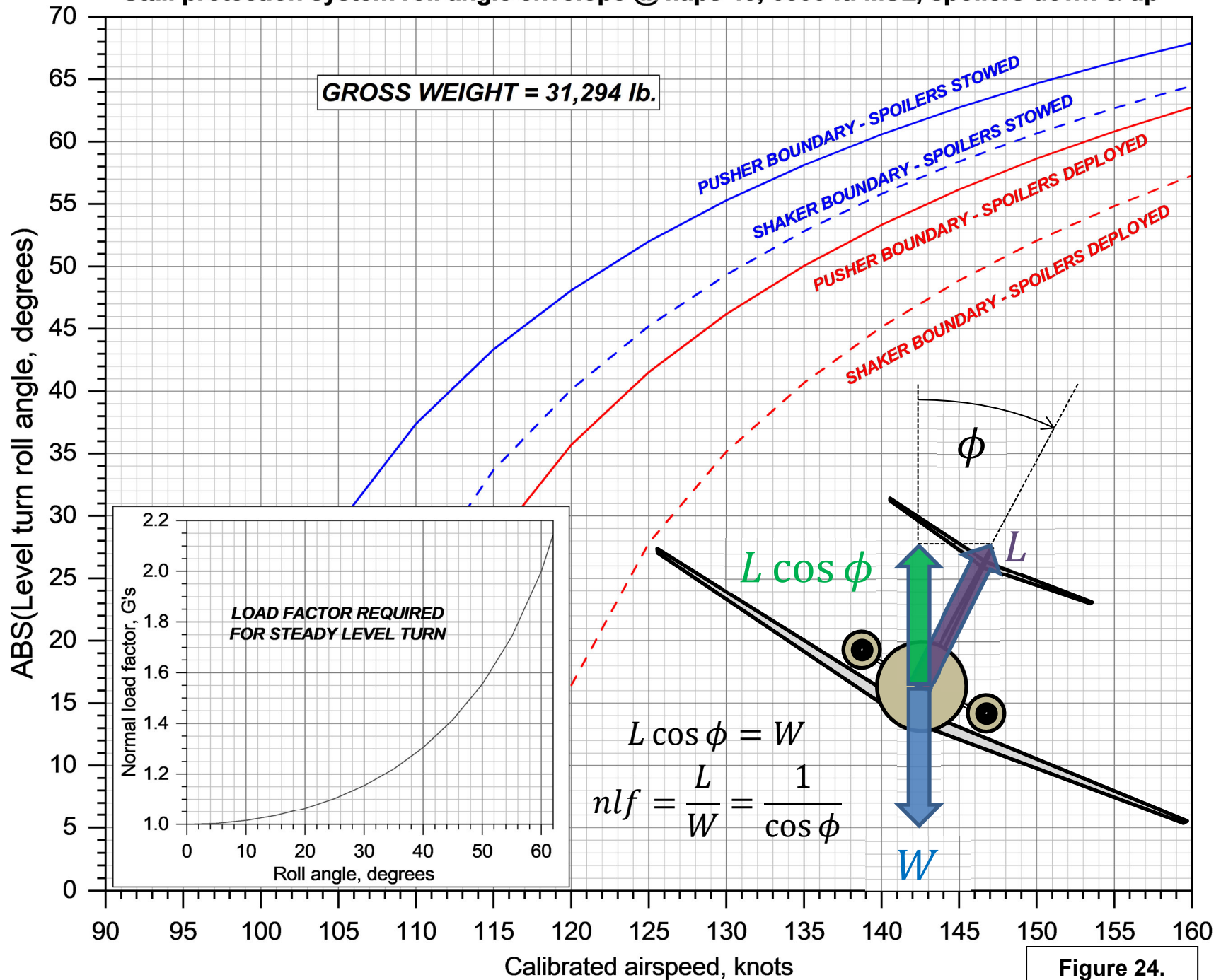


Figure 23.

WPR21FA286: Bombardier CL-600-2B16, N605TR, Truckee, CA, 07/26/2021
Stall protection system roll angle envelope @ flaps 45, 6300 ft. MSL, spoilers down & up



THIS PAGE DELIBERATELY LEFT BLANK

APPENDIX A:

KTRK airport diagram and other information

Airports

Nav aids

Airspace Fixes

Aviation Fuel

Hotels

iPhone App

My AirNav

1463 users online [LOGIN](#)**KTRK Truckee-Tahoe Airport**
Truckee, California, USA**GOING TO TRUCKEE?**[Reserve a Hotel Room](#)[Reserve Online](#)**FAA INFORMATION EFFECTIVE 27 JANUARY 2022**[Loc](#) | [Ops](#) | [Rwys](#) | [IFR](#) | [FBO](#) | [Links](#)
[Com](#) | [Nav](#) | [Sves](#) | [Stats](#) | [Notes](#)**Location**

FAA Identifier: TRK

Lat/Long: 39-19-12.2000N 120-08-22.5000W

39-19.203333N 120-08.375000W

39.3200556,-120.1395833

(estimated)

Elevation: 5904.3 ft. / 1799.6 m (surveyed)

Variation: 14E (2015)

From city: 2 miles E of TRUCKEE, CA

Time zone: UTC -8 (UTC -7 during Daylight Saving Time)

Zip code: 96161

Airport Operations

Airport use: Open to the public

Activation date: 10/1962

Control tower: yes

ARTCC: OAKLAND CENTER

FSS: RENO FLIGHT SERVICE STATION

NOTAMs facility: TRK (NOTAM-D service available)

Attendance: 0700-2130

Pattern altitude: 7004.3 ft. MSL

Wind indicator: lighted

Segmented circle: yes

Lights: WHEN ATCT CLSD ACTVT REIL RWY 11; MIRL
RWY 2/20 & 11/29; VASI RWY 20 - CTAF.

Beacon: white-green (lighted land airport)

Operates sunset to sunrise.

Landing fee: yes

Airport Communications

CTAF: 120.575

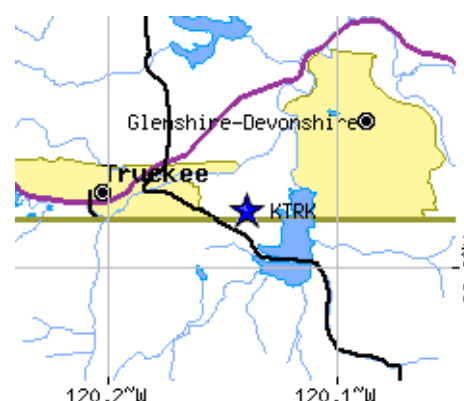
UNICOM: 122.95

**One clear choice to land.**

Lake Tahoe Airport

KTVL - 122.85

530-541-2110

Road maps at: [MapQuest](#) [Bing](#) [Google](#)**Aerial photo**

WARNING: Photo may not be current or correct

WX AWOS-3PT: 118.0 (530-587-4599)
 TRUCKEE GROUND: 118.3 [0700-1900 APR-MAY; 0700-2000 JUN-SEP;
 0700-1800 OCT-MAR]
 TRUCKEE TOWER: 120.575 [0700-1900 APR-MAY; 0700-2000 JUN-
 SEP; 0700-1800 OCT-MAR]

- APCH/DEP CTL SVC PRVDD BY OAKLAND ARTCC (ZOA) ON FREQ 127.95 (SQUAW VALLEY RCAG) AND FREQ 316.1 (SACRAMENTO RCAG).

Nearby radio navigation aids

VOR radial/distance	VOR name	Freq	Var
SWR r020/10.3	SQUAW VALLEY VOR/DME	113.20	16E
FMGr 225/25.7	MUSTANG VORTAC	117.90	16E

Airport Services

Fuel available: 100LL JET-A JET-A1+
 100LL:FUEL AVBL 0700-1900
 Oil available: WHEN ATCT CLSD.
 Parking: hangars and tie-downs
 Airframe service: MAJOR
 Powerplant service: MAJOR
 Bottled oxygen: NONE
 Bulk oxygen: NONE

Runway Information

Runway 11/29

Dimensions: 7001 x 100 ft. / 2134 x 30 m
 Surface: asphalt/grooved, in good condition
 Weight bearing capacity: Single wheel: 50.0
 Double wheel: 80.0

Runway edge lights: medium intensity

RUNWAY 11

Latitude: 39-19.490865N
 Longitude: 120-09.164548W
 Elevation: 5901.3 ft.
 Traffic pattern: left
 Runway heading: 106 magnetic, 120 true
 Markings: nonprecision, in good condition

Runway end identifier lights: yes
 Touchdown point: yes, no lights

RUNWAY 29

39-18.914562N
 120-07.879025W
 5892.6 ft.
 left
 286 magnetic, 300 true
 nonprecision, in good condition

no
 yes, no lights

Runway 2/20

Dimensions: 4654 x 75 ft. / 1419 x 23 m
 Surface: asphalt, in good condition

Weight bearing capacity: Single wheel: 35.0
 Double wheel: 50.0

Runway edge lights: medium intensity

RUNWAY 2

RUNWAY 20



Photo courtesy of Mitch Bowers Imagewerx.us Aerial Photography
 Photo taken 10-May-2012 from 12,000' looking east.

Do you have a better or more recent aerial photo of Truckee-Tahoe Airport that you would like to share? If so, please [send us your photo](#).

Sectional chart



Airport diagram

CAUTION: Diagram may not be current



Airport distance calculator

Flying to Truckee-Tahoe Airport? Find the distance to fly.

From to KTRK

[CALCULATE DISTANCE](#)

Sunrise and sunset

Times for 17-Feb-2022
 Local Zulu
 (UTC-8) (UTC)

Latitude: 39-18.871247N	39-19.535112N
Longitude: 120-08.399323W	120-07.906053W
Elevation: 5890.2 ft.	5890.3 ft.
Traffic pattern: left	right
	GLDRS USE LEFT TFC
	RWY 20.
Runway heading: 016 magnetic, 030 true	196 magnetic, 210 true
Displaced threshold: no	115 ft.
Markings: nonprecision, in good condition	nonprecision, in good condition
Visual slope indicator:	2-box VASI on left (3.50 degrees glide path)
Runway end identifier lights: no	no
Touchdown point: yes, no lights	yes, no lights

Morning civil twilight	06:23 ^{A4}	14:23
Sunrise	06:51	14:51
Sunset	17:38	01:38
Evening civil twilight	18:06	02:06

Current date and time

Zulu (UTC)	17-Feb-2022 14:27:14
Local (UTC-8)	17-Feb-2022 06:27:14

METAR

KTRK 171320Z AUTO 00000KT 10SM CLR M10/M11 A3035 RMK AO2
KRNO 171355Z 00000KT 10SM CLR
 20nm NE M04/M07 A3039 RMK AO2 SLP303 T10391072 \$

TAF

KTRK 171120Z 1712/1812 VRB04KT P6SM SKC FM180400 VRB03KT P6SM SCT100 BKN180
KRNO 171120Z 1712/1812 VRB04KT P6SM SKC FM180400 VRB03KT P6SM SCT120 BKN200

NOTAMs

[Click for the latest NOTAMs](#)

NOTAMs are issued by the DoD/FAA and will open in a separate window not controlled by AirNav.

Airport Ownership and Management from official FAA records

Ownership: Publicly-owned
 Owner: TRUCKEE-TAHOE AIRPORT DIST
 10356 TRUCKEE AIRPORT RD
 TRUCKEE, CA 96161
 Phone 530-587-4540
 Manager: KEVIN SMITH
 10356 TRUCKEE AIRPORT RD
 TRUCKEE, CA 96161
 Phone 530-587-4119

Airport Operational Statistics

Aircraft based on the field: 114	Aircraft operations: avg 96/day *
Single engine airplanes: 98	60% local general aviation
Multi engine airplanes: 7	37% transient general aviation
Jet airplanes: 1	3% air taxi
Helicopters: 3	<1% military
Gliders airplanes: 4	* for 12-month period ending 31 December 2017
Ultralights: 1	

Additional Remarks

- RWY 20 & RWY 11 DIST-TO-GO MKRS INSTLD ON LEFT SIDE.
- ACFT & HEL NOISE ABATEMENT RULES IN EFCT. PLEASE AVOID FLT OVER RESIDENTIAL AREAS, N,W, & S; CTC ARPT NOISE ABATEMENT OFC 530-587-4119 EXT 106 FOR COPY OF PROCS & RULES PRIOR TO ARR OR DP WWW.TRUCKEETAHOEAIRPORT.COM
- NO DE-ICE SER AVAIL INDEF
- SIMULUS OPS ON RWYS 11/29 AND 2/20.
- CLSD TO ULTRALIGHT ACT EXC BY PRIOR PMSN.
- ACFT CPBL OF OPERG ABV 80,000 LBS MUST SMT CERTIF TO AMGR VFYG ACFT OPERG WT IS LESS THAN 80,000 LBS.
- VOLUNTARY CURFEW: NO ENG STARTS ARR OR DEPS EXC PPR OR LIFEGUARD FLTS 2200-0700.
- PREF CALM WIND RWY USE RWY 02/20.
- NO ASR COVERAGE BLO 10,000 FT OVER KTRK
- SPECIAL HAZARD: MOUNTAINOUS TRRN SRNDS ARPT AND RWYS; EXPC

WINDSHEER AND DOWNDRAFTS.

- SUMMER DENSITY ALTS IN AFTNS FRQLY EXCEED 9000 FT.
- COLD TEMPERATURE AIRPORT. ALTITUDE CORRECTION REQUIRED AT OR BELOW -18C.
- WHEN ATCT CLSD, FOR CD CTC OAKLAND ARTCC AT 510-745-3380.
- WILDLIFE ON AND INVOF ARPT.
- GLDR AND SKYDIVING OPNS NE OF ARPT MAY-SEP.

Instrument Procedures

NOTE: All procedures below are presented as PDF files. If you need a reader for these files, you should [download](#) the free Adobe Reader.

NOT FOR NAVIGATION. Please procure official charts for flight.

FAA instrument procedures published for use from 27 January 2022 at 0901Z to 24 February 2022 at 0900z.

IAPs - Instrument Approach Procedures

RNAV (GPS) RWY 11	download (355KB)
RNAV (GPS) RWY 20	download (365KB)
RNAV (GPS)-A	download (306KB)
NOTE: Special Alternate Minimums apply	download (118KB)

Departure Procedures

TAHOE ONE (RNAV)	download (173KB)
TRUCK FOUR (OBSTACLE)	download (261KB)
NOTE: Special Take-Off Minimums/Departure Procedures apply	download (181KB)

Other nearby airports with instrument procedures:

[KRNO](#) - Reno/Tahoe International Airport (20 nm NE)



[KCXP](#) - Carson City Airport (20 nm E)

[KRTS](#) - Reno/Stead Airport (24 nm NE)

[KMEV](#) - Minden-Tahoe Airport (26 nm SE)



[KTVL](#) - Lake Tahoe Airport (26 nm S)

FBO, Fuel Providers, and Aircraft Ground Support

Business Name	Contact	Services / Description	Fuel Prices	Comments
 TRUCKEE TAHOE AIRPORT	UNICOM 122.95 530-587-4119 530-587-4540 [web site] [email]	Airport management, Aviation fuel, Aircraft parking (ramp or tiedown), Courtesy transportation, Restrooms More info and photos of Truckee Tahoe Airport	 100LL Jet A	not yet rated
			FS \$6.11 \$6.69 SS \$5.56 --- <small>Updated 15-Feb-2022</small>	2 read write

Alternatives at nearby airports

IMPORTANT: Note that the FBOs below are NOT at KTRK but at other nearby airports. Do not expect services from these FBOs to be available at KTRK.

Located at KRNO 	122.85 775-800-4244 [web site] [email]	At KRNO (Reno/Tahoe International Airport), 20 miles ENE Reno's newest FBO is now operating mid-field at RNO. Come join the Stellar family and enjoy service that is out of this world at reasonable prices.	Located at KRNO  100LL Jet A FS \$6.83 \$5.98 <small>Updated 16-Feb-2022</small>	★★★★★ 7 read write
---	--	---	--	---

FS=[Full service](#)
SS=[Self service](#)

UPDATE PRICES

Would you like to see your business listed on this page?

If your business provides an interesting product or service to pilots, flight crews, aircraft, or users of the Truckee-Tahoe Airport, you should consider listing it here. To start the listing process, click on the button below

ADD YOUR BUSINESS OR SERVICE

Other Pages about Truckee-Tahoe Airport

- [www.truckeetahoeairport.com](#)
- [Noise Abatement Procedures](#)
- [Webcam](#)

UPDATE, REMOVE OR ADD A LINK

eNASR

Cycle:	Current (2021-09-09)	Resource:	Airport	Query Screen
--------	----------------------	-----------	---------	------------------------------

Airport TRK

General	Location	Associated FAA Facilities	Contacts	Services and Facilities	Usage, Rules, and Regulations	Pad Rwy	Linear Rwy
----------------	-----------------	----------------------------------	-----------------	--------------------------------	--------------------------------------	----------------	-------------------

Item 2 of 2

Status:	EXISTING	Rwy ID:	11/29	Gross Wt SW:	50.0	Gross Wt DW:	80.0	Gross Wt DTW:	
Gross Wt DDTW:		PCN Number:		Pavement Type:		Subgrade Strength Category:		Tire Pressure:	
Evaluation Method:									

Rwy General

Edge Intensity:	MED	Length:	7001	Length Source:	3RD PARTY SURVEY	Length Source Date:	2017-09-26	
Width:	100							

Rwy Surface

Condition:	GOOD	Surface Type:	ASPH	Treatment:	GRVD
-------------------	------	----------------------	------	-------------------	------

Base Rwy End

Rwy End ID:	11	Arresting Systems			
		System Code			

Apch Lights:		Centerline:		Marking Cond:	GOOD	Marking Type:	NPI	REIL:	
RVR:		RVV:		TDZ:		Thr Crossing Hgt:		VGSI:	
Visual Glide Angle:									

Obstruction

Clearance Slope:	20	Close In:		Cntrln Offset		Ctlg Obstn:		Displaced Thr Len:	
				Offset:					
				Direction:	L/R				
Dist From Rwy End:		FAR 77 Category:	C	Hgt Above Rwy End:		Marked Lighted:		Slope to Displaced Thr:	

Displaced Threshold	Runway End
Elevation	Elevation
Elevation ft:	Elevation ft: 5901.3
Source:	Source: 3RD PARTY SURVEY
Source Date:	Source Date: 2017-09-26
Datum:	Datum: NAVD88
Position	Position
Latitude:	Latitude: 39-19-29.4519N
Longitude:	Longitude: 120-9-9.8729W
Source:	Source: 3RD PARTY SURVEY
Source Date:	Source Date: 2017-09-26

Touchdown Zone	Rwy Distances
Elevation ft: 5904.3	Acft Stop Dist Avbl:
Source: 3RD PARTY SURVEY	Lndg Dist Avbl:
Source Date: 2017-09-26	Overrun Len:
Datum: NAVD88	Stopway Len:
	Tkof Dist Avbl:
	Tkof Run Avbl:

LAHSO	Rwy End General
LAHSO Lndg	Gradient:
Hold Short of Intersecting	Grad Drctn:

Dist:	Rwy:	Right Traffic:	True Heading: 120					
Hold Short of Other:	<table border="1"> <tr><td>Hold Short Point</td></tr> <tr><td>Latitude:</td></tr> <tr><td>Longitude:</td></tr> <tr><td>Source:</td></tr> <tr><td>Source Date:</td></tr> </table>	Hold Short Point	Latitude:	Longitude:	Source:	Source Date:		
Hold Short Point								
Latitude:								
Longitude:								
Source:								
Source Date:								

Reciprocal Rwy End

Rwy End ID: 29	<table border="1"> <tr><td>Arresting Systems</td></tr> <tr><td>System Code</td></tr> </table>	Arresting Systems	System Code
Arresting Systems			
System Code			

Apch Lights:	Centerline:	Marking Cond: GOOD	Marking Type: NPI	REIL:
RVR:	RVV:	TDZ:	Thr Crossing Hgt:	VGSI:
Visual Glide Angle:				

Obstruction

Clearance Slope: 34	Close In:	<table border="1"> <tr><td>Cntrln Offset</td></tr> <tr><td>Offset:</td></tr> <tr><td>Direction:</td></tr> </table>	Cntrln Offset	Offset:	Direction:	Ctlg Obstn:	Displaced Thr Len:
Cntrln Offset							
Offset:							
Direction:							
Dist From Rwy End:	FAR 77 Category: B(V)	Hgt Above Rwy End:	Marked Lighted:	Slope to Displaced Thr:			

Displaced Threshold
Elevation
Elevation ft:
Source:
Source Date:
Datum:
Position
Latitude:
Longitude:
Source:
Source Date:

Runway End
Elevation
Elevation ft: 5892.6
Source: 3RD PARTY SURVEY
Source Date: 2017-09-26
Datum: NAVD88
Position
Latitude: 39-18-54.8737N
Longitude: 120-7-52.7415W
Source: 3RD PARTY SURVEY
Source Date: 2017-09-26

Touchdown Zone
Elevation ft: 5900.8
Source: 3RD PARTY SURVEY
Source Date: 2017-09-26
Datum: NAVD88

Rwy Distances
Act Stop Dist Avbl:
Lndg Dist Avbl:
Overrun Len:
Stopway Len:
Tkof Dist Avbl:
Tkof Run Avbl:

LAHSO					
LAHSO Lndg Dist:					
Hold Short of Intersecting Rwy:					
<table border="1"> <tr><td>Hold Short Point</td></tr> <tr><td>Latitude:</td></tr> <tr><td>Longitude:</td></tr> <tr><td>Source:</td></tr> <tr><td>Source Date:</td></tr> </table>	Hold Short Point	Latitude:	Longitude:	Source:	Source Date:
Hold Short Point					
Latitude:					
Longitude:					
Source:					
Source Date:					
Hold Short of Other:					

Rwy End General
Gradient:
Grad Drctn:
Right Traffic:
True Heading: 300

APPENDIX B:

Bombardier memorandum to NTSB

Air Safety Investigation Office (ASIO)

TECHNICAL MEMO

BOMBARDIER

DATE Thursday, February 17th, 2022
MEMO REFERENCE NO. ASIO-2021-ML-022
SUBJECT Stall Assessment - Challenger 605 N605TR (MSN 5715) - Impact with Terrain on Approach to Runway 11 at Truckee Tahoe Airport (KTRK) on July 26th, 2021
FROM Bombardier Air Safety Investigation Office (ASIO)
TO U.S. National Transportation Safety Board (NTSB)
CC Transportation Safety Board of Canada (TSB)
ASIO CASE REF. NO. CL600-2B16 (604 Variant).5715.26-7-21
NTSB CASE REF NO. WPR21FA286
TSB CASE REF NO. A21F0101

Introduction

On July 26th, 2021, at approximately 1318 Pacific Daylight Time (PDT), Challenger 605 N605TR (MSN 5715) impacted terrain while conducting a circling approach to runway 11 at Truckee Tahoe Airport (KTRK). The aircraft was destroyed by impact forces and post-impact fire. All on-board (two flight crew, four passengers and two domestic animals) were fatally injured.

The U.S. National Transportation Safety Board (NTSB) opened an investigation into the circumstances of the accident. The Transportation Safety Board of Canada (TSB), representing the State of Design and Manufacture of the aircraft, in accordance with International Civil Aviation Organization (ICAO) Annex 13 protocols, designated a non-traveling Accredited Representative to the investigation and appointed Bombardier's Air Safety Investigation Office (ASIO) as a Technical Advisor to the TSB Accredited Representative.

This memo has been prepared by the ASIO, at the request of the NTSB, to provide the following:

1. a qualitative description of how the natural stall develops on the Challenger 605 at low altitude and the resulting expected aircraft behavior;
2. in relation to 1, an explanation of why the Challenger 605 Stall Protection System is designed the way it is; and
3. a review of approximately the last five seconds of the accident data retrieved from the Flight Data Recorder (FDR) with regards to the displayed stall characteristics.

Challenger 605 Natural Stall

The wing design of the Challenger 605 is essentially the same as that of the original Challenger 600, thus all of the Challenger 600 series aircraft have common stall characteristics, and observations of any specific model are applicable to the entire series.

The Challenger 600 series wing design is characterized by a “leading edge” stall; as the angle-of-attack (AoA) increases towards the stall, a separation bubble begins to form near the leading edge on the upper surface; at first, this is a localized phenomenon and is not evident in the aircraft-level characteristics. Specifically, no pre-stall buffet occurs. If the AoA is further increased, the bubble grows and then suddenly, without any precursor indications, “bursts”; the upper surface airflow separates almost entirely aft of the burst bubble. This occurs at a critical spanwise location at close to mid span, but this “bursting” disrupts the flow both inboard and outboard of that location, which is already approaching local flow separation conditions anyway, and thus the stall spreads rapidly – almost instantaneously – both inboard and outboard of the initiating location – not reaching fully inboard, but close to fully outboard.

As this is a “sudden” behaviour, in most practical circumstances the stall occurs and fully develops on one wing before the other wing has even begun to separate. The sudden loss of lift on one wing therefore not only causes a sudden drop in overall lift and thus load factor but also causes an abrupt rolling moment, and the resulting rapid rate of roll induces an increase in AoA on the already stalled wing, driving that wing into a more stalled condition, while simultaneously reducing the apparent AoA on the opposite wing, tending to prevent a stall developing on the “unstalled” wing. Thus, the rolling moment is if anything reinforced. The Challenger 600 series has relatively small ailerons for roll control, and with one wing almost fully stalled outboard, the effectiveness of that wing’s aileron is negligible. It is thus impossible to arrest the rolling motion until the AoA is reduced and the stalling condition removed.

The natural stall characteristics of the Challenger 600 series (and thus the Challenger 605 specifically as well) are thus a stall with no pre-stall warning, an abrupt load factor reduction at the instant of stall, and an uncontrolled and uncontrollable rolling motion. Any recovery action other than reducing the AoA is ineffective.

Challenger 605 Stall Protection System

The natural stall characteristics described in the preceding section are not certifiable to 14 CFR Part 25 (Airworthiness Standards: Transport Category Airplanes) or any comparable regulations. There was an extensive attempt during Challenger 600 initial development to obtain “certifiable stall characteristics” by means of adding wing “dressing” to the design; these attempts were ultimately unsuccessful.

Therefore, it was deemed necessary to rectify the natural characteristics by adding a system which would provide acceptable characteristics by artificial means. This is the design intent of the Stall Protection System.

In order to address the lack of stall warning inherent in the natural stall, stick shakers are added to both control columns, with their firing triggered once the AoA passes a specific threshold, generally called the (shaker) “firing angle”. In order to obtain acceptable characteristics if the stall were to progress past stall shaker onset, a stall pusher system was installed, which commands a full nose-down elevator input if the AoA passes a higher threshold, called the “pusher firing angle”. The nose-down elevator creates a nose down pitch motion which is similar to the pitch down seen with acceptable, “certifiable”, stall characteristics; the pitch down also creates a loss of lift as the AoA is reduced. The firing angle for pusher activation was selected such that for any expected stall manoeuvre, the pusher would activate and allow the stall to be safely recovered from, even accounting for higher entry rates to the stall and possible AoA overshoots in recovery, without encountering the natural stall. The firing angle for shaker was then derived from the pusher firing angle to allow the required "certification" warning margin, such that a crew encountering shaker and recovering promptly would avoid pusher activation.

Stall Analysis of Accident Flight

There are two distinct stall “events” during the accident flight.

At approximately FDR time 19775, the pilot commands an increasing load factor with an increasing nose-up elevator input; the AoA increases in response. The shaker activates but the crew continues to command an increasing load factor/AoA, and thus the pusher activation AoA is reached. When the pusher activates a significant nose-down elevator is seen and the increase in AoA is stopped, followed by a marked reduction in AoA. There is also a marked pitch down and reduction in load factor proportional to the reduction in AoA. During this stall event the bank angle appears to remain under control and does not vary significantly. This is entirely representative of the expected behaviour for the aircraft following pusher activation and recovery.

At approximately FDR time 19779, four seconds after the first event, the pilot has reacted to the previous pitch-down by then commanding significantly more nose-up elevator than previously. The AoA increases again, this time passing through the pusher AoA with some evidence of pusher activation, as the elevator input is reduced to close to neutral, but no nose-down input is seen. As a consequence the AoA is not abruptly reduced, and a sudden drop in load factor (n_z) from $\sim 1.50g'$ to $\sim 1.25g'$ then occurs with no corresponding change in AoA, at the same time as a build up occurs in sideforce (n_y) and a significant rolling motion occurs. The characteristics observed here are consistent with the expected natural stall characteristics.

Conclusion

Two stall events occur in the last few seconds of the accident flight. The initial event has characteristics consistent with a pusher-defined stall, with the aircraft remaining under pilot control in the roll axis, while the second event is consistent with encountering the natural stall, with apparently uncommanded and uncontrolled rolling motion.